UNIVERSIDADE DE VIGO
DEPARTAMENTO DE FÍSICA APLICADA
Environmental Physics Laboratory

Universidade Vigo

PhD Thesis

Thermohaline variability in the Bay of Biscay: causes and physical implications

Memoria presentada por
Jorge Costoya Noguerol
para optar al título de DOCTOR POR LA UNIVERSIDADE DE VIGO

Enero, 2016

Universidade de Vigo, Campus de Ourense
Jorge Costoya Noguerol (xurxocostoya@uvigo.es)
Thermohaline variability in the Bay of Biscay: causes and physical implications.
Ourense, enero de 2016.

Imagen de la portada:
http://earthobservatory.nasa.gov/NaturalHazards/view.php?id=14900, do Observatorio da Terra da NASA (http://earthobservatory.nasa.gov/).

Informe del director

Dra. María Teresa de Castro Rodríguez, profesora titular del Departamento de Física Aplicada de la Universidad de Vigo, y **Dr. Ramón Gómez Gesteira**, catedrático del Departamento de Física Aplicada de la Universidad de Vigo:

CERTIFICAN

Que la presente memoria "*Thermohaline variability in the Bay of Biscay: causes and physical implications*", resume el trabajo de investigación realizado, bajo su dirección, por DON JORGE COSTOYA NOGUEROL en el departamento de Física Aplicada en el programa de doctorado en Marine Sciences, Technology and Management (Campus do Mar) para optar al título de "DOCTOR POR LA UNIVERSIDAD DE VIGO".

Y para que conste y en cumplimiento de la legislación vigente, firman el presente informe en Ourense a 20 de octubre de 2015.

Dra. María Teresa de Castro Rodríguez

Dr. Moncho Gómez Gesteira

Agradecementos/Acknowledgements

En primeiro lugar teño que expresar todo o meu agradecemento a Maite e Moncho. Prestáronme a súa axuda antes incluso de coñecerme en persoa e tanto durante a miña etapa de máster como durante os tres anos que me levou realizar esta tese sempre tiven a sensación de ser un privilexiado ao poder contar ca súa axuda e orientación, preocupados tanto polo traballo diario como polo meu futuro.

Teño que dar as gracias a tódalas persoas cas que compartín laboratorio habitualmente: Fran, Anxo, Orlando, Ángel, Álex, Jose e Roger. Sempre atopei solucións cando lles pedín axuda e o ambiente de traballo sempre foi moi bo, moitas risas. Dar as gracias tamén ós integrantes do laboratorio perico Diego, Rubén, Laura, Manolo, Marisela e David, polos bos momentos tanto dentro como fóra da universidade. Ademais, das gracias as persoas que nos visitaron cas que tamén compartín bos momentos: Renato, Magda, Carlos e Ricardo.

A meus pais, Elena e Moncho, e a miña irmá, Ara, porque independentemente do número de kilómetros que me separaron da miña casa durante toda a miña etapa universitaria (en León, Trieste, Santiago ou Ourense) sempre estiveron ahí a modo de salvavidas preocupados sempre de que nunca me faltase nada.

Dar infinitas gracias a Lucía, en primeiro lugar por animarme a facer a tese, foi unha moi boa decisión, e tamén por confiar máis en min e nas miñas capacidades do que eu o farei nunca, polo seu ánimo e apoio sempre que o precisei e, o que é máis importante, por ser sinónimo de felicidade todos estes anos.

Moitas gracias aos que foron compañeiros/as de carreira en León e que, a pesar do paso do tempo, e da distancia nalgúns casos, seguen estando moi presentes: Javi, Marina, Bertza, Marcos, Óscar, Victoria...e tamén a Miguel, co cal levo unha vida paralela e sempre rematamos por atoparnos alá onde vou, por fortuna para min. Dar gracias ós colegas de Vigo, en especial a Jorge, Rubén e Krusty e tamén ó Iago, que me fixo máis fácil a miña vida en Ourense.

This work was supported by the Xunta de Galicia through the Plan galego de investigación, innovación e crecemento 2011–2015 (Plan I2C) in collaboration with the International Campus do Mar (PRE/2012/431)

Resumen

Durante las últimas décadas se han detectado importantes cambios en el sistema climático a nivel global (IPCC, 2013). La variación que, tal vez, ha despertado un mayor interés entre la comunidad científica ha sido el incremento de temperatura tanto en los océanos como en la atmósfera. El océano desempeña un papel fundamental a la hora de regular este calentamiento ya que se estima que aproximadamente el 93% del calor absorbido por la Tierra ha ido a parar a los océanos (Church et al., 2011; Levitus et al., 2012). De esta forma el contenido de calor oceánico se ha incrementado, especialmente en los primeros 700 m de la columna de agua (Palmer et al., 2007; Domingues et al., 2008; Ishii and Kimoto, 2009; Levitus et al., 2012).

Es importante señalar que las variaciones de temperatura, y en general los cambios en las variables físicas oceánicas, son dependientes tanto del período como de la zona que se analiza. De tal forma que es posible encontrar tendencias opuestas cuando se varía el periodo de análisis para una misma zona (e.g: Casey and Cornillon, 2001; deCastro et al., 2009; Gouretski et al., 2012). Además, se ha visto que la tasa de aumento de temperatura varía dependiendo de la cuenca oceánica (Tabla 1). Estos cambios son incluso más marcados a escalas espaciales menores porque existen una serie de factores locales (vientos, corrientes oceánicas, cambios en la capa de mezcla, fenómenos de afloramiento…) que pueden variar más rápidamente a escala regional (Ginzburg et al., 2004; Goreau et al., 2005; Santos et al., 2005; Gómez-Gesteira et al., 2008).

Cuenca oceánica	***Tendencia en el Contenido de Calor*** *(10^{22} J por década)*	***Tendencia en la Temperatura*** *(ºC por década)*
Océano Global	3.0	0.18
Hemisferio Norte	1.5	0.23
Hemisferio Sur	1.5	0.14
Atlántico	1.4	0.31
Pacífico	1.0	0.12
Índico	0.5	0.15

Tabla 1. Cambio en el contenido de calor (10^{22} J por década) y tendencia en la temperatura (ºC por década) en los primeros 700 m de la columna de agua para el Océano Global y para cada cuenca. Las tendencias fueron calculadas de forma lineal para el período 1955-2010. Fuente: Levitus et al. (2012).

Durante las últimas décadas también se han notificado variaciones en la salinidad. En general, la tendencia ha sido a aumentar en aquellas regiones en las que la salinidad media es superior, y a disminuir en aquellas zonas donde es más baja (Boyer et al., 2007; Hosoda et al., 2009; Roemmich and Gilson, 2009; Durack and Wijffels, 2010). Así, el Océano Atlántico es donde más ha aumentado la salinidad superficial, especialmente en el Atlántico Norte. Cambios en los valores medios de temperatura o

salinidad traen consigo otras modificaciones, como por ejemplo, cambios en la profundidad de la capa de mezcla (MLD, *Mixed Layer Depth*) (deBoyer et al., 2004; Monterrey and Levitus, 1997). A su vez, la MLD condiciona variables biológicas como la disponibilidad de nutrientes (Sverdrup, 1953; García-Soto and Pingree, 2009). Por tanto, cambios en las variables termohalinas en el océano desencadenan importantes modificaciones a diferentes niveles, especialmente a escala regional, donde los cambios son más acentuados.

Aparte de los cambios en los valores medios de las variables termohalinas, en las últimas décadas se ha puesto de relieve la importancia de analizar las variaciones en eventos extremos ya que un aumento en la frecuencia o intensidad de los mismos se ha definido como uno de los aspectos más peligrosos del cambio climático (IPCC, 2013). Además, variaciones en la estacionalidad de los parámetros físicos como por ejemplo cambios en la duración de la estación cálida son también de interés porque determinan cambios importantes en las respuestas bióticas (e.g: Selig et al., 2010). Por tanto, cambios en los valores medios, variaciones en valores extremos y cambios en la estacionalidad son aspectos fundamentales para entender los cambios en los ecosistemas marinos y determinar políticas para mitigarlos (e.g: Thieltges, 2006; Occhipinti-Ambrogi, 2007; Halpern et al., 2008).

Los párrafos anteriores ponen de relieve los cambios globales relacionados con la temperatura y la salinidad, así como la importancia de analizar dichos cambios a escala local y a diferentes escalas temporales. Para lograr este objetivo, es fundamental contar con bases de datos que proporcionen altas resoluciones espaciales y temporales. Durante las últimas décadas se ha dedicado un gran esfuerzo a desarrollar series de datos oceánicas fiables. En relación a la temperatura superficial del mar (SST, *Sea Surface Temperature*), los satélites proporcionan información global con un nivel de detalle espacial inalcanzable utilizando solamente datos in-situ. Según el IPCC (2013), el principal sensor de radiación infrarroja es el *Advanced Very High Resolution Radiometer* (AVHRR) (ver información detallada en NOAA, 2009). Los datos de este sensor se utilizaron para construir diferentes bases de datos tales como *Pathfinder*, que contiene datos de SST desde 1981 (Kilpatrick et al., 2001; Casey et al., 2010). Además, los datos de SST provenientes de los sensores AVHRR se combinaron con datos in situ tomados por buques y boyas utilizando un método especial de kriging, la interpolación óptima, con el fin de construir una base de datos con una malla regular de alta resolución espacial y temporal, *NOAA ¼º daily Optimum Interpolation Sea Surface Temperature (OISST$_{1/4}$) database* (Reynolds, 2009). Más recientemente, se puso en funcionamiento el sensor *Moderate Resolution Imaging Spectroradiometer (MODIS)*, que es considerado el sucesor del sensor AVHRR. MODIS proporciona una mayor resolución espacial y una resolución espectral mayor ya que adquiere información en 36 bandas espectrales (NASA, 2015).

En cuanto a la disponibilidad de datos termohalinos bajo la superficie del mar, el inicio del proyecto Argo supuso un gran avance (GCOS, 2009). Las boyas Argo

producen más de 100.000 perfiles de temperatura y salinidad de los primeros 2000 m cada año desde 2012. Antes del inicio del proyecto Argo, los datos termohalinos disponibles a lo largo de la columna de agua, especialmente para la salinidad, eran escasos y dependían principalmente del desarrollo de campañas oceanográficas. Sin embargo, algunos proyectos de asimilación de datos, como por ejemplo el *Simple Ocean Data Assimilation (SODA)*, lograron generar una base de reanálisis utilizando datos de cruceros en combinación con datos satélite y simulaciones llevadas a cabo con modelos con el objetivo de crear una malla regular de muestras desde 1958 (Carton et al., 2005).

	BASE DE DATOS	VARIABLE	RESOLUCIÓN ESPACIAL	RESOLUCIÓN TEMPORAL
OCEANOGRÁFICAS	*Argo*	Tª y salinidad	Movimiento libre (Hasta 2000m)	Desde 2002 (10-días)
	SODA	Tª y salinidad	0.5°x0.5° (Hasta 5000m)	Desde 1958 (mensuales)
	OISST$_{1/4}$	SST	0.25°x0.25° (Valores superficiales)	Desde 1982 (diarios)
	MODIS	SST y Radiancia	0.01°x0.01° (Valores superficiales)	Desde 2002 (diarios)
ATMOSFÉRICAS	*NCEP/NCAR*	Viento, T^{aire}, Flujo calor latente y precipitación	1.91°x1.91°	Desde 1948 (mensuales)
	CFSR	Viento y flujos de calor	0.3°x0.3°	Desde 1979 (6-horas)

Tabla 2. Bases de datos oceanográficas y atmosféricas utilizadas en esta tesis

La totalidad de las bases de datos mencionadas se utilizaron para analizar los cambios en las variables físicas en el Golfo de Vizcaya, que es el objetivo principal de esta tesis. Por lo tanto, bases de datos modernas como MODIS o Argo se combinaron con las bases de datos que contienen datos de mayor duración (OISST$_{1/4}$ y SODA) con el fin de proporcionar una visión completa de estos cambios. Este enfoque es crucial para determinar los cambios físicos a escala regional.

El Golfo de Vizcaya se ubica en el Atlántico Norte, al norte de la Península Ibérica y al oeste de Francia (Figura 1). Esta zona forma una unidad geomorfológica diferenciada que se caracteriza por una plataforma continental muy ancha a lo largo de la costa francesa (entre 60-150 km) y una mucho más estrecha a lo largo de la costa cantábrica (Lavín et al., 2006). El área central de la bahía alcanza profundidades medias de 4000 m, y entre la plataforma y esta área central se localiza el talud continental. Estas tres zonas con diferente batimetría son claves para definir la circulación en el golfo (Charria et al., 2013), que varía dependiendo de la estación. Es importante señalar que el

Golfo de Vizcaya se encuentra en una situación intermedia entre los dos giros que definen la circulación en el Atlántico Norte, lo que le confiere unas características especiales (Borja and Colins, 2009). Esta peculiaridad define la masa de Agua Central del Este del Atlántico Norte (ENACW, *Eastern North Atlantic Central Water*) que ocupa la parte superior de la columna de agua y, por tanto, se encuentra influenciada por el giro subpolar ($ENACW_{sp}$) y subtropical ($ENACW_{st}$) del Atlántico Norte (Fraga et al., 1982; Pérez et al., 2000). A una mayor profundidad fluye la masa de Agua Mediterránea (MW, *Mediterranean Water*), que alcanza el Golfo de Vizcaya al desplazarse hacia el norte a lo largo del oeste de la Península Ibérica (Mazé et al., 1997; Iorga and Lozier, 1999; van Aken, 2000).

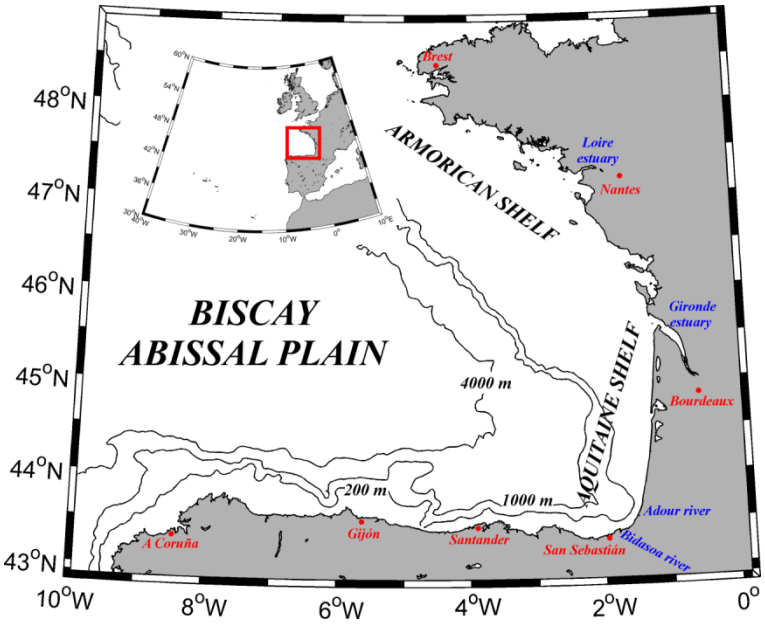

Figura 1. Batimetría del Golfo de Vizcaya. Las líneas de contorno representan las isobatas de 200, 1000 y 4000m. Ubicación del Golfo de Vizcaya (señalado en cuadro rojo) en la parte superior izquierda.

Históricamente el Golfo de Vizcaya es una región que ha recibido poca atención desde el punto de vista oceanográfico si se compara con otras zonas del Atlántico Norte (Lavín et al., 2006). Así, son muy pocos los estudios que se pueden citar durante los siglos XIX y XX (Borja and Collins, 2004; Rallo and Borja, 2004), y no es hasta los años 80 cuando los estudios centrados en el Golfo de Vizcaya se incrementan notablemente (Lavín et al., 2006). En cuanto a los diferentes estudios que se han desarrollado en el campo de la oceanografía física durante las últimas décadas, es importante señalar que la mayor parte se caracterizan por abarcar una región concreta del Golfo de Vizcaya siendo muy limitados los estudios que analizan todo el golfo en conjunto. Precisamente, este es uno de los aspectos en los que se trata de avanzar en esta tesis, ya que todos los estudios que la forman se caracterizan por cubrir todo el golfo.

El parámetro físico más analizado en los estudios previos tal vez haya sido la SST. Así, diferentes estudios (deCastro et al., 2009; Michel et al., 2009a;b; Koutsikopoulos et

al., 1998) analizaron variaciones en la SST durante las últimas décadas en toda la región y detectaron una tendencia común al calentamiento desde los años 70. Este calentamiento presenta diferencias espaciales, por ejemplo Michel et al. (2009b) observó un mayor calentamiento en la zona norte del Golfo, y también temporales, con un mayor incremento durante los meses de primavera y verano (deCastro et al., 2009). La tendencia al aumento de la SST también fue descrita en diferentes análisis llevados a cabo para zonas más concretas. Gómez-Gesteira et al. (2008) detectaron un aumento a lo largo de las costa cántabra y francesa y varios estudios notificaron este calentamiento en las proximidades de San Sebastián (Usabiaga et al., 2004; Fontán et al., 2008; Goikoetxea et al., 2009; González et al., 2013).

En cuanto a los cambios en las masas de agua, González-Pola et al. (2005) analizaron cambios tanto en ENACW como en la MW durante el periodo 1992-2003 en el sureste del golfo. Estos autores detectaron un incremento de la temperatura tanto en ENACW como en la MW. En relación a cambios en la salinidad a lo largo de la columna de agua, Pérez et al. (1995); (2000) observaron una disminución de la salinidad en ENACW hasta 1990 y un aumento a partir de esas fecha. De la misma forma, Llope et al. (2006) detectaron un aumento durante para el periodo 1993-2003 y González-Pola et al. (2005) un incremento de la salinidad en la MW.

A la hora de analizar los forzamientos que causan estos cambios es importante tener en cuenta diferentes aspectos. La atmósfera juega un papel muy importante ya que influye directamente en las propiedades del océano (salinidad, temperatura) y condiciona los procesos físicos que en él tienen lugar (ej. la estratificación de la columna de agua, afloramiento). Por lo tanto es necesario tener en cuenta las variaciones en la atmósfera (ej: cambios en la temperatura del aire, cambios en el patrón de precipitaciones, cambios en el intercambio del flujo de calor…) ya que influyen directamente en el océano. A lo largo de esta tesis, se analizaron los cambios en algunos parámetros atmosféricos y se tuvieron en cuenta los patrones de teleconexión con mayor influencia en la región de estudio (Oscilación del Atlántico Norte (NAO, *North Atlantic Oscillation*) y el Patrón Atlántico Este (EA, *East Atlantic Pattern*)). Otros forzamientos que se analizaron son los aportes de agua dulce ya que pueden llegar a modificar las propiedades del agua oceánica costera así como modificar la circulación. En el caso del Golfo de Vizcaya, los ríos con valores de descarga más altos son el Loira y el Gironde.

Como se dijo anteriormente, el objetivo principal de esta tesis es analizar los cambios, desde un punto de vista físico, que han tenido lugar en el Golfo de Vizcaya durante las últimas décadas. El contenido de cada uno de los capítulos que compone esta tesis es el siguiente:

El capítulo 1 recoge el contexto global en el que se encuadra el contenido científico de la tesis. En él se subraya el contexto de cambio global en el planeta Tierra y los cambios más destacables detectados durante las últimas décadas. Por otra parte se explica la importancia del Golfo de Vizcaya y se caracteriza desde un punto de vista

físico esta región. Además se recopilan los diferentes trabajos previos que analizan cambios en las variables físicas.

En el capítulo 2 se describen todas las bases de datos, oceánicas y atmosféricas, que se utilizaron para realizar los diferentes estudios. Además también se describen los patrones de teleconexión (NAO y EA) y el modo de variabilidad oceánico "Oscilación Multidecadal del Atlántico (AMO)".

El capítulo 3 analiza los cambios en las propiedades termohalinas de la masa de agua ENACW a través de datos de reanálisis (base de datos SODA) para el periodo 1975-2010. Se detectó un aumento tanto en la temperatura como en la salinidad de ENACW (0.11°C por década y 0.03 por década, respectivamente). Este incremento fue mayor en la parte media de la bahía y cerca de la frontera noreste (Figura 2). Estas variaciones no fueron causadas por procesos locales en el interior del golfo. En realidad, las tendencias parecen estar relacionados con los cambios en el modo subpolar de ENACW ya que se observaron tendencias al incremento tanto en temperatura como en salinidad al norte de la bahía, especialmente en la zona poco profunda que se extiende desde Brest a Irlanda, que se caracteriza por la mezcla profunda en invierno. También se analizó la influencia de los dos modos principales de variabilidad en el Atlántico Norte (NAO y EA) sobre los cambios en ENACW, mostrando una mayor influencia del patrón EA. Además, se observó que la temperatura del aire y la diferencia entre las tasas de evaporación y precipitación (P-E) también contribuyeron al calentamiento y a la salinización de ENACW.

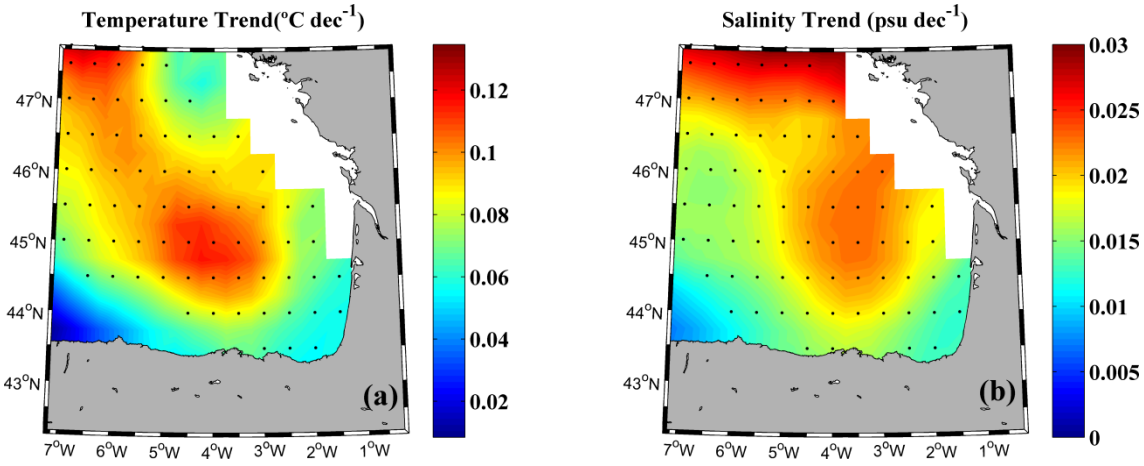

Figura 2. (a) Tendencia anual de la temperatura (ºC por década) y (b) tendencia anual de la salinidad (por década) para ENACW en el Golfo de Vizcaya durante el periodo 1975-2010. Los puntos negros representan puntos con un nivel de significancia superior al 99%.

El capítulo 4 también analiza cambios en las propiedades termohalinas de ENACW pero en este caso el estudio se realizó con datos in-situ (boyas Argo) y además se extendió el análisis a la masa de Agua Mediterránea durante la década 2004-2013. Con el fin de conocer el origen de las variaciones detectadas se aplicó la metodología desarrollada por Bindoff y McDougall (1994). Se detectó un aumento tanto de la temperatura como de la salinidad en ENACW, en consonancia con lo observado a través

de datos de reanálisis, y por el contrario, se observó un enfriamiento y una reducción de la salinidad en la MW (Tabla 2). Estos cambios se debieron principalmente a cambios intrínsicos en las masas de agua, es decir, a variaciones en las zonas donde estas masas de agua se crean, aunque en la parte superior de ENACW el desplazamiento hacia la superficie de las isopicnas tuvo un papel importante a la hora de explicar las variaciones en esta masa de agua.

	Tendencia en la temperatura (°C por década)	***Tendencia en la salinidad (por década)***
SW	-0.05	0.06*
ENACW	0.12*	0.04*
MW	-0.11*	-0.05*

Tabla 2. Tendencias lineales de temperatura y salinidad en el Golfo de Vizcaya para el periodo 2004-2013. Agua superficial (SW) (0-100m), ENACW (100-600m) y MW (600-1200m). Los asteriscos indican una significancia mayor del 95%.

Los cambios detectados en las propiedades termohalinas de las diferentes masas de agua traen consigo modificaciones en otras variables físicas, como por ejemplo la profundidad de la capa de mezcla (MLD). Es por ello que el capítulo 5 analiza los cambios en la MLD que tuvieron lugar desde 1975. Con este propósito se definió la capa de mezcla utilizando como parámetros tanto la temperatura como la densidad. Además se analizó la influencia de los forzamientos atmosféricos sobre estas variaciones. Las tendencias en la MLD mostraron ser dependientes de la zona. De tal forma que la MLD tendió a ser más profunda en la parte sureste del Golfo de Vizcaya y, por el contrario, más superficial en el resto del Golfo (Figura 3). A la hora de explicar esta variabilidad espacial se observó que las variaciones en la temperatura superficial del aire desempeñan un papel importante ya que se observaron tendencias a disminuir la temperatura en la esquina sureste donde la MLD tiende a ser más profunda, mientras que se detectó un aumento de la temperatura del aire en las zonas donde la MLD tiende a ser más superficial. Además, la tendencia de la temperatura oceánica para los primeros 700 m está en consonancia con este patrón de variación de la MLD.

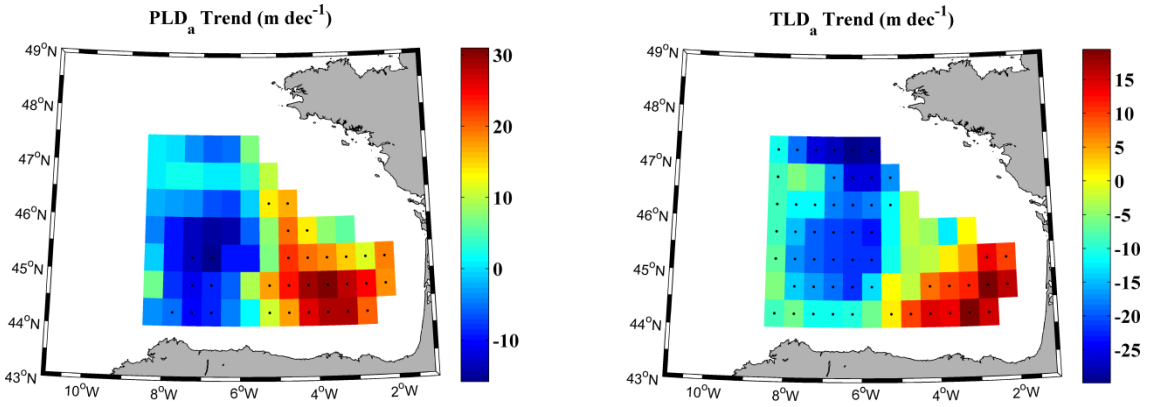

Figura 3. Tendencia de la profundidad de la capa de mezcla (m por década) durante los meses de invierno calculada por medio de anomalías mensuales utilizando como parámetro la densidad (PLD, figura izquierda) y la temperatura (TLD, figura derecha) en el Golfo de Vizcaya para el periodo 1975-2010. Los puntos negros representan puntos con un nivel de significancia superior al 90%.

En el capítulo 6 se estudian los cambios en la estacionalidad de la temperatura superficial del mar durante las tres últimas décadas. Además se analizan las variaciones en la duración de la estación cálida y también las tendencias en el número de días extremadamente cálidos. A escala anual se detectó un incremento de la SST (0.26 ± 0.03°C por década) para el periodo 1982-2014. Sin embargo, a la hora de analizar las variaciones a escala mensual se observó que la intensidad del calentamiento varía dependiendo del mes. Los mayores aumentos se registraron entre septiembre y noviembre, mientras que las tendencias más bajas se observaron entre enero y marzo y durante los meses de julio y agosto. Por tanto, estos resultados sugieren que el calentamiento anual se debió principalmente a un aumento en la duración de la estación cálida más que a inviernos más suaves o veranos más cálidos. Este hecho es el principal responsable del aumento en la frecuencia de días con una SST extremadamente cálida que se detectó durante los meses de primavera y otoño. En contraste, las tendencias observadas durante el mes con una SST media más alta, es decir, agosto, se caracterizan por un aumento del número de días extremadamente cálidos cerca de la costa y una disminución en la parte oceánica de la bahía.

Finalmente el capítulo 7 estudia la influencia de las descargas de los dos ríos más caudalosos que desembocan en el Golfo de Vizcaya, Loira y Gironde, sobre la temperatura superficial del mar por medio de dos bases de datos complementarias: MODIS y $OISST_{1/4}$. El área bajo la influencia de la pluma fluvial (Figura 4) mostró un patrón de variación de la SST diferente en comparación con la zona oceánica adyacente durante los meses en que la pluma alcanza su mayor extensión (diciembre, enero y febrero). La parte oceánica incrementó su temperatura, mientras que la temperatura en

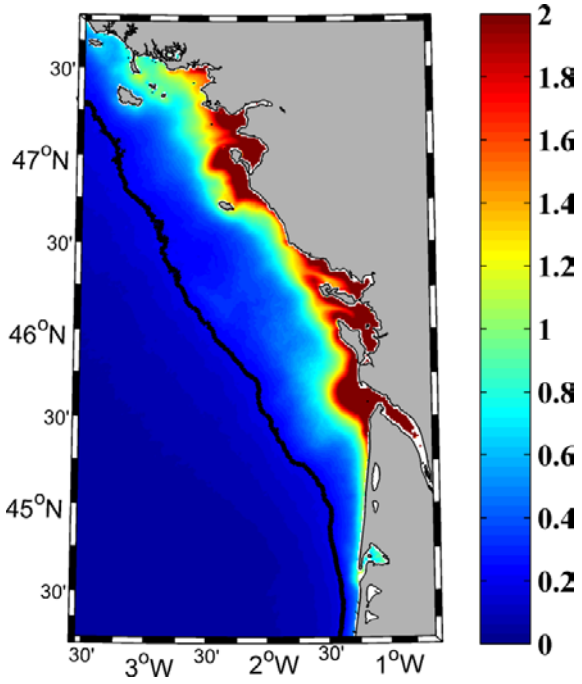

Figura 4. Extensión promedio de la pluma turbia ($mWcm^{-2}\mu m^{-1}sr^{-1}$) generada por las descargas de los ríos Loira y Gironde durante los meses de diciembre, enero y febrero para el periodo 2002-2014. La línea negra marca el límite entre las aguas oceánicas claras y la zona bajo influencia de la pluma.

el área de influencia de las descargas de ambos ríos tendió a enfriarse durante el período 1982-2014. Se concluyó que la mera presencia de una capa de agua dulce es capaz de modular el calentamiento observado en la franja costera bajo influencia de la pluma fluvial. Además se observó que esta franja costera es la única zona de la bahía donde los cambios en la SST se correlacionan de forma significativa con NAO y no lo hacen con la AMO. El patrón de enfriamiento-calentamiento es aún más patente durante el periodo 2002-2014, caracterizado por unas condiciones atmosféricas más favorables a la presencia de la pluma, ya que aumentaron tanto el caudal de los ríos como los vientos de componente suroeste, que favorecen el confinamiento de la pluma contra la costa.

Abstract

There is a wide consensus among climatologist and oceanographers that the climate system has undergone rapid changes during the last decades of the 20th century and the beginning of the 21st. The most remarkable variation is the increase in temperature both in oceans and atmosphere. Ocean plays a key role to mitigate global warming since it absorbs the vast majority of the heat gained by the Earth. So, small changes in ocean`s properties can lead to unforeseeable consequences. Numerous studies showed that these variations are highly dependent on temporal and spatial scales, in such a way that changes are more marked at regional scale.

The Bay of Biscay is a semi-enclosed sea located in the North Atlantic Ocean, off the north coast of Spain and the west coast of France. Its bathymetry is characterized by a wide continental shelf along the French coast, especially in its northern part (more than 100 km), and a narrower one along the Spanish coast. The Biscay Abyssal plain, with depths around 4000 m, occupies the central part of the bay. This area is influenced by the general circulation in the North Atlantic following an anticyclonic gyre. In the rest of the bay, bathymetric conditions together with local forcings (wind pattern, river discharges…) give as result a circulation pattern that changes depending on the season. So, the scientific interest of the Bay of Biscay resides in that it is a semi-enclosed sea representing a complex merger between ocean features and local processes that show their influence at different temporal and spatial scales.

The main aim of this thesis is to analyze oceanic physical changes occurred in the Bay of Biscay during the last decades. To carry out this purpose the newest databases were selected in order to ensure appropriate spatial and temporal resolutions. Thus, in-situ databases (Argo floats), satellite data (MODIS sensor) and reanalysis databases (SODA, $OISST_{1/4}$ and CFSR) were combined to analyze changes in salinity and temperature, as well as, variations in other physical variables such as mixed layer depth, for the whole Bay of Biscay.

Thermohaline variability of the two main upper water masses, Eastern North Atlantic Central Water (ENACW) and Mediterranean Water (MW), were studied over the periods 1975-2010 and 2004-2013. ENACW has been observed to warm and salinificate over both periods, whilst a cooling and a freshening were detected for MW over the period 2004-2013. These variations were mainly due to changes in the region were both water masses originated. This fact was evidenced applying the methodology developed by Bindoff and McDougall (1994) and also analyzing air temperature trends and precipitation less evaporation balance trend in the Northeastern Atlantic.

Wintertime MLD trends in the Bay of Biscay over the period 1975–2010 were calculated using a potential temperature criterion to define the isothermal layer depth

and a potential density criterion to define the isopycnal layer depth. MLD tended to deepen at the southeastern corner and shallow at the rest of the bay. It was observed that air temperature trends play a key role to explain the different MLD trend pattern.

Apart from changes in the mean values of thermohaline variables, variations in the seasonality and in the frequency of extreme hot SST days were also studied for the whole Bay of Biscay since 1982. Overall, a warming was detected in all months for the whole bay. This warming was higher during spring and autumn months. This fact led to an increase in the duration of the warm season in more than one month for most of the bay. In addition, an increase in the number of extreme hot SST days was detected during spring and autumn months, while no clear trend was observed during august, when the highest mean SST values occur.

Finally, the influence of Loire and Gironde Rivers discharges over SST trends was analyzed using reanalysis and satellite data. The oceanic area under the influence of the turbid plume is the only area of the bay where a cooling was detected during winter months. In addition, it was concluded that river discharges and southwestern winds over their mean values favors the maintenance of the turbid plume and also the cooling in this area. So, river discharges in the Bay of Biscay can modulate the warming pattern.

In conclusion, significant changes in physical properties and processes were detected in the Bay of Biscay during the last decades. The combination between ocean features and local processes, which show their influence at different temporal and spatial scales, explain these variations. This thesis evidences the importance of carrying out regional studies to understand physical changes in oceans, as well as to understand its influence on marine ecosystems in order to determine scenarios and policies to mitigate those changes.

Table of contents

Table of contents I

Chapter 1: Introduction 5

1.1 Motivation 6

1.2. Bay of Biscay 10

1.2.1 Topography 10

1.2.2 Freshwater inputs 11

1.2.3 Circulation 12

1.2.4 Water masses 13

1.2.5 Thermal balance and mixed layer 16

1.2.6 River plumes and upwelling events 17

1.2.7 Physical changes 18

Chapter 2: Databases 23

2.1. Ocean database 24

2.1.1 Argo floats 24

2.1.2 Simple Ocean Database Assimilation (SODA) 25

2.1.3 Daily ¼ Optimum Interpolation SST ($OISST_{1/4}$) 25

2.1.4 Moderate Resolution Imaging Spectroradiometer (MODIS) 26

2.2 Atmospheric database 27

2.2.1 National Center for Environmental Prediction/National Center of Atmospheric Research (NCEP/NCAR) Reanalysis 27

2.2.2 Climate Forecast System Reanalysis (CFSR) 27

2.3. Oceanographic modes 28

2.3.1 Atlantic Multidecadal Oscillation (AMO) 28

2.4 Atmospheric modes 29

2.4.1 North Atlantic Oscillation (NAO) 29

2.4.2 East Atlantic pattern (EA) 30

Chapter 3: Eastern North Atlantic Central Water variability by means of reanalysis data 33

3.1 Methods 34
3.2 Results and discussion 35
3.2.1 ENACW salinity and temperature trends 35
3.2.2 Atmospheric modes influence on ENACW salinity and temperature trends 40
3.2.3 Influence of atmospheric variables on ENACW variability 41
3.3 Conclusions 43

Chapter 4: Intermediate water masses variability by means of in-situ data 45
4.1 Methods 46
4.2 Results and discussion 48
4.2.1 Water masses temperature and salinity trends 48
4.2.2 Mechanisms controlling intermediate water masses variability 51
4.3 Conclusions 54

Chapter 5: Mixed layer depth trends 55
5.1 Methods 56
5.2 Results and discussion 58
5.2.1 Argo and SODA correlation 58
5.2.2 MLD variability 59
5.2.3 Influence of atmospheric variables on MLD variability 61
5.3. Conclusions 64

Chapter 6: Changes in sea surface temperature seasonality 67
6.1 Methods 68
6.1.1 SST trends 68
6.1.2 Duration of the warm season 68
6.1.3 Extreme SST trends 68
6.2 Results 69
6.2.1 Mean SST and SST trends 69
6.2.2. Duration of the warm season 73
6.2.3. Trends in the number of extreme hot SST events 74
6.3 Discussion 76

6.4 Conclusions 79

Chapter 7: Warming modulation by Loire and Gironde river discharges 81
7.1 Methods 82
7.1.1 River plume detection 82
7.1.2 SST trend calculation 82
7.1.3 Wind and heat fluxes 82
7.1.4 River discharge data 83
7.2 Results 83
7.3 Discussion 90
7.4 Conclusions 92

General conclusions 93

Acronym and abbreviation list 95

List of figures 97

List of tables 103

Bibliography 105

List of publications 127

Chapter 1: Introduction

The aim of this chapter is twofold. On the one hand, it will be given a general view of the context in which the scientific content of this thesis fits. Thus, it will be highlighted the importance of the ocean in the Earth system and the main changes that have occurred during the last decades, as well as, the most recent databases that allow us to analyze these changes using different approaches. On the other hand, the importance and interest of the Bay of Biscay will be commented. Previous studies related to changes in physical variables will be mentioned and the Bay of Biscay will be characterized from a physical point of view.

1.1 Motivation

The scientific community has focused its attention in the climate system due to the rapid changes detected during the last decades. According to the last report of the Intergovernmental Panel on Climate Change (IPCC), changes detected in the climate system since 1950 are unprecedented (IPCC, 2013). Overall, the most remarkable change is the atmosphere and ocean warming (Figures 1.1 and 1.2), which in turn drives other modifications such as a reduction of the amount of snow and ice or sea level rise.

Ocean plays a key role in regulate global warming since about 93% of the total heat gained by the Earth over the last 50 years has been absorbed by oceans (Church et al., 2011; Levitus et al., 2012). In addition, it is estimated that oceans have captured about 30% of human emissions of carbon dioxide (Mikaloff-Fletcher et al., 2006; Le Quéré et al., 2010). Therefore, little changes in oceans can lead to important changes in the climate system due to feedbacks that can increase or reduce the rate of climate change.

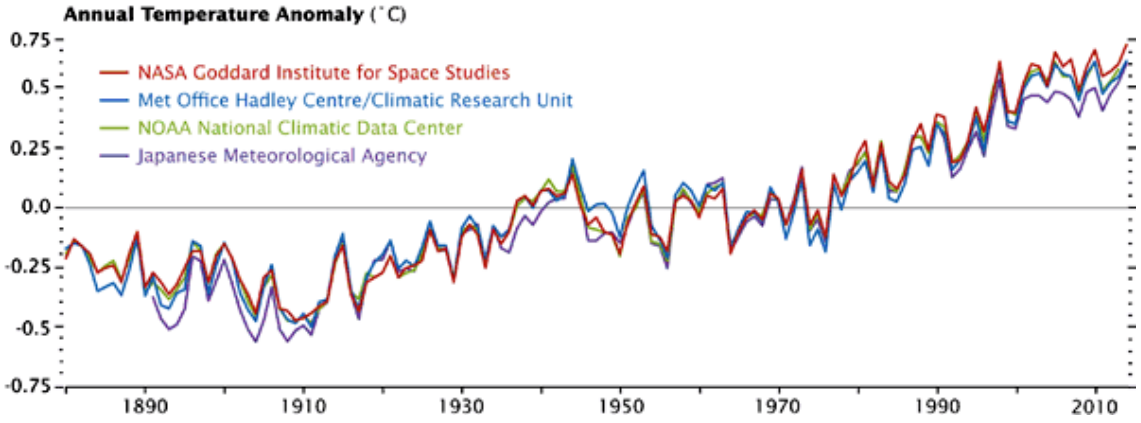

Figure 1.1. Average annual surface air temperature anomalies from 1880 to 2014 analyzed using independent methods by four different institutions. Source: NASA Earth Observatory

The most important changes in the heat content observed in the world ocean in the last decades correspond to the upper 700 m (Palmer et al., 2007; Domingues et al., 2008; Ishii and Kimoto, 2009; Levitus et al., 2012) (Table 1.1). The magnitude of these changes decrease with increasing depth. Thus, a global average warming ranging between 0.09 to 0.13 ºC per decade was detected in the upper 75 m over the period 1971-2010. However, it decreases to 0.015 ºC per decade at a depth of 700 m (IPCC, 2013). Below 700 m, it is more difficult to carry out long-term trends due to a lower data coverage but a warming was detected from 700 to 2000 m between 1957 and 2009 (Levitus et al., 2012), whilst no significant trends were observed from 2000 to 3000 m between 1992-2005 (Purkey and Johnson, 2010).

Although ocean warming occurs in a global context, it is important to take into account that ocean temperature trends are highly dependent on time and spatial scales. Thus, warming rates change from basin to basin (Levitus et al., 2012) (Table 1.1). Higher warming rates were detected in the Northern Hemisphere, especially in the North Atlantic where the highest temperature increase was found (Palmer et al., 2007; Roemmich et al., 2012). Ocean temperature variability is even more marked at the regional scale (Ginzburg et al., 2004; Goreau et al., 2005; Santos et al., 2005). This fact is related to local processes (winds, mixed layer depth, ocean currents, upwelling intensity…) that can change faster involving larger changes in regional ocean temperature than global average trends (Gómez-Gesteira et al., 2008). With regard to the dependence on time scale, opposite trends can be observed when different periods of time are considered (e.g: Casey and Cornillon, 2001; deCastro et al., 2009; Gouretski et al., 2012). So, it is important to take into account the cyclic behavior of the different parameters (climatic, meteorological, hydrodynamic and topographic) that influence ocean temperature. In addition, it has been noticed that ocean temperature trends are also dependent on the period of the year considered in such a way that different trends can mask or cancel each other when annual scales are considered.

Ocean Basin	***Heat Trend*** *(10^{22} J per decade)*	***Temperature Change*** *(ºC per decade)*
World Ocean	3	0.18
Northern Hemisphere	1.5	0.23
Southern Hemisphere	1.5	0.14
Atlantic	1.4	0.31
Pacific	1	0.12
Indian	0.5	0.15

Table 1.1. Change in ocean heat content (10^{22} J per decade) and change in mean temperature (ºC per decade) for the upper 700 m for the World Ocean and individual basins calculated using linear trends over the period 1955-2010. Source: Data from Levitus et al. (2012).

Apart from changes in temperature, ocean has suffered other modifications in its properties. Some of them are indirect changes mainly provoked by the warming, whilst other are independently of temperature increase, such as changes in salinity that will be commented below. From a physical point of view, one of the most important changes derived from warming is that the global increase around 0.25ºC between 0-200 m from 1971 to 2010 (Levitus et al., 2009) corresponds to a 4% increase in density stratification on average in world`s oceans (IPCC, 2013). So, it is supposed that variations in the mixed layer depth (MLD) have occurred. MLD is the deepest layer affected by turbulent mixing, which marks the width of the upper ocean that interacts with atmosphere. Thus, it is fundamental in the exchange of heat and freshwater between the ocean and the atmosphere and influences other processes such as the formation of water masses. MLD presents a high spatial and temporal variability since it varies from diurnal (Brainerd and Gregg, 1995) to decadal scales (Carton et al., 2008) and from mesoscale to large spatial scales (deBoyer et al., 2004; Monterrey and Levitus, 1997). The deepest MLDs

in the North Atlantic occur in winter and early spring. During spring the onset of surface heating produces a restratification of the upper ocean, giving as result shallower MLDs. These variations that reach hundreds of meters over the year, have important biological implications since it conditions the availability of nutrients in the upper layers and also phytoplankton blooms (Sverdrup, 1953; García-Soto and Pingree, 2009).

Study of ocean salinity trends is also important because it influences changes in circulation and stratification due to changes in water density. In a global context, the amount of salt does not change, so, the salinity of seawater can vary only by addition or removal of freshwater. Trends in sea surface salinity (SSS) are mainly related to the atmospheric patterns of evaporation minus precipitation (E-P) and trends in total precipitable water. Several studies have proved that SSS trends are related to the distribution of surface salinity itself, in such a way that salinity tends to increase (decrease) in regions of high (low) mean salinity (Boyer et al., 2007; Hosoda et al., 2009; Roemmich and Gilson, 2009; Durack and Wijffels, 2010). So, interbasin salinity differences were enhanced (Figure 1.2). The relatively salty Atlantic has become more saline, while the relatively fresh Pacific has become fresher. In particular, North Atlantic has become saltier since 1950s (Boyer et al., 2007) mainly due to an increase in salinity in the Gulf Stream region (Wang et al., 2010) and also in the pathway followed by the Mediterranean Outflow Water (Fusco et al., 2008).

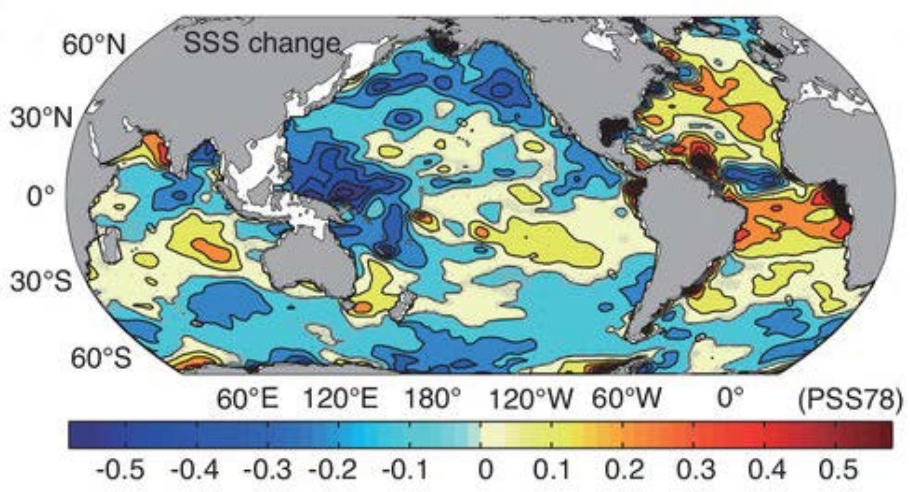

Figure 1.2. Sea surface salinity change from 1950 to 2008. Seasonal and El Niño-Southern Oscillation signals were removed. Salinity values are expressed on the Practical Salinity Scale 1978 (Fofonoff and Lewis, 1979). Source: IPCC (2013) based on Durack and Wijffels (2010).

Apart from changes in the mean values of thermohaline variables, special attention has been paid to extreme climate events during the last decades (IPCC, 2013). Although these events have been extensively documented in the atmosphere (Dessai, 2002; Trigo et al., 2009; deCastro et al., 2011b), there is a lack of knowledge on extreme temperature events in the ocean despite the fact that there is a general consensus that an increase in the frequency and/or intensity of extreme weather events can be one of the most hazardous consequences of climate change (e.g. Alexander et al.,

2006; Houghton, 2009; Sura, 2011). Changes in the seasonality of ocean temperature, such as changes in the timing of seasonal warming, are also of interest since it determines biotic responses due to the importance that temperature plays in the life cycle of marine species (e.g. Selig et al., 2010). Therefore, changes in the seasonality of SST and the frequency of extreme sea temperatures such as extremely hot or cold events is fundamental to understand changes in marine ecosystems and to determine scenarios and policies to mitigate those changes (e.g: Thieltges, 2006; Occhipinti-Ambrogi, 2007; Halpern et al., 2008).

Previous paragraphs have highlighted the global changes related to temperature and salinity, as well as the importance of analyzing changes at local scales and different temporal scales due to the spatial and temporal heterogeneity of these changes. To achieve this goal, it is fundamental account with databases that provide high spatial and time resolutions. A great effort has been devoted to develop reliable oceanic series during the last century. Regarding sea surface temperature (SST), satellite datasets provides global information with a level of spatial detail unachievable by in situ data only. According to the IPCC (2013), the main infrared radiation sensor is the Advanced Very High Resolution Radiometer (AVHRR) (see detailed information in NOAA (2009)). Data from this sensor was used to build up different datasets such as Pathfinder that contains SST data since 1981 (Kilpatrick et al., 2001; Casey et al., 2010). In addition, SST data from AVHRR sensors was combined with in-situ data from ships and buoys using a special method of kriging, the optimal interpolation, in order to construct a regular global dataset with high spatial and temporal resolution, the NOAA ¼º daily Optimum Interpolation Sea Surface Temperature (OISST) database (Reynolds, 2009). More recently, was launched the Moderate Resolution Imaging Spectroradiometer (MODIS) database, which is considered the successor of AVHRR sensors. MODIS provides a higher spatial resolution and also a greater spectral resolution since acquires data in 36 spectral bands (NASA, 2015).

Regarding thermohaline data beneath surface, the beginning of the Argo global array of profiling floats system supposed a major achievement (GCOS, 2009). Deployments of Argo floats started in 2002 and it produces more than 100.000 profiles each year since 2012. To compare data, the World Ocean Database 2009 (Boyer et al., 2009) contains approximately 500.000 profiles deeper than 1000 m from the 20th century onwards. In this way, Argo database provides in-situ data of temperature and salinity, as well as information about currents of the upper 2000 m in all ocean`s world. Prior to Argo project, the available thermohaline data along the water column, especially for salinity, was sparse and it depended mainly on oceanographic cruises. However, some data assimilation projects, like Simple Ocean Data Assimilation (SODA), have reanalyzed data from these cruises in conjunction with satellite and model simulations with the aim of create a regular mesh of samples since 1958 (Carton et al., 2005).

The entire above mentioned databases will be used to analyze changes on physical processes inside the Bay of Biscay that is the main goal of this thesis. Thus, modern databases like MODIS or Argo were combined with long-term databases ($OISST_{1/4}$ and SODA) in order to provide a complete view of these changes. This approach is crucial to determine physical changes at regional scales since, as it was previously highlighted, the magnitude of these changes depends clearly on the region under study. So, regional studies improve the knowledge to apply policies with the aim of mitigate harmful effects derivate from these changes.

1.2. Bay of Biscay

This section will try to characterize the Bay of Biscay in physical terms and also to provide the state-of-the-art until the beginning of this thesis. First of all, it is important to mention that oceanography has developed slowly in this region and it has received historically less attention when compared with others areas in the North Atlantic (Rallo and Borja, 2004; Lavín et al., 2006).

1.2.1 Topography

The Bay of Biscay is an embayment located in the North Atlantic Ocean, Western Europe, off the north coast of Spain and the west coast of France (Figure 1.3). According to the International Hydrographic Organization (IHO, 1971), the limits of the bay are marked by "*a line joining Cap Ortegal (43º 46'N, 7º 52'W) to Penmarch Point (47º48`N, 4º 22'W)*". Although this is the most common criterion used, some authors (e.g: Sánchez and Olaso, 2004) consider the southern limit up to Cape Finisterre, at 43ºN latitude. So, the bay is a well-differentiated geomorphological unit in the north-east Atlantic (Lavín et al., 2006). The Spanish coast, also called Cantabrian coast, has a marked E-W orientation, whilst the French coast follows a N-S orientation from the mouth of the Bidassoa River to La Rochelle and a NW-SE from there to Brest.

A distinctive feature of the bay is the wide of the continental shelf along the French coast, especially the northern area, ranging from 60 to 150 km with a very gentle slope of 0.12% (Pascual et al., 2004). In contrast, the Cantabrian coast is characterized by a narrower continental shelf (7-20 km wide) (Figure 1.3). The continental slope, an area of transition between the shelf and the central part of the bay, the abyssal plain, is defined by a mean slope of the order of 10-12% (Lavín et al., 2006) and by numerous canyons. For example, the Avilés Canyon System (Gómez-Ballesteros et al., 2014) or the Cap Breton Canyon in the southeastern corner of the bay, where the 1000 m isobaths is just 3 km far from the coast. The Biscay Abyssal plain, with depths around 4000 m and reaching 5500 m (Charria et al., 2013), occupies the central part of the bay (Figure 1.3).

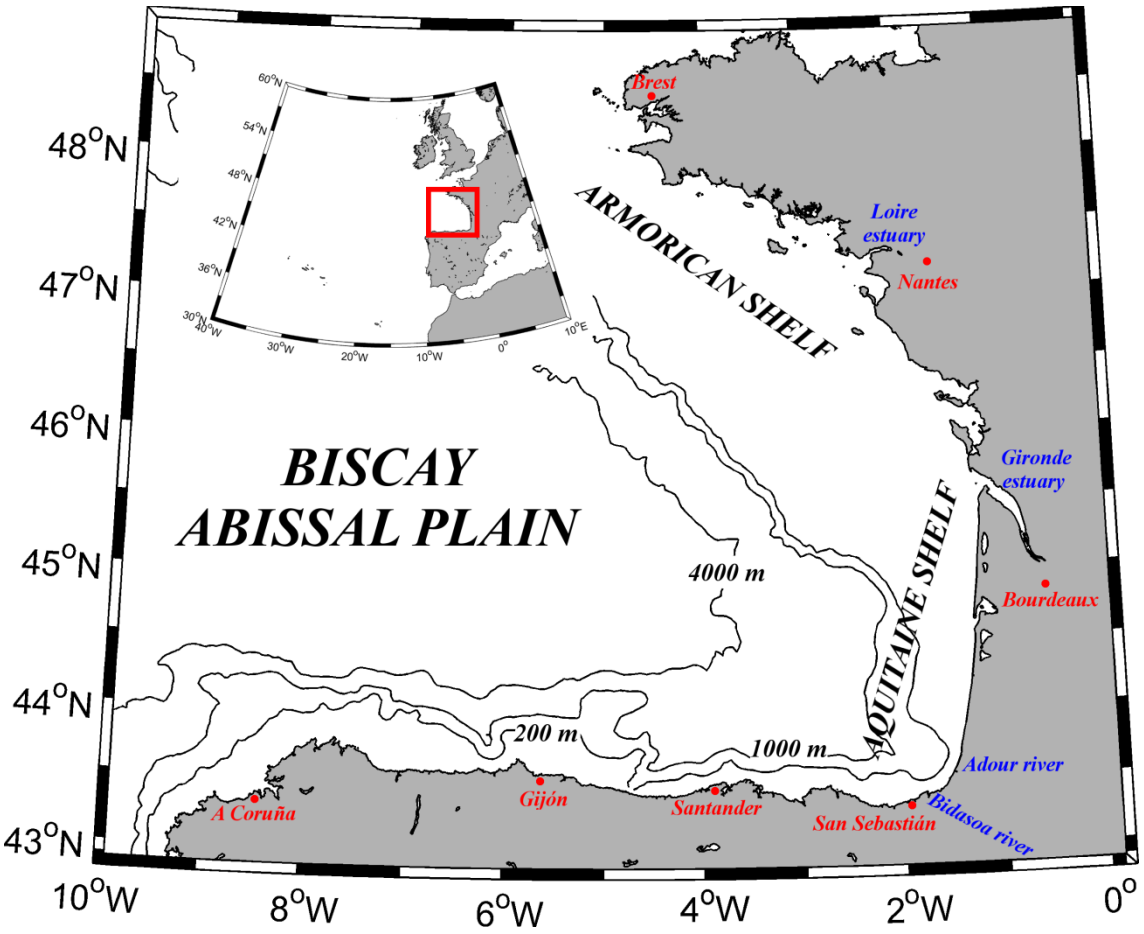

Figure 1.3. Bathymetry of the Bay of Biscay. Contour lines represent 200, 1000 and 4000 m isobaths. Location of the Bay of Biscay (marked with a red square) in the upper left figure.

1.2.2 Freshwater inputs

The main rivers that drain into the bay are located along the French coast since rivers in the Cantabrian coast are small due to the proximity of the mountains to the sea. The major freshwater inputs affecting the area are provided by the discharge of Loire and Gironde Rivers (Puillat et al., 2004). These rivers provide 80% to the freshwater discharges onto the French shelf. The Loire River has a length of about 1020 km from Mont Gerbier de Jonc, in the Massif Central, to Nantes at St Nazaire. Its basin occupies about 117,000 km^2 with an annual mean flow of ~900 m^3s^{-1}. The highest river discharges occur in January and February with mean values that surpass 1500 m^3 s^{-1} (Figure 1.4). Gironde River (estuary) is formed by the contributions of Garonne and Dordogne Rivers. Garonne River has a length of ~ 600 km from Aran Valley, in the Pyrenees (Spain), to the Gironde Estuary, in Bec d'Ambès, north of Bordeaux. Its basin occupies about 61,000 km^2 with a mean flow of ~ 500 m^3s^{-1}. Dordogne River has a length of ~ 485 km from the Puy of Sancy, in the mountains of Auvergne, to the Gironde Estuary. Its basin occupies about 24,000 km^2 with a mean flow of ~ 250 m^3s^{-1}.

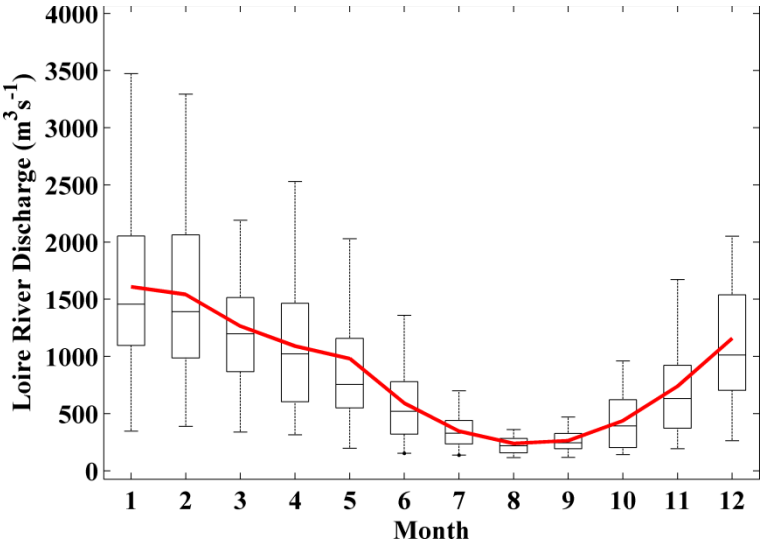

Figure 1.4. Annual hydrologic cycle variability (m^3s^{-1}) for Loire runoff over the period 1982-2014. Solid red line represents the monthly average flow and the line inside each box represents the median for each month. Lower and upper whiskers show minimum and maximum river flow, respective, whilst lower and upper box indicate first and third quartiles, respectively.

1.2.3 Circulation

The circulation in the Bay of Biscay is influenced by bathymetric conditions commented previously. Overall, it is possible to distinguish three different circulation patterns. The oceanic area of the bay is part of the North Atlantic open ocean circulation. This area is characterized by a weak (1-2 cm s^{-1}) and variable anticyclonic circulation at depths of around 400 m (Saunders, 1982; Pingree, 1993; Koutsikopoulos and Le Cann, 1996). Along the slope, circulation becomes cyclonic, giving rise to a poleward current (5-10 cm s^{-1}) that shows seasonal variations (Pingree and Le Cann, 1992; Garcia-Soto et al., 2002; Garcia-Soto and Pingree, 2012). Currents over the continental shelf are seasonally dependent because they are explained as a combination of wind-driven, tidally induced and density-driven flows (Charria et al., 2013; Pingree and Le Cann, 1989). Figure 1.5 summarizes the main hydrographic features in the Bay of Biscay.

Although the previous paragraph describes the general circulation, the location of the bay in an intergyre zone favors high seasonal variability in the circulation at mesoscale due to interactions between atmosphere and sea surface. In this way, the slope current that flows eastward North of Spain (Iberian Poleward Current, IPC) and poleward along the Aquitaine and Armorican slopes shows its maximum intensity during autumn and winter. IPC transports warm and saline water along the west coast of the Iberian Peninsula and usually reach the Cantabrian slope around Christmas (for this reason is also called “Navidad”) (García-Soto et al., 2002; deCastro et al., 2011a). In summer, circulation along the slope turns equatorward (Charria et al., 2013; Le Boyer et al., 2013). A similar process occurs along the French shelves since a poleward circulation prevails from October to March, whilst weak equatorward currents are

observed during spring and summer. This fact is related to the prevalence of southwesterly winds during autumn and winter and northwesterly winds from April to September in this region (Puillat et al., 2004; 2006). In addition, along the French continental shelf, freshwater input during winter and spring plays an important role inducing density gradients that favor poleward circulation (Lazure and Jégou, 1998). Regarding the Cantabrian shelf, winter eastward current is replaced by a westward flow with velocities reaching 13.5 cm s^{-1} during summer (Charria et al., 2013). Another important feature during winter is the presence of eddies, which are formed in the continental slope due to the interaction between the slope current and topography. These structures have been named "SWODDIES" (Slope Water Oceanic Eddies) by Pingree and Le Cann (1992) and its movements has been studied using satellite images (Bardey et al., 1999; García-Soto et al., 2002) and floats (van Aken, 2002; Huthnance et al., 2002). In summary, the basin represents a complex mix between open ocean features and local processes.

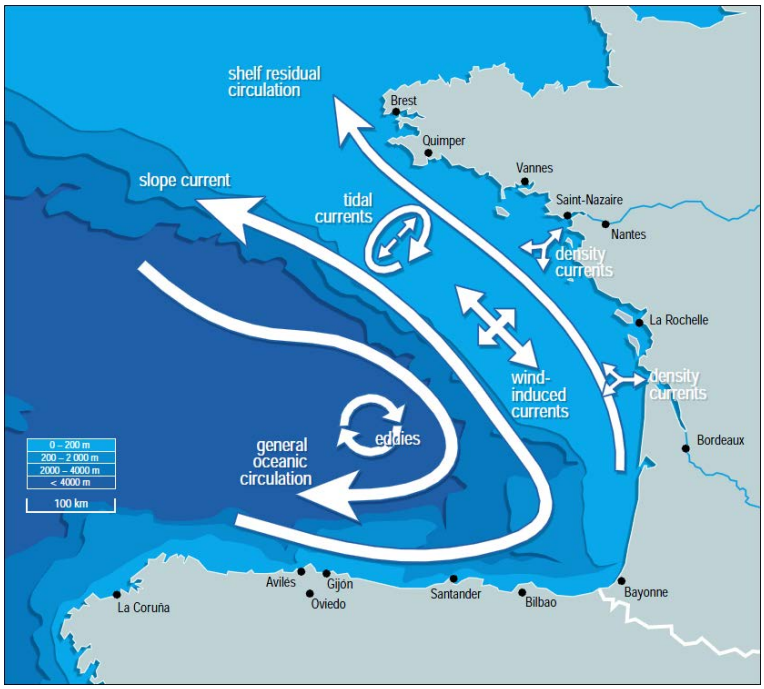

Figure 1.5. Schematic illustration of circulation in the Bay of Biscay. Source: Reproduced from Koutsikopoulos and Le Cann (1996) modified by OSPAR Commission (2000).

1.2.4 Water masses

In this section water masses present in the Bay of Biscay will be characterized from up to down of the water column. First of all, it is important to notice that the depth at which a water mass spreads and its thermohaline properties varies depending on the region (Figure 1.6). For this reason the same water mass can be defined by a different depth or density range depending on the area (e.g: Harvey, 1982, Valencia et al., 2004).

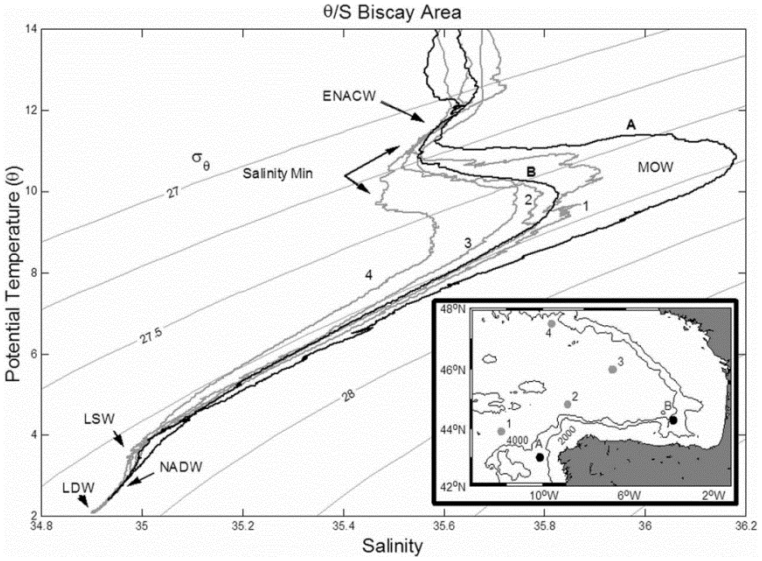

Figure 1.6. Diagram that summarizes the thermohaline properties of the water masses present in the Bay of Biscay in six hydrographic stations (its position can be seen in the small plot on the bottom right). Superimposed lines in the diagram represent isopycnals (kg m−3) Source: Lavín et al. (2006), it was produced with data from ICES and IEO databank.

The Bay of Biscay is located at mid latitudes in the intergyre zone of the North Atlantic (Figure 1.7). Thus, the southerly branch of the subpolar current and the northerly stream of the subtropical Azores current converge at the latitude where the Bay of Biscay is located (Ríos et al., 1992; Pollard et al., 1996). This peculiarity defines the Eastern North Atlantic Water Mass (ENACW), which occupies the upper waters. ENACW develops each year as a result of winter mixing in an area ranging from northeast Azores to the European margin (Pollard and Pu, 1985; Pollard et al., 1996). The fact that the Bay of Biscay is located in an inter-gyre region, influenced by subpolar and subtropical Atlantic gyres, allows defining two subtypes of ENACW: the subpolar (ENACWsp) and the subtropical (ENACWst) modes (Fraga et al., 1982; Pérez et al., 2000). The limit between them was established at 12.20 ºC and 35.66 by Ríos et al. (1992). ENACW characteristics become progressively modified with increasing distance from their area of formation (Pollard and Pu, 1985). Overall, the OSPAR commission (2000) established that ENACW spreads in the first 600 m in the Bay of Biscay in a potential temperature range between 10.5 and 11.5 ºC and a salinity range between 35.55 and 35.60 giving as result a potential density range between 27.15 and 27.25 kg m^{-3}. However, other studies defined ENACW in a wider density range (27.0-27.2 kg m^{-3}), in accordance with studies such as Botas et al. (1989) who established that ENACW ranges from 11-13 ºC and 35.53-35.74. Pollard et al. (1996) located the core of ENACW at around 350 m depth with a mean density value of 27.1 kg m^{-3}. The different characteristics of ENACW depending on the region of the bay can be seen in Figure 1.6. This figure summarizes the main thermohaline characteristics of the water masses present at different locations in the Bay of Biscay and its surrounding area.

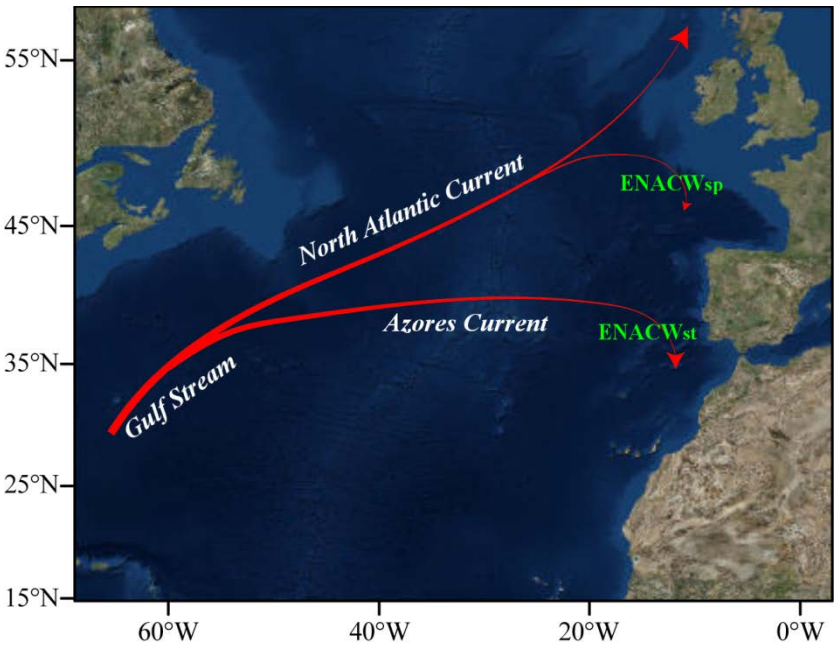

Figure 1.7. Surface circulation in the Northeastern Atlantic.

Below ENACW it spreads the Mediterranean Water (MW). This water body spreads at around 1000 m depth with a mean density range of 27.6-27.7 kg m^{-3}, which corresponds to a mean temperature of 9-10 ºC and a salinity value of 35.8 (Figure 1.6). MW results from the mixture of Mediterranean Outflow Water (MOW, Bozec et al., 2011) with the near-surface Atlantic water at the Strait of Gibraltar (Mauritzen et al., 2001). MW leaves the western Gulf of Cadiz separating in two branches. One branch spreads in the North Atlantic westward to the central Atlantic and the other one northward along the Western Iberian slope (Mazé et al., 1997) reaching the Bay of Biscay and influencing intermediate waters northward to the Rockall Trough (Iorga and Lozier, 1999; van Aken, 2000). MW, which is in its origin warmer and more saline than ENACW, can produce temperature inversions along the water column (Valencia et al., 2004). The salinity of the MW core decreases poleward along the continental slope due to isopycnal and diapycnal mixing with less saline waters (del Río et al., 1998, van Aken, 2000; Lavín et al., 2006).

Deeper than the MW it is located the North Atlantic Deep Water (NADW), which is the result of a complex mixture of waters (Valencia et al., 2004; Lavín et al., 2006). The sources are Labrador Sea Water (LSW), Norwegian Sea Water (NSW) and Antarctic Bottom Water (AABW). The core of LSW, located at 1800 m, is characterized by a deep salinity minimum, especially in the northern and western part of the bay. In the Biscay Abyssal Plain the influence of the AABW is higher in the NADW (Valencia et al., 2004).

1.2.5 Thermal balance and mixed layer

Temperature in the upper levels of the water column in the Bay of Biscay is highly influenced by air temperature. In this way, high correlations were found between air temperature and SST in different areas of the bay (e.g: Borja et al., 2000; Fontán et al., 2008). So, heat fluxes between the ocean and the atmosphere are the main responsible for the seasonal SST cycle. The Bay of Biscay is a region of weak net heat flux since it is located at midlatitude in a region of transition between areas where the ocean gains heat at the south and areas that loss heat north of the bay (Michel et al., 2009a). Figure 1.8 represents the annual cycle of radiative (shortwave and longwave) and turbulent (sensible and latent) heat fluxes averaged for the whole bay. The annual cycle is characterized by its dependence on the shortwave flux, which is the unique parameter that represents a gain of heat (positive sign) by the ocean. This heat flux attains it maximum in June, however is during August when the highest mean SST (~ 19.5 ºC) is observed in the bay due to the high heat capacity of the sea. The range of change of turbulent and longwave heat fluxes is clearly lower but it is enough to compensate the heat gain by the ocean from October to March (Figure 1.8). Michel et al. (2009b) quantified the heat budget in the 0-200 m layer in the Bay of Biscay and its surrounding area by means of an ocean circulation model. The main heat input come from the transport across the western boundary related to current that cross the Atlantic from the Gulf Stream. In addition, these investigators quantified the contribution of atmospheric flux, diffusion process and total transport to the thermal balance in the first 200 m for the whole bay. They found that air-sea flux in conjunction with oceanic transport are the main drivers of temperature interannual variations, whilst diffusion has its importance along the French coast south to Brest.

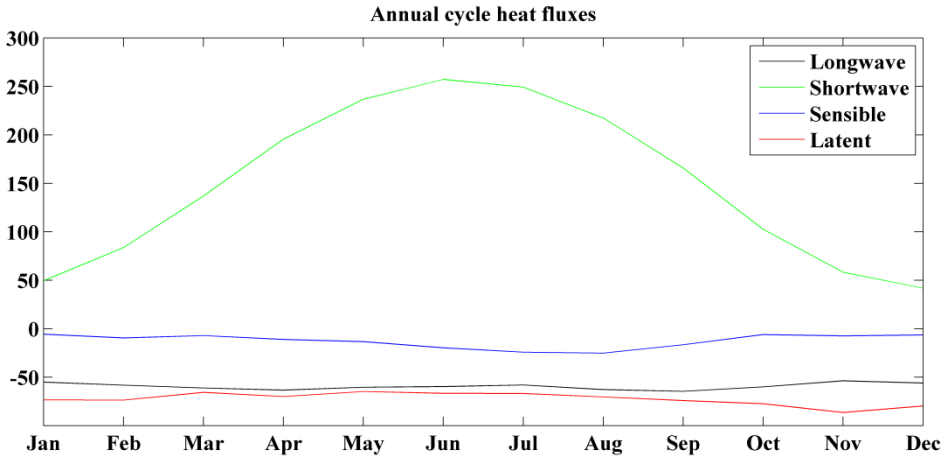

Figure 1.8. Annual cycle of the heat fluxes averaged for the whole Bay of Biscay (W m^{-2} per decade) over the period 1982-2014. Data retrieved from the Climate Forecast System Reanalysis database.

Heat fluxes play a key role to explain mixing and stratification processes. Overall, the upper ocean remains stratified since May to October and the mixing of the water column persists from November to April coinciding with months when the ocean losses

heat. Previous studies focus on the analyses of mixed layer in the Bay of Biscay are scarce and do not cover the whole bay. González-Pola et al. (2007) developed a method for characterizing the upper ocean structure and they applied it to profiles from a linear section sampled off Santander. They found that the mixed layer depth do not surpasses the 200 dbar level. Hartman et al. (2014) using the algorithm developed by González-Pola et al. (2007) with data from Argo floats found maximum MLD reaching 476 m during the cold winter in 2009/2010. Somavilla et al. (2011) use data from the same section combined with a one dimensional water column model (GOTM) and data from NCEP/NCAR reanalysis over the period 1948–2008 to analyze MLD variability. They found that during 1970s and 1980s, MLDs were strikingly shallower than from 1995 onwards. In addition, Somavilla et al. (2009) studied the consequences in the hydrographic structure of an extreme mixing event that occurred during winter of 2005.

1.2.6 River plumes and upwelling events

Atmospheric forcing also plays a key role to explain some mesoscale processes along the coast of the bay, such as river plumes or upwelling. Several studies about river plumes have been conducted in the Bay of Biscay by means of numerical models (Lazure and Jegou, 1998), in situ data (Kelly-Gerreyn et al., 2006; González-Nuevo and Nogueira, 2014), satellite imagery (Petus et al., 2010; 2014), or by combining several of these methods (Ferrer et al., 2009). As it was previously commented, Loire and Gironde are the two largest rivers in the bay. Turbid plumes generated by both rivers can merge forming a great plume under high discharge conditions due to the synchronism of both rivers (Koutsikopoulos and Le Cann, 1996; Lazure and Jegou, 1998). Although Loire and Gironde plumes are usually oriented to the NW due to Coriolis effect, the development of both plumes depends mainly on the variability of river runoff and winds (Lazure and Jegou, 1998). Winds over the French continental shelf are characterized by a marked interannual variability. Thus, southwesterly winds prevails from October to March and northwesterly winds from April to September (Puillat et al., 2004; 2006). In addition, surface circulation is also important since it affects the plume displacement. Currents over the shelf are conditioned by wind, density gradients and tides (Pingree and Le Cann, 1989). Overall, a poleward circulation prevails during winter in this area (Charria et al., 2013), contributing to the NW orientation of plumes. Freshwater discharges give as results a cooler strip in the area occupied by the turbid plume during winter. In addition, thermal inversions are often observed due to the haline stratification (e.g: Koutsikopoulos and Le Can, 1996). River discharges along the French coast has it signal when sea surface salinity is analyzed (Figure 1.9). Salinity values are higher than 35 over most of the bay. However, salinity reduces along the French continental shelf, especially close to Gironde, Loire and Adour estuaries (values around 30). The movement and the effect of low salinity structures were studied in detail over the Aquitaine shelf by Reverdin et al. (2013).

Easterly winds in the Cantabrian coast produce upwelling during spring and summer. In this way, different upwelling episodes have been described in the western part of the southern Bay of Biscay (Fraga, 1981; Botas et al., 1990; Lavín et al., 1998; Llope et al., 2006; Borja et al., 2008; Álvarez et al., 2010). Regarding the French coast, northerly winds can generate upwelling episodes in the southern part, whilst northwesterlies winds are favorable to upwelling along the Brittany coast (Froidefond et al., 1996; Puillat et al., 2003). The magnitude and the persistence of upwelling events are lower when compared to upwelling intensity along close areas, such as the western part of the Iberian Peninsula (Álvarez et al., 2011). The importance of upwelling in these areas is that upwelled water is cooler than the surrounding surface water and it represents a nutrient supply during the period of water column stratification (later spring and summer).

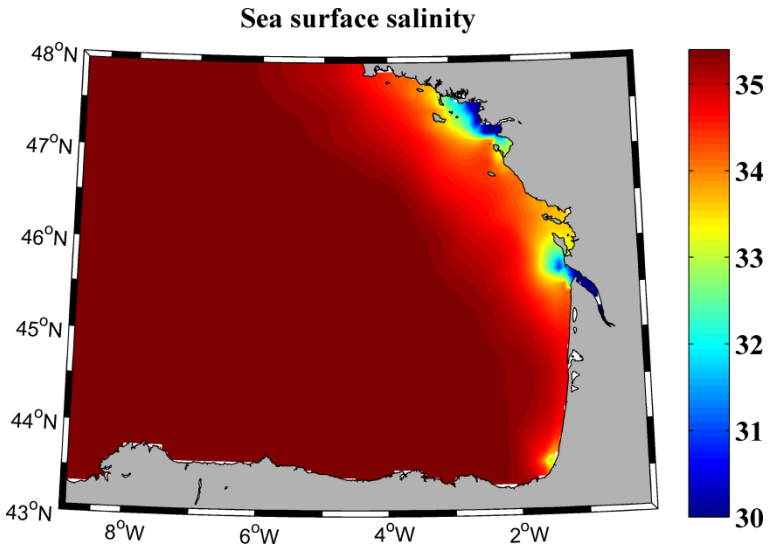

Figure 1.9. Sea surface salinity averaged over the period 2003-2011. Data retrieved from the Physical IBI reanalysis product (Copernicus project, http://marine.copernicus.eu/)

1.2.7 Physical changes

The variable that has received more attention related to physical changes in the Bay of Biscay is the SST. In this way, deCastro et al. (2009) carried out a long-term analysis of SST trend for the whole bay since 1867. They detected a warming-cooling cycle with cooling periods between 1867-1910 and 1945-1974 (-0.14 ºC per decade and -0.10 ºC per decade, respectively) and warming between 1910-1945 and 1974-2007 (0.17 ºC per decade and 0.22 ºC per decade, respectively). Similar results were obtained by Goikoetxea et al. (2009) by means of data from the Aquarium of San Sebastian. deCastro et al. (2009) also analyzed SST trends from 1985-2006. They observed a warming ranging between 0.15-0.45 ºC per decade depending on the area. Thus, the highest warming was detected in the northwestern part and along the French coast, whilst the lowest were found in the southwestern part. Moreover, they found the highest

increase in SST during spring and summer. Other authors that analyzed SST trends for the whole Bay of Biscay, considering also its surrounding area, were Michel et al. (2009a;b). Michel et al. (2009a) notified a warming trend ranging from 0.22ºC to 0.37ºC per decade using simulations and satellite data over the period 1985 to 2003. Michel et al. (2009b) also detected spatial and temporal variations of the warming rate. They noticed the highest warming over the northern part of the bay (roughly 0.5ºC per decade) and they also found the highest SST trends in summer and spring over the period 1986-2005. However, Koutsikopoulos et al. (1998) noticed a SST increase of about 0.64ºC per decade during the period 1972-1993 mainly due to mild winters than to warm summers.

As far as we know, the above studies are the unique that analyzed SST trends for the whole Bay of Biscay. Most of the studies were focused on a certain region and carried out with data from punctual sampling or taking into account only coastal areas. Thus, Gómez-Gesteira et al. (2008) analyzed SST trends along the entire coast of the bay by means of satellite-derived data. They found a warming both along the Cantabrian coast (0.21 ºC per decade) and along the French coast (0.27 ºC per decade). Several studies have analyzed SST trends with data from the Aquarium of San Sebastian (Usabiaga et al., 2004; Fontán et al., 2008; Goikoetxea et al., 2009; González et al., 2013). Goikoetxea et al. (2009) detected a cooling tendency over the period 1947-1977 and a warming from 1977 to 2007. In addition, Fontán et al. (2008) and Goikoetxea et al. (2009) found a change in the classical seasonal cycle ("deseasonality") that was cause by the prevalence of long warm summers and cold winters. Llope et al. (2006) noticed a warming over the period 1993-2003 with data from a punctual sampling in the central Cantabrian Sea (43º 36'). Planque et al. (2003) analyzed SST trends by means of Meteo-France data over the period 1971-1998 and they detected a maximum warming rate in the southeastern area of the bay (~0.5 ºC per decade). It is important to take into account that the southeastern corner of the bay is a region with a high continental influence. So, SST tends to be higher during summer (Valencia et al., 2004).

With regard to the changes observed in water masses, several studies have shown that the temperature and salinity characteristic of ENACW vary interannually. Pérez et al. (1995), (2000) observed a persistent freshening of salinity until 1990 and a subsequently salinity increase in the 1990's by means of data from several oceanographic cruises carried out in the North Atlantic in the eighties and at the beginning of the nineties. High salinity values were detected at the beginning of the 1970s and minimum values were measured during the 1980s. From 1991 to 1993 a sudden change in ENACW was detected with an abrupt increase in salinity. González-Pola et al. (2005) obtained a warming trend in ENACW on the order of 0.3 ºC per decade over the period 1992–2003 using stations located at the southeastern part of the Bay of Biscay. In addition, Llope et al. (2006) measured a decreasing salinity in the southern Bay of Biscay for a similar period of time (1993–2003). González-Pola et al. (2005) also noticed a warming and a salinification of the upper MW (700-1000 dbars).

Michel et al. (2009a) also studied temperature trends along the water column although they did not link them to changes in water masses. They observed a decreasing in the warming rate with increasing depth by means of data from the World Ocean Database and ORCA simulations in the Bay of Biscay and its surrounding area over the period 1965-2003. In this way, they detected a warming up to 500 m and a cooling between 500-600 m.

The atmospheric forcing over different physical processes has been analyzed by means of the teleconexion patterns that influenced the bay. The North Atlantic Oscillation (NAO) is the dominant mode of atmospheric interannual variability in the North Atlantic (Hurrel, 1995). However, the Bay of Biscay is located between two regions with different wind and precipitation responses to NAO (Pérez et al., 2000). García-Soto et al. (2002) found a negative correlation between November-December NAO index and January SST in the southern Bay of Biscay only during years with a marked presence of the Iberian Poleward Current. This fact was related to a relaxing of the northeasterly wind stress that favors a penetration of this current in the bay. García-Soto and Pingree (2012) found that the westerly winds, which favors the entrance of the IPC in the bay, prevails during negative NAO. However, Llope et al. (2006) did not found correlations between NAO index and the IPC. Planque et al. (2003) related NAO with SST, scalar wind and river run-off. They did not find clear correlations during the 1990s. However, significant but weak relationships were found between NAO index and SST and river runoff when they analyzed the period 1850-2000. The second most important atmospheric pattern in the North Atlantic is the East Atlantic (EA) pattern. According to Borja et al. (2008), southwesterly (northeasterly) winds prevail during positive (negative) EA phases over the Bay of Biscay. A negative EA phase prevails from 1950 to 1976 and a positive phase occurred from 1977 on (NOAA, 2008). Thus, Goikoetxea et al. (2009) related the SST trends detected in San Sebastian (cooling over the period 1947-1977 and warming from 1977 to 2007) with these cycles of EA. Moreover, EA pattern was related to ocean-atmosphere heat fluxes (Cayan, 1992) and winter SST (Sáenz et al., 2011) over the southern part of the bay.

The biological implications of physical changes have been highlighted in several studies. Fisheries, such as anchovy (*Engraulis encrasicolus*), sardine (*Sardina pilchardus*), mackerel (*Scomber scombrus*), horse mackerel (*Trachurus trachurus*) or albacore (*Thunnus alalunga*) represent an important economic activity in the bay (MEECE, 2013). Temperature plays a key role in the life cycle of marine species (e.g: Selig et al., 2010). Thus, changes in the SST can cause changes in biodiversity both at the ecosystem level (e.g. latitudinal shifts in species distributions) and at the population level due to changes in phenological events (e.g. reproductive period, larval season or migrations) (Giménez, 2011). Lavín et al. (2007) analyzed the influence of SST and winds on horse mackerel and albacore dynamics. Albacore catches correlated positively with the wind component and horse mackerel recruitment was negatively correlated with SST. Quéro et al. (1998) studied the distribution of several species and they found

that warming has favored a northernmost distribution limits. The influence of river plumes and less saline lenses in anchovy and sardine spawning has been also analyzed by different authors (Motos et al., 1996; Planque et al., 2007; Bellier et al., 2007). The role of extreme events was also studied along the coast of the bay. Thus, for example, Wethey et al. (2011) studied changes in the biogeographic distribution of intertidal populations due to extreme events. Changes in the mixed layer depth plays an important role in determine the availability of nutrients. In this way, the onset of the stratification in March-early April has important biological implications since it develops phytoplankton blooms that can cover the whole bay (Lavín et al., 2006).

On the basis of the above, it can be concluded that the Bay of Biscay is an embayment with special characteristics that plays an important role in influencing oceanographic processes at mid-latitudes. Since the eighties, the number of analysis and studies has increased in the bay (see Borja and Collins (2009) for detailed information). Most of the studies that analyzed changes in physical processes (water masses, SST, salinity, circulation, mixed layer…) were carried out for a certain region of the bay and usually considering a short period of time. The main aim of this study is to describe changes in physical terms, in particular changes in thermohaline variables that have occurred during the last decades. The different studies that compound this thesis are characterized by analyzing the whole Bay of Biscay. For this purpose, an effort was done to account with some of the newest databases in order to ensure appropriate spatial and temporal resolutions. The content of the subsequent chapters of this study is the following:

- Oceanic and atmospheric databases used to carry out this study will be described in detail in **Chapter 2**. In addition, information about the teleconexion patterns (NAO and EA) and the Atlantic Multidecadal Oscillation (AMO), which is the main oceanographic mode in the area under scope, will be included.

- A complete analysis of thermohaline changes detected in ENACW (upper 700 m of the water column) will be carried out in **Chapter 3** by means of reanalysis data. These changes will be related to atmospheric forcings in the Northeastern Atlantic.

- Thermohaline variations in intermediate water masses (ENACW and MW) will be analysed in **Chapter 4** by means of in-situ data provided by Argo floats. In addition, the methodology developed by Bindoff and McDougal (1994) will be applied in order to know the origin of the changes.

- Trends in the mixed layer depth will be studied using different criterions since 1975 in **Chapter 5**. Thus, an iso-thermal layer depth (TLD) and an iso-pycnal

layer depth (PLD) will be defined. The influence of atmospheric forcings will be analyzed.

- Changes in the seasonality of the bay during the last three decades will be analyzed in **Chapter 6**. In addition, variations in the duration of the warm season and trends in the number of extreme hot SST days will be also studied.

- The influence of Loire and Gironde River discharges over the sea surface temperature will be studied in **Chapter 7** by means of MODIS and $OISST_{1/4}$ databases.

Chapter 2: Databases

The main features of databases used to carry out this thesis are shown in this chapter. The choice of each one was based on the purpose of each study and on an attempt to use the most recent databases. Thus, in-situ data from Argo floats or satellite data from MODIS, both projects started during the past decade, were used. In the same way, recent reanalysis products such as Daily ¼ Optimum Interpolation SST or Climate Forecast System Reanalysis were also selected due to its high spatial and temporal resolution and because they provide data for the last decades. So, data with a different origin (in-situ, satellite or reanalysis) were combined to achieve the goals of this thesis.

2.1. Ocean database

2.1.1 Argo floats

The Argo Project (Argo Science Team, 2001) began as a collaboration between different countries with the aim of creating a global array of floats in order to sample the upper layers of the ocean all over the world. Under this project, floats were deployed starting in 2000, with deployments increasing every year. Thus, more than 3800 active floats were operating all over the world in 2015. In this way, most of the goals that the Argo Project had when it was designed, such as a global resolution of 3° × 3°, were reached. More than 100,000 in-situ profiles are produced each year. Overall, profiles reach a maximum depth between 1500 and 2000m, being their resolution higher in the first layers. The accuracy of pressure, temperature and salinity measurements is ±2.4 dbar, ±0.005 °C and ±0.01, respectively (Argo Science Team, 2001).

Argo floats drift following oceanic currents. In general, each float is designed to generate a profile every 10 days. The process to obtain a new profile begins with the descent of the buoy to a depth of 1000 meters, where it remains during 9 days. Then, it descends to a depth of 2000 meters and initiates the ascent to surface measuring temperature and salinity (Figure 2.1). Once on surface, data is transmitted, using satellite technology, to the Argo Global Data Assembly Centers located in France and EEUU. These centers are responsible for storing and processing data collected. Data used in this thesis were retrieved from the US Global Ocean Data Assimilation Experiments server (http://www.usgodae.org/argo/argo.html).

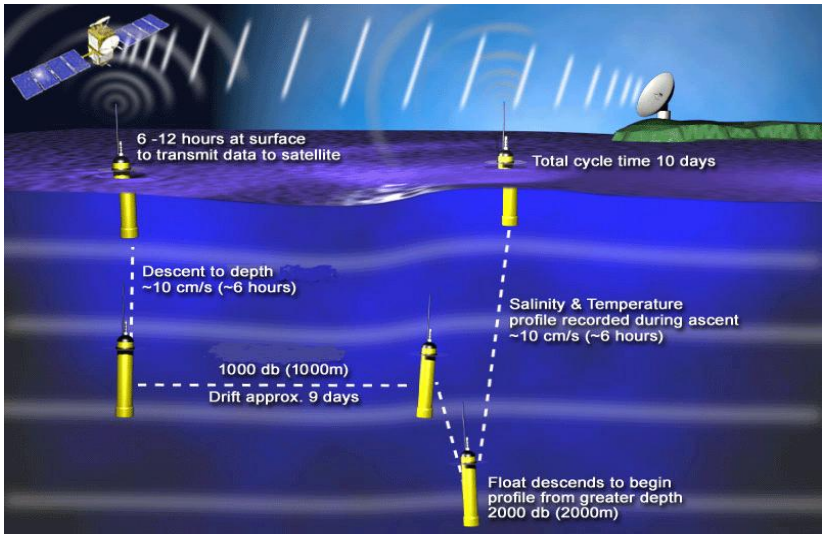

Figure 2.1. Process followed by an Argo float to generate each profile. Source: http://www.argo.ucsd.edu/.

All profiles in the Argo Project are labelled in function of the quality and accuracy of the data that it contains following the Argo quality control manual v2.8 (Wong et al., 2013) (http://www.argodatamgt.org/Documentation). Thus, only profiles with a control flag equal to 1 were selected. This control flag means that all Argo real time quality control tests, which are specified in the manual, were passed. These tests were applied to filter out spurious or inconsistent values outside of statistical limits. Additionally, other procedures were developed to prevent anomalous behavior in the floats and ensure a spatial distribution as homogeneous as possible. In this way, a visual inspection of each profile position and the trajectory of each buoy was carried out. Thus, buoys that had traveled a long distance over a short period of time, buoys with only a profile in the region of interest or buoys with multiple profiles at exactly the same location were discarded from the analysis. Moreover, only profiles with more than 20 valid measurements were considered.

2.1.2 Simple Ocean Database Assimilation (SODA)

Simple Ocean Database Assimilation (SODA) is a reanalysis database that offers several versions (Carton et al., 2005). Version 2.2.4 was selected to carry out different analysis in this thesis. It uses a model based on Parallel Ocean Program physics. Data used to create this database come from different sources. Temperature and salinity profiles were assimilated from the World Ocean Atlas-94 (MBTs, XBTs, CTDs and station data) (Levitus and Boyer, 1994), as well as additional hydrography, sea surface temperature (Reynolds and Smith, 1994) and altimeter sea level were assimilated from the Geosat, ERS-1 and TOPEX/Poseidon satellites. Detailed information about SODA product can be found in Carton et al. (2005) and Carton and Giese (2008).

Reanalysis of world ocean climate variability are available from 1958 to 2010 at monthly scale, with a horizontal spatial resolution of 0.5º x 0.5º and a vertical resolution of 40 levels, ranging from 5 m to more than 5000 m decreasing the resolution with depth. Data were downloaded from the website: http://sodaserver.tamu.edu/.

2.1.3 Daily ¼ Optimum Interpolation SST ($OISST_{1/4}$)

The ¼º daily Optimum Interpolation Sea Surface Temperature ($OISST_{1/4}$) database depends on the NOAA's National Centers for Environmental Information. Observations from satellites, ships and buoys were used to generate this database. Two products were developed using a special method of kriging (Optimum interpolation). On the one hand, one product only uses data from the Advanced Very High Resolution Radiometer (AVHRR) infrared satellite sensor (Figure 2.2). On the other hand, the other product uses AVHRR data and Advance Microwave Scanning Radiometer (AMSR) on the NASA Earth Observing System satellite SST data. In this thesis, only the AVHRR sensor data was used since AMSR data is only available since June 2002. The spatial resolution is 0.25º x 0.25º and it is available since 1982. Additional information on

Optimum Interpolation algorithm and its bias treatment can be found in Reynolds et al. (2007) and Reynolds (2009).

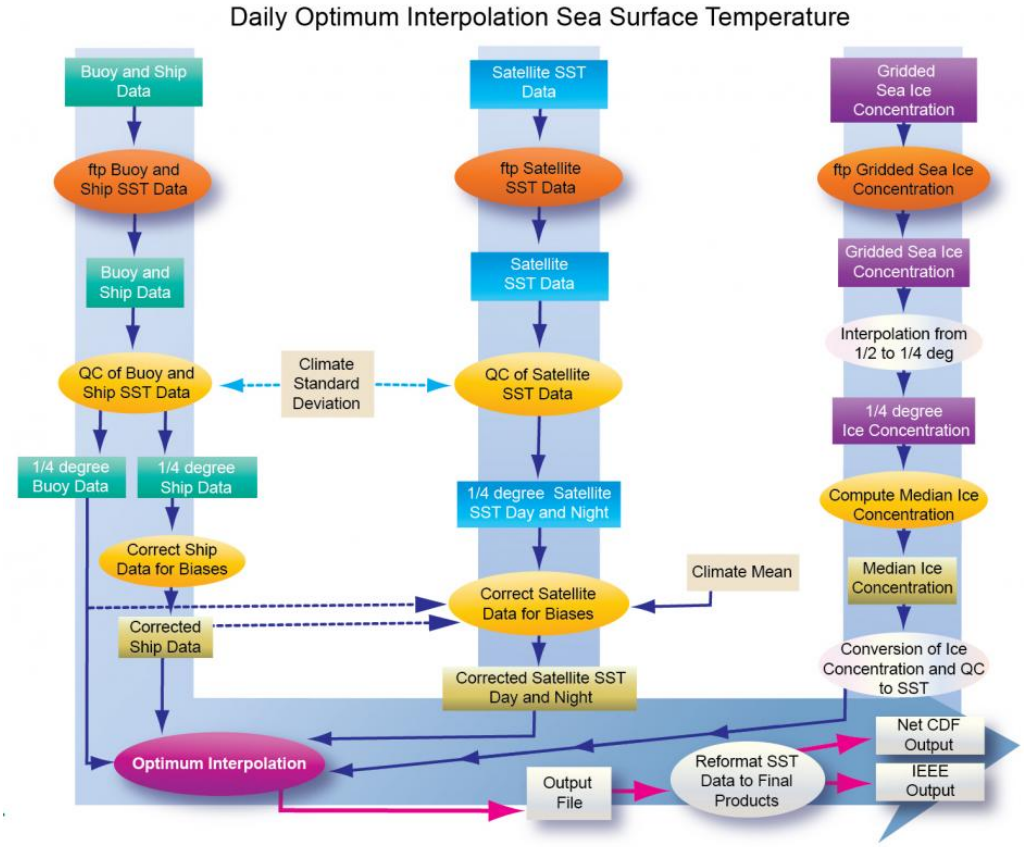

Figure 2.2. Flowchart followed to process the data contained in the OISST ¼.. Source: NOAA's National Centers for Environmental Information website.

2.1.4 Moderate Resolution Imaging Spectroradiometer (MODIS)

Moderate Resolution Imaging Spectroradiometer (MODIS) is a sensor located onboard Aqua and Terra satellites that provides information on several parameters. In general, Aqua satellite moves from south to north, passing over the Equator in the afternoon, whilst Terra satellite goes from north to south, passing over the Equator in the morning. The MODIS instrument provides high radiometric sensitivity in 36 spectral bands ranging in wavelength from 0.4 µm to 14.4 µm (NASA, 2015). Two MODIS ocean products were used in this thesis: MODIS Sea Surface Temperature and MODIS Remote Sensing Reflectance. Both datasets were retrieved from the NASA Ocean Color web site (http://oceancolor.gsfc.nasa.gov).

Level 2 of MODIS Sea Surface Temperature was selected. It has a global coverage with a spatial resolution of 1-km and it contains a day and night measurement every 24 hours (detailed information about the algorithm used to construct this product can be found in Brown and Minnett (1999). SST data was obtained using 11-12 µm thermal IR infrared channels since these bands are located close to the maximum of the

Earth's emission and have larger bandwidth than other available channels (Reinart and Reinhold, 2008). This SST product has been shown to be suitable to analyze water surface temperatures in previous studies (Barré et al., 2006; Chavula et al., 2009).

MODIS Remote Sensing Reflectance product allows selecting several values of normalized water-leaving radiance (nLw). The 645 nm band was selected since it fits best to the purpose of this study. Nighttime SST images and daytime nLw 645 from MODIS-Aqua and MODIS-terra were merged following Mendes et al. (2014). Thus, a larger number of available pixels were obtained increasing the consistency of the data.

2.2 Atmospheric database

2.2.1 National Center for Environmental Prediction/National Center of Atmospheric Research (NCEP/NCAR) Reanalysis

Meteorological large-scale reanalysis data was obtained from the NCEP/NCAR reanalysis database that was developed by the Physical Sciences Division (PSD) of the NOAA. A wide variety of weather observations (ships, planes, RAOBS, station data, satellite observations…) were assimilated to create this database (Kalnay et al., 1996). Data are supplied on a T62 Gaussian grid corresponding to a 1.9º both in latitude and longitude and monthly time resolution from 1948 on. Data of four variables (air temperature, precipitation, latent heat flux and wind speed above sea surface) were extracted from the PSD website (http://www.esrl.noaa.gov/psd/data/gridded/reanalysis/). Air temperature was considered at 2 m from surface, while wind was regarded at 10 m.

2.2.2 Climate Forecast System Reanalysis (CFSR)

The Climate Forecast System Reanalysis (CFSR) is a global, high-resolution, coupled atmosphere-ocean-land surface-sea ice system (Saha et al., 2010). It was developed by NOAA's National Centers for Environmental Prediction. CFSR includes many variables and, in general, it provides a 0.3º×0.3º and a 6 hour spatial and time resolutions from 1979 on. A second version was developed beginning on 2011. Although it can be considered as a seamless extension, it includes some improvements such as a better spatial resolution (from 0.3º to 0.2º) of surface and flux fields. Data from two variables (wind and heat fluxes) were extracted from the website http://rda.ucar.edu/pub/cfsr.html.

Table 2.1 summarizes the main properties of the oceanographic and atmospheric databases used to carry out this thesis:

	DATABASE	VARIABLE	SPATIAL RESOLUTION	TEMPORAL RESOLUTION
OCEANOGRAPHIC	*Argo*	ST & Salinity	Free drift (Up to 2000m depth)	From 2002 on (10-days values)
	SODA	ST & Salinity	0.5°x0.5° (Up to 5000m depth)	From 1958 on (Monthly values)
	OISST$_{1/4}$	SST	0.25°x0.25° (Surface values)	From 1982 on (Daily values)
	MODIS	SST & Reflectance	0.01°x0.01° (Surface values)	From 2002 on (Daily values)
ATMOSPHERIC	*NCEP/NCAR*	Wind, T^{air}, Latent heat flux & Precipitation	1.91°x1.91°	From 1948 on (Monthly values)
	CFSR	Wind & Heat fluxes	0.3°x0.3°	From 1979 on (6-hour values)

Table 2.1. Oceanographic and atmospheric databases used in this thesis.

2.3. Oceanographic modes

2.3.1 Atlantic Multidecadal Oscillation (AMO)

The Atlantic Multidecadal Oscillation (AMO) is a mode of natural variability that has its main expression in the North Atlantic SST. The duration of its cycle ranges between 35 to 80 years depending on the author (Timmermann, 1998; Kerr, 2000; Dima and Lohmann, 2007). Several studies have shown the global and regional influence of AMO (e.g: Polyakov and Johnson, 2000; Chylek et al., 2006; 2014, Muller et al., 2013; Kawada et al., 2013). AMO index is calculated as the average of SST anomaly in the Atlantic north of equator (Enfield et al., 2001). Monthly unsmoothed series from 1948 on are available in the NOAA website (http://www.esrl.noaa.gov/psd/data/timeseries/AMO/). Negative anomalies prevailed

from mid-1960s to mid-1990s, whilst positive anomalies predominated from mid-1990s on (Figure 2.3).

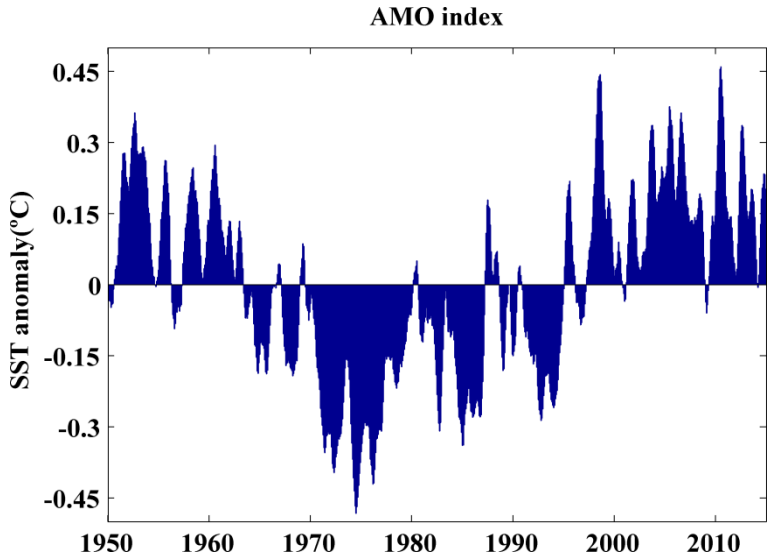

Figure 2.3. Monthly values for the AMO index over the period 1950-2014 (A ± 1 month running average was considered).

2.4 Atmospheric modes

2.4.1 North Atlantic Oscillation (NAO)

NAO is the most prominent teleconnection pattern that influences the North Atlantic (Barnston and Livezey, 1987). Thompson and Wallace (1998) described the NAO as the local manifestation of a global pattern called the Arctic Oscillation (AO) which is the result of the coupling between the stratospheric polar vortex and tropospheric circulation in the Northern Hemisphere. In a later study, Thompson and Wallace (2000) found that the variation in the North Hemispheric polar vortex is stronger in wintertime, and that is the season when the correlation with NAO is stronger. NAO consists of a north-south dipole with one center located over Greenland and the other over a region spanning between 35-40ºN. This index is calculated as the difference in geopotencial anomalies between both centers. Monthly NAO index, which is available since 1950, was extracted from the Climate Prediction Center at the National Center of Environmental Prediction (http://www.cpc.noaa.gov).

Although NAO shows its influence in all seasons it is higher during winter. Positive phase of NAO is associated with a reinforcement of the two centers cited above, whilst the negative phase is related to a weakening of them. The persistence of positive or negative phases generates basin-wide changes in the location and intensity of the North Atlantic jet stream and storm track during winter, which in turn influences

changes in temperature and precipitation patterns from eastern North America to western and central Europe (Hurrell, 1995). Thus, strong positive phase results in an

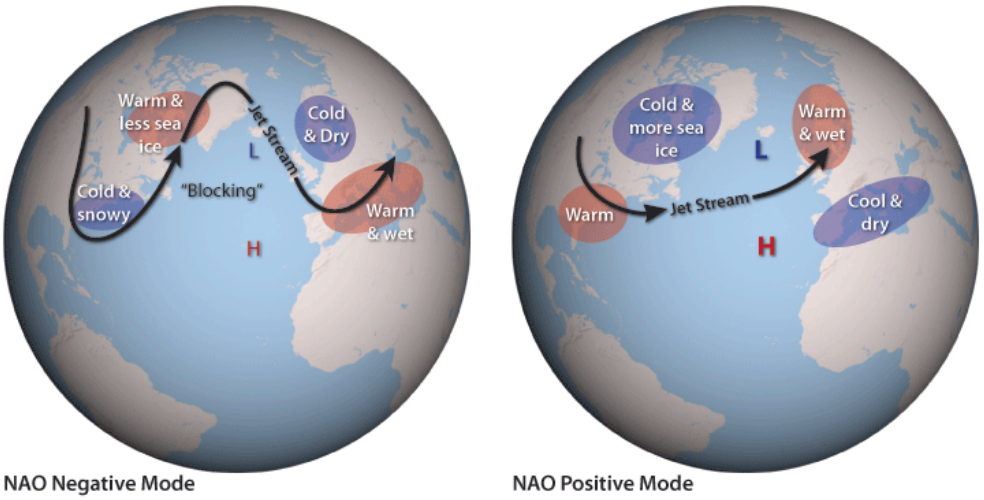

Figure 2.4. Effects of the positive and negative phases of NAO over the North Atlantic. Source: www.climate.gov.

increase in frequency and strength of winter storms crossing the Atlantic Ocean. This fact tend to be associated with an increase in temperature and precipitation over Greenland and also in the south of Europe, whilst colder and drier conditions occur in the East Coast of America and over northern Europe and Scandinavia. The opposite pattern occur during strong negative phases (Figure 2.4)

2.4.2 East Atlantic pattern (EA)

EA is the second teleconnection pattern with a higher influence over the North Atlantic. It is structurally similar to NAO but with its center displaced southeastward

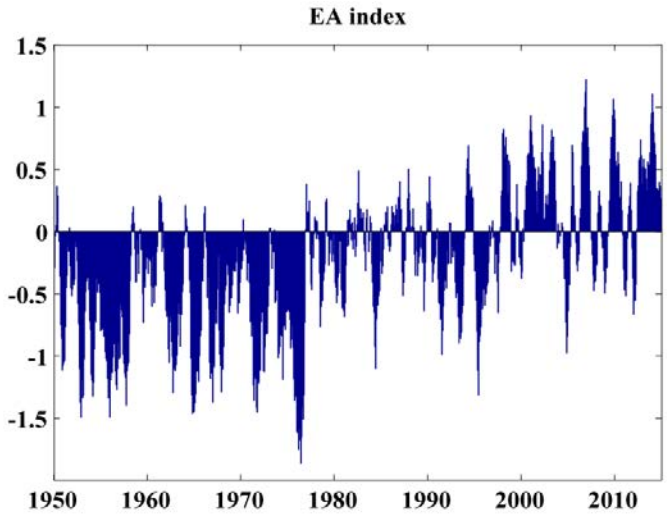

Figure 2.5. Monthly values for the EA index over the period 1950-2014 (A ± 1 month running average was considered).

(55ºN, 20–35ºW and 25–35ºN, 0–10ºW) covering the North Atlantic from west to east (Barnston and Livezey, 1987). The main difference with NAO is that the lower-latitude center is related to a strong subtropical link in association with modulations in the subtropical ridge intensity and location. The positive phase is associated with above-average temperature in Europe for all months and with negative anomalies of temperature in the southern United States during January-May and in the north-central United States during July-October. Regarding precipitation, positive values are related with above-average values over northern Europe and Scandinavia and with below-average values across southern Europe. Negative values of EA index clearly prevailed from 1950 to 1980, whilst positive values dominated from mid-1990s on (Figure 2.5).

Chapter 3: Eastern North Atlantic Central Water variability by means of reanalysis data

The aim of this chapter is to analyze thermohaline changes in the Eastern North Atlantic Central Water (ENACW) mass in the Bay of Biscay over the period 1975-2010. The dependence of these changes on teleconnection patterns (NAO and EA) will be also studied. In addition, temperature and salinity changes in ENACW will be correlated with air temperature and precipitation minus evaporation (P-E) trends in the Northeastern Atlantic in order to know the dependence on variations that occur outside the Bay of Biscay.

3.1 Methods

Temperature and salinity data was obtained from SODA database from 1975 to 2010. This time period corresponds to the strongest warming period detected in the North Atlantic area (Koutsikopoulos et al., 1998; García-Soto et al., 2002; Gómez-Gesteira et al., 2008; deCastro et al., 2009; Gómez-Gesteira et al., 2011). The area selected ranges from 0 to 7.25ºW and from 43.25º to 47.75ºN (Figure 3.1). The first 21 vertical levels from near surface (5 m) to the upper permanent thermocline depth (700 m) were considered. The thickness of vertical layers increases from 10 m near surface to 100 m below 300 m.

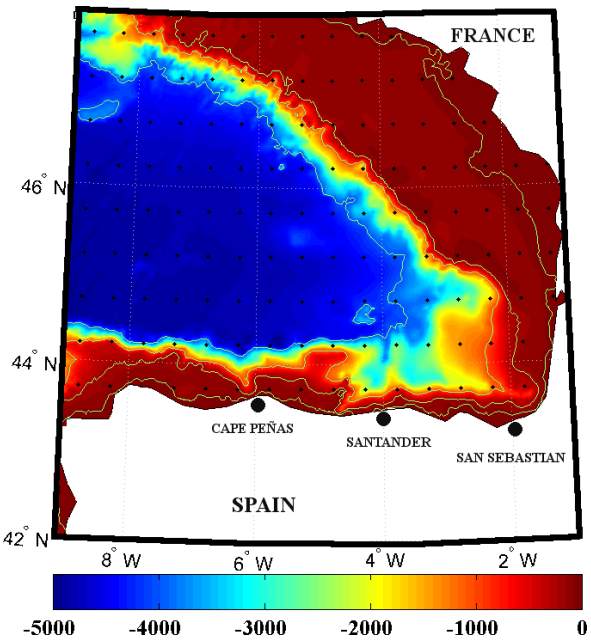

Figure 3.1. Bay of Biscay bathymetry. Dots represent the 0.5ºx0.5º grid of data. The marked isobaths corresponds to −50, −200, −1000 and −4000 m.

ENACW will be identified by means of salinity and temperature values that generate density values inside the interval 27.0–27.2 kg m^{-3}. First of all, the grid points where ENACW was rarely sampled (less than 800 valid samples) were discarded. Note that, working at monthly scale, the period under study contains 432 months and 21 vertical layers, which results in about 9000 samples per point. The imposed threshold (800 ENACW samples) corresponds to less than a 10% of the samples although the results were almost insensitive to changes in this threshold. Salinity and temperature data corresponding to each grid point were averaged to convert them into annual values. All salinity and temperature data corresponding to the density interval 27.0–27.2 kg m^{-3} for a certain year were averaged, no matter their layer, in order to obtain the value of the mean ENACW salinity and temperature for that year. The mean ENACW depth was calculated in the same way.

Long-term processes like warming–cooling or salinification–freshening and their implications in the water column stratification were analyzed at annual scale. First of all, the annual mean and standard deviation were calculated at every point. Then, the trends, which were assumed to be linear, were calculated. The regression procedure accounted for the standard deviations by using weighted least squares, with weights proportional to the inverse of the variance. First of all, annual values were calculated by the average of monthly values and then they were linearly fitted. All trends were calculated on raw mean data, without using any filter or running mean. The validity of the obtained trends was checked by imposing that the standard deviation was less than 25% of the absolute value of the trend.

Correlations between teleconnection patterns (NAO and EA) and annual salinity and temperature trends of ENACW were carried out by filtering the indices using a backward-looking 9-year Blackman window and a 1-year lag. This approach accounts for the memory of ocean circulation with regard to atmospheric patterns. It was previously used by Curry and McCartney (2001) and Johnson and Gruber (2007).

Air temperature, precipitation and latent heat flux were retrieved at a monthly scale from the NCEP/NCAR reanalysis data. Monthly air temperature was considered at 2 m from surface. Evaporation was calculated as the latent heat flux loss divided by the latent heat of water (2.5×10^6 J kg^{-1}) following González-Pola et al. (2005). The Spearman rank correlation coefficient was used to analyze the significance of trends and correlations due to its robustness to deviations from linearity and its resistance to the influence of outliers (Saunders and Lea, 2008).

3.2 Results and discussion

3.2.1 ENACW salinity and temperature trends

The vertical profiles of temperature and salinity trend were calculated considering the entire area under scope (0-7.25ºW // 43.25º-47.75ºN) over the period 1975-2010 (Figure 3.2). Figure 3.2a shows a significant (>95%) warming trend near surface and from 100 till 700 m deep. The warming rates range from values close to 0.11 ºC near surface to 0.04 ºC per decade at 700 m deep. Warming decreases quickly along the upper 100 m reaching values lower than 0.06 ºC per decade, then it increases till values close to 0.10 ºC per decade between 200 and 400 m and, finally, it decreases quasi-linearly till 700 m deep.

The surface warming trend observed is on the same order of magnitude as observed in previous studies carried out in the area (e.g. Koutsikopoulos et al. (1998): 0.64 ºC per decade for the period 1972–1993 with a grid based on vessels and buoys;

Planque et al. (2003): 0.6 ºC per decade in the southeastern corner using SST data from Meteo-France; Llope et al. (2006): 0.5 ºC per decade over the period 1993–2003 using the coefficients of an empirical model; Goikoetxea et al. (2009): 0.23 ºC per decade over the period 1977–2007 with data from the Aquarium of San Sebastian (south of Bay of Biscay); Gomez-Gesteira et al. (2008): 0.35 ºC per decade from 1985 to 2005 using satellite SST data and deCastro et al. (2009): 0.22 ºC per decade over the period 1974–2007 by means of extended reconstructed SST data). In addition, Michel et al. (2009), who used simulations (ORCA) and in situ (WOD) measurements, observed a similar vertical profile of temperature trends with warming rates ranging from 0.10 ºC per decade (ORCA) to 0.19 ºC per decade (WOD) near surface to −0.10 ºC per decade (ORCA) and −0.04 ºC per decade (WOD) at 600 m over the period 1965–2003. The warming tendency, observed throughout the water column, suggests that it is not only forced at surface by the air–sea interaction but also generated internally in the subsurface layers of the ocean. In fact, the quasi-linear decrease in the warming rate between 200 and 700 m deep suggests the existence of a warming trend for ENACW.

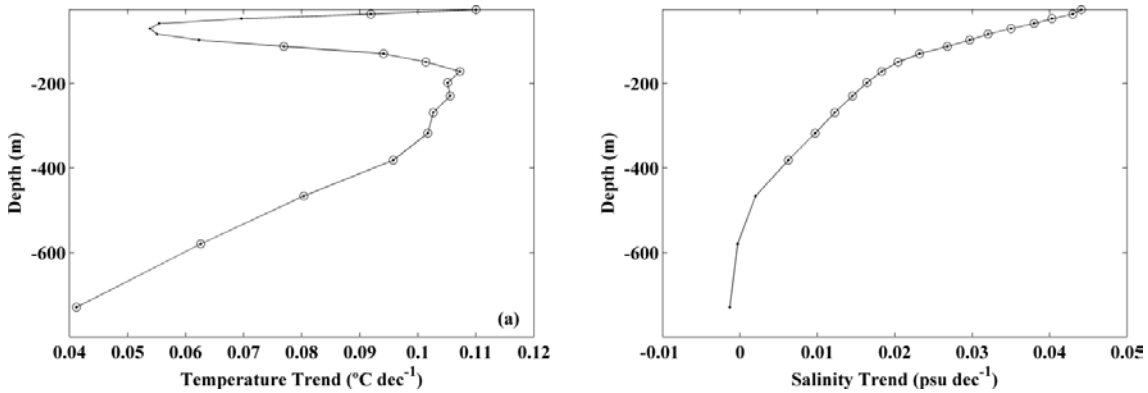

Figure 3.2. Vertical profile of (a) temperature trends (ºC per decade) and (b) salinity trends (per decade) for the entire Bay of Biscay from 1975 to 2010. Circles represent trends with a significance level greater than 95%.

A significant positive salinity trend is observed till 400 m deep (Figure 3.2b). The salinification rate decreases monotonically from 0.044 per decade near surface to null values at 600 m deep. Similar values were observed by Boyer et al. (2005) in the south of North Atlantic from 1955 to 1998. They found a linear salinification of 0.03 per decade till 100 m deep decreasing to 0.01 per decade at 200 m deep and reaching 0.005 per decade from 200 to 500 m deep.

As mentioned above, ENACW mass was identified by salinity and temperature values generating density values centered on 27.1 kg m^{-3}. The T–S diagram represented in Figure 3.3 shows the water masses present in the Bay of Biscay at a particular point (3.25°W, 44.75°N) from 1975 to 2010 at the upper 700 m. The points marked in gray lie inside the interval 27.0–27.2 kg m^{-3}. This T–S diagram is similar to the one described by González-Pola et al. (2005) near Santander (south of Bay of Biscay) from 1991 to 2003. A similar plot can be observed for most of the points inside the Bay.

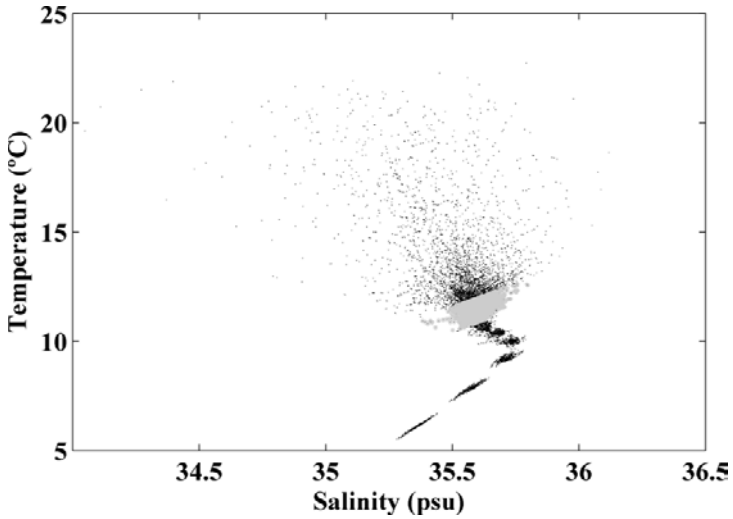

Figure 3.3. T-S diagram of the water masses present in the Bay of Biscay at 3.25ºW and 44.75ºN from 1975 to 2010 till a depth of 700m calculated using SODA database. ENACW is highlighted by means of gray dots.

The temperature and salinity trends corresponding to ENACW over the period 1975-2010 are depicted in Figure 3.4. Black dots represent the grid points where trends with a significance level higher 99% were obtained. The blanks observed on the French continental shelf, correspond to points where ENACW was scarcely detected for the period under study following the protocol described above. The temperature trend (Figure 3.4a) is positive for the entire area with maximum values around to 0.11 °C per decade in the central and northwestern part. In fact, the ENACW warming is negligible at the southwestern corner (values lower than 0.02 °C per decade) and small (around 0.08 °C per decade) along the southern coast of the Bay. A similar pattern is observed for the ENACW salinity trend (Figure 3.4b) with positive values in the entire area and with maximum values between 0.02 and 0.03 per decade in the central and northern part of the Bay. ENACW salinification is negligible at the southwestern corner of the Bay (close to 7.25°W).

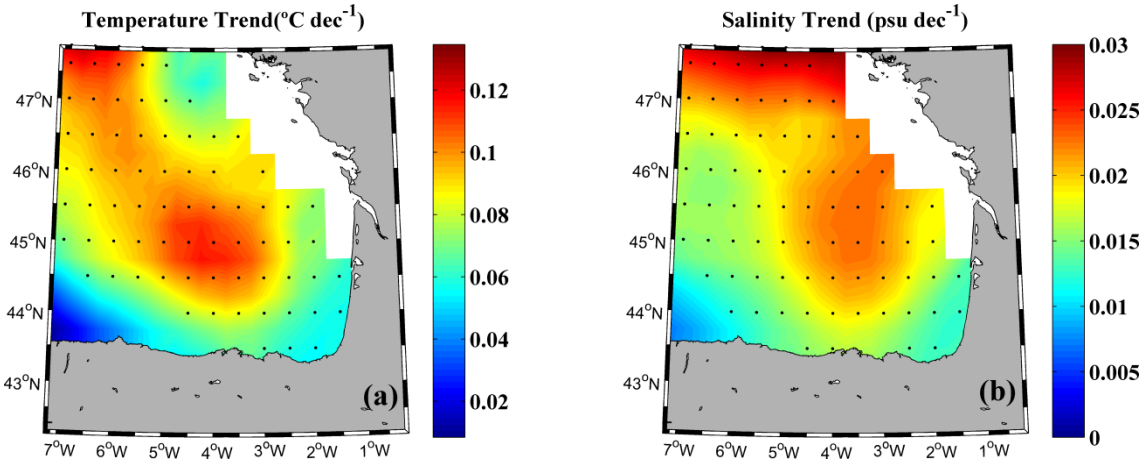

Figure 3.4. (a) Annual temperature trends (ºC per decade) and (b) annual salinity trends (per decade) corresponding to ENACW in the Bay of Biscay from 1975 to 2010. Black dots represent the grid points where trends with a significance level greater than 99%% were obtained. The blanks represent points where ENACW was scarcely detected.

Both temperature and salinity trends show warming and salinification of ENACW from 1975 to 2010 being more pronounced at the north-central part of the bay. These tendencies are not homogeneous in space, being more pronounced at the north-western part of the bay and almost negligible at the south-western part. Results can be compared to the local analysis carried out by González-Pola et al. (2005), who observed an intense ENACW warming ranging from 0.2 to 0.4 °C per decade from 1992 to 2003 at 200–500 db. They also indicate a moderate decrease in ENACW salinity at 200–500 db, which ranged from 0.01 to 0.02 per decade. Although there is a qualitative agreement in temperature, the salinity trends are opposite. This is possibly due to the different extent of both intervals. In fact, the salinity series showed by Llope et al. (2006) in the area close to Cape Peñas, about 150 km away from the area described by González-Pola et al. (2005), shows a clear oscillatory behavior, which cannot be accurately described by a linear fitting. There, small changes in the extent of the interval can lead to opposite trends.

Examining trends in salinity and temperature calculated in the Bay of Biscay, one can observe how the origin of the changes seems to be located outside the domain. In this way, the most intense trends in salinity and temperature are found in the middle part of the Bay although they are not exactly located at the same place. On the other hand, it is rather clear that trends are negligible and without statistical significance at the SW boundary. In addition, the maximum trends are observed at the northern boundary. Thus, it requires a wider context to determine how this ENACW (warmer and saltier) enters the Bay. The analysis previously described for Figure 3.4 was carried out for the North Atlantic area (0–22.25°W and 41.75–54.25°N) (Figure 3.5).

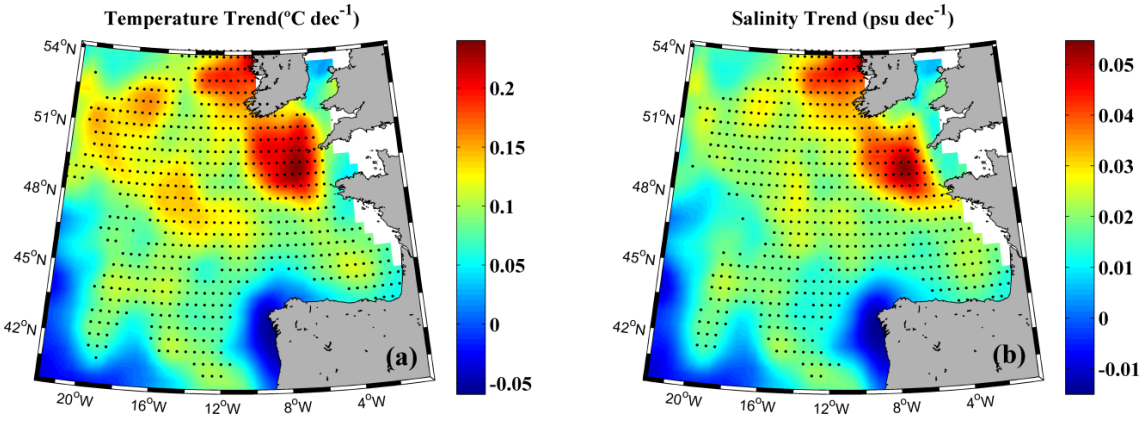

Figure 3.5. (a) Annual temperature trends (°C dec^{-1}) and (b) annual salinity trends (dec^{-1}) of ENACW mass in the North Atlantic area (0–22.25°W and 41.75–54.25°N) from 1975 to 2010. Black dots represent the grid points where trends with a significance level greater than 99% were obtained. The blanks represent points where ENACW was scarcely detected.

As in previous case, black dots represent the grid points where trends with a significance level of 99% were obtained and the blanks represent the grid points where

ENACW was scarcely detected. Significant positive trends were observed on the North Atlantic area influenced by the subpolar branch of ENACW ($ENACW_{sp}$). The maximum positive trends were detected both for temperature (~0.3 °C per decade; Figure 3.5a) and salinity (~0.05 per decade; Figure 3.5b) in the north Atlantic region characterized by deep winter mixing and cascading from the shelf (Pollard et al., 1996; van Aken, 2000; González-Pola et al., 2005).

The mean ENACW depth calculated over the North Atlantic area from 1975 to 2010 (Figure 3.6) ranges from −50 to −400 m. The minimum depth of ENACW (~ −50 m) was observed in the region characterized by deep winter mixing where salinification and warming are stronger. The maximum depth (>−350 m) was observed at the western part at latitudes between 42°N and 45° N. Note that the changes in ENACW observed at this area are negligible. The mean ENACW depth inside the Bay of Biscay ranges from −200 to −250 m, which is on the same order of magnitude than measured by other authors. Thus, for example, the depth found for ENACW by González-Pola et al. (2005) near Santander was on the order of 325–350 m analyzing the 27.1 and 27.2 kg m^{-3} isopycnals. Note that the region where the minimum ENACW depth is measured coincides with the area where the highest changes in ENACW are observed (Figure 3.5). This area is characterized by its shallowness and deep winter mixing and it is strongly affected by atmospheric forcing, in such a way that changes pass to the water column due to winter mixing and are advected from there to the rest of the area. Thus, salinity and temperature changes are mostly influenced by the atmospheric forcing at this area and not at the formation area (from northeast Azores to the European margin). This picture is consistent with research by González-Pola et al. (2005) who observed that climate anomalies at the subduction area of ENACW do not fully explain the salinity and temperature anomaly.

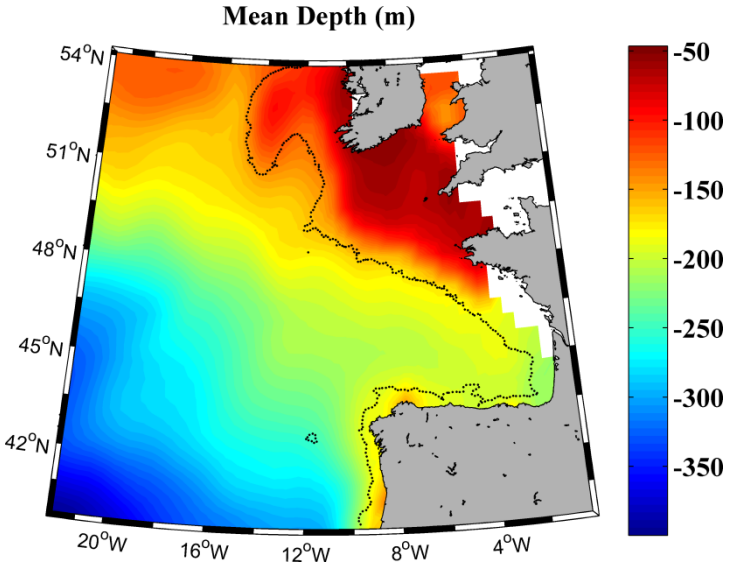

Figure 3.6. Mean depth of ENACW (m) in the North Atlantic area for the period 1975-2010. The blanks represent points where ENACW was scarcely detected. Dotted line represents the 500 m isobath.

3.2.2 Atmospheric modes influence on ENACW salinity and temperature trends

Decadal water mass variations in the Northern Hemisphere were described by Johnson and Gruber (2007) along 20° W. They related the observed changes to the 1995–1996 shift of the NAO (Halpert and Bell, 1997), which is the leading mode of variability in the area. Following this shift, the subpolar gyre retreated to the northwest, which gave rise to changes in the $ENACW_{sp}$, which became saltier and warmer. This fact was also mentioned by González-Pola et al. (2005) to put into context the warming observed in ENACW near Santander. In the present study, the annual salinity and temperature trends observed for ENACW were compared with the extended winter indices corresponding to the two main modes of atmospheric variability over the North Atlantic (NAO and EA). Previous researches carried out in the area under scope (deCastro et al., 2008a and deCastro et al., 2008b) had pointed out that more than a single atmospheric mode can be necessary to explain the ocean variability. In particular deCastro et al. (2008a) and deCastro et al. (2008b) showed that the EA mode was the main atmospheric forcing explaining upwelling. The spatial mean temperature (or salinity) in the North Atlantic region was calculated by averaging the grid points with trends significant at a level higher than 99% (see Figure 3.5). These spatial means were correlated with the lagged and filtered atmospheric indices as described in section 3.1. Figure 3.7a shows the time evolution of the three series: NAO for the extended winter (December-March) thick black line, temperature thin black line and salinity solid gray line, which were normalized to be represented together. Note that NAO increases till 1995 and decreases from then on, which is related to the NAO shift described in the literature (Halpert and Bell, 1997; González-Pola et al., 2005; Johnson and Gruber, 2007). The shaded areas highlight the different trends (positive and negative) observed for NAO index over the period 1975–2010. This contrasts with salinity and temperature series which increase all over the period. Thus, no significant correlations were obtained between salinity and NAO (R=0.14, p<0.4) or between temperature and NAO (R=0.07, p<0.7). The lack of dependence on NAO is in apparent contradiction with previous research carried in the Bay of Biscay. Michel et al. (2009) compared the anomalies in December NAO with temperature increase, obtaining a significant correlation. However, they focused on the year-to-year scale and they removed the linear trend in the signal, which can only be done when the series show a clear increasing or decreasing trend, but not in the case under study, where the NAO signal increased till 1995–1996 and decreased from then on. Other authors like Pérez et al. (2000) or Llope et al. (2006) compared salinity trends with the accumulated anomaly of NAO. This parameter is not the NAO signal itself and can be misleading due to the fact that it considers the whole previous history of the variable. We did not consider this accumulated variable in a long-term series like ours since it can impose unphysical memory effects, where indices from the beginning of the series can apparently have some influence on salinity and temperature several decades later. We have adopted the approach used by Johnson and Gruber (2007), who used a backward window that only considers the previous 9 years with decreasing weight. Finally, not all authors have

found significant correlation between NAO and salinity or temperature (see for example González-Pola et al., 2005).

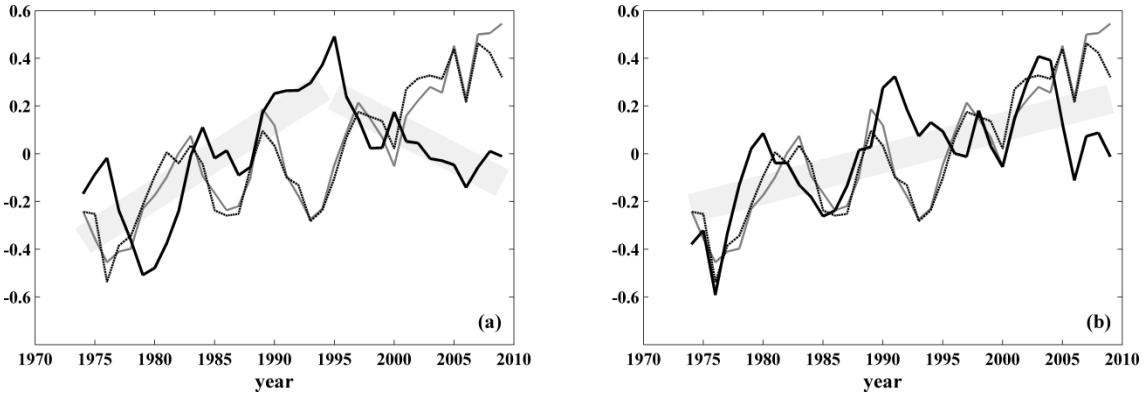

Figure 3.7. (a) Time evolution of temperature (black dotted line) and salinity (solid gray line) of ENACW and NAO index (black solid line) over the period 1975-2010. (b) Time evolution of temperature (black dotted line) and salinity (solid gray line) of ENACW and EA index (black solid line) over the period 1975-2010. The atmospheric indices were calculated for the extended winter (DJFM). Signals were normalized to be represented together. The mean temperature and salinity were calculated using only the grid points with significant trends (>99%) in Figure 3.5, respectively. Shaded areas represent the trends observed for NAO and EA indices.

Figure 3.7b shows the time evolution of the three series: EA thick black line, temperature thin black line and salinity solid gray line, which were normalized to be represented together. The shaded gray area represents the positive trend observed for the EA index over the period under study. A significant correlation was obtained between the EA index and salinity (R=0.52, p<0.01) and between EA and temperature (R=0.55, p<0.01). Thus, changes observed for salinity and temperature are consistent with the evolution of EA mode. This atmospheric mode had already shown to be the main atmospheric forcing in ocean variability over the area under study (deCastro et al., 2006, deCastro et al., 2008a, deCastro et al., 2008b and deCastro et al., 2011a). The positive phase of the EA is associated with below-average precipitation across southern Europe (Rodríguez-Puebla et al., 1998) and with above-average surface temperatures in Europe. In particular in the northern part of the Iberian Peninsula, the EA pattern is the most important variation pattern explaining temperature variability (Saenz et al., 2001).

3.2.3 Influence of atmospheric variables on ENACW variability

The variability of ENACW was also analyzed in terms of air temperature at 2 m (Figure 3.8). Dots represent annual air temperature trends with significance higher than 95%. The air temperature increases significantly in the whole area from 1975 to 2010 with maximum values (0.26 °C per decade) in the north-western corner of the domain and with the minimum warming, 0.14 °C per decade, at the southern part. Inside the Bay of Biscay, the air warming is around 0.16 °C per decade. The air temperature trend is consistent with ENACW temperature trends over the North Atlantic region shown in Figure 3.5a. The spatial mean of air temperature in the North Atlantic region was calculated by averaging the temperature series at the grid points with significant

(>95%). This mean air temperature was correlated with the ENACW temperature (Figure 3.7, thin black line), showing positive correlation (R=0.72, p<0.01) between both signals.

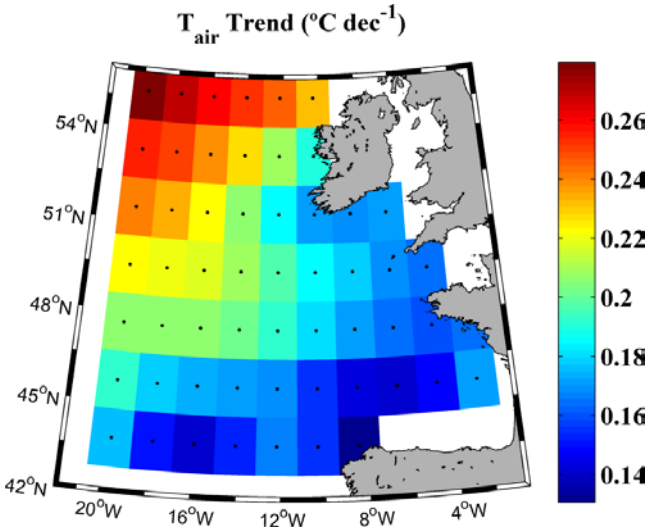

Figure 3.8. Air temperature trend (ºC per decade) calculated over the North Atlantic region from 1975 to 2010. Black dots represent the grid points with significant trends (>95%)

Trends of the balance between precipitation and evaporation (P−E) were also considered over the North Atlantic region (Figure 3.9). Dots represent $P-E$ trends with significance higher than 95%. In this case, significant negative trends (between −0.25 and −0.15 mm mo^{-1} per decade) were only observed in the eastern part of the region. The pattern of $P-E$ trends is consistent with ENACW salinification shown in Figure 3.5b. Once again, only the points with significant trends (>95%) in the $P-E$ balance were averaged over the North Atlantic area and correlated with ENACW salinity (Figure 3.7, solid gray line), showing negative correlation (R=−0.57, p<0.01) between both signals.

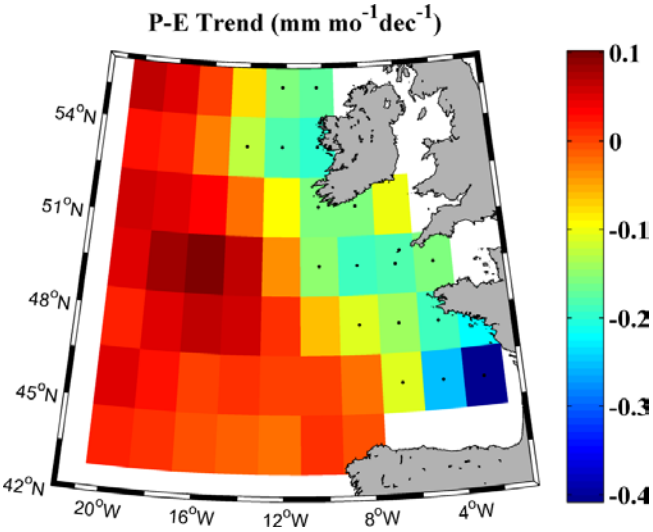

Figure 3.9. P-E (precipitation minus evaporation) balance trend (mm mo^{-1} per decade) calculated over the North Atlantic from 1975 to 2010. Black dots represent the grid points with significant trends (>95%)

3.3 Conclusions

Changes in ENACW have been observed in the Bay of Biscay over the period 1975-2010, coinciding with the last warming period in the North Atlantic. The main conclusions are summarized as follows:

- ENACW has been observed to warm and salinificate in most of the area at a maximum rate of 0.11ºC per decade and 0.03 per decade, respectively. These changes were more intense in the middle part of the Bay and at the northern boundary.

- Changes in ENACW are not locally generated inside the Bay. Actually, changes are especially significant at places influenced by $ENACW_{sp}$ mode over a wider region. The highest trends (0.3°C per decade in temperature and 0.05 per decade in salinity) were observed north of the bay, especially at the shallow area that stretches from Brest to Ireland, which is characterized by deep winter mixing.

- The increase in salinity and temperature is consistent with changes observed in the EA pattern, which also increases over the period under study.

- Salinity increase is consistent with changes in the P−E balance and temperature increase with warming in air temperature.

Chapter 4: Intermediate water masses variability by means of in-situ data

The aim of this chapter is to analyze the variability of ENACW and MW masses in the Bay of Biscay over the period 2004-2013 with in-situ data from Argo floats. The mechanisms controlling these changes will be analyzed using the model proposed by Bindoff and McDougall (1994). Thus, it is possible to establish if temperature and salinity changes are due to heat flux or freshwater flux variability in the water formation area or due to changes that occurred inside the Bay.

4.1 Methods

All available data from Argo database for the Bay of Biscay (43.5–48°N/350–359°E) were extracted from the US Global Ocean Data Assimilation Experiment (USGODAE) server (http://www.usgodae.org/argo/argo.html) for the decade 2004–2013. In this way, 3540 temperature and salinity profiles were obtained from 60 floats. All profiles were submitted to the quality control specified in section 2.1.1, which includes several steps. After this process, 3084 profiles from an initial set of 3540 were used. Therefore, less than 15% of the initial profiles were removed.

Figure 4.1 shows the time and spatial distribution of the 3084 good quality profiles selected. The recent onset of the Argo Program and the progressive deployment of Argo floats since 2002 reveal that the number of profiles for the first years of the Argo Program in the Bay of Biscay were limited. In fact, there were no profiles in February 2004. However, the number of profiles increased since mid-2004, reaching a maximum in 2008 and a progressive reduction from then on (Figure 4.1a). Regarding the spatial distribution, Figure 4.1b shows how the bay is well covered since more than 20 profiles have been generated for most of the pixels over the period under study. The number of profiles is higher in the central part of the bay although there are no marked spatial differences.

Profiles were vertically interpolated, following a linear interpolation, in 50 pressure levels with a resolution that decreases with depth. Thus, a pressure level every 10 dbar was established for the first 100 m, every 25 dbar for depths ranging from 100 to 600 m and every 50 dbar for depths from 600 to 1200 m. Potential temperature and density values were calculated to avoid pressure problems with depth following the method described in UNESCO (1983). The Spearman rank correlation coefficient was used to analyze the significance of trends due to its robustness to deviations from linearity and its resistance to the influence of outliers. Trends were calculated using monthly anomalies and were assumed to be linear. Moreover, all trends were calculated using raw data without any filter or running mean.

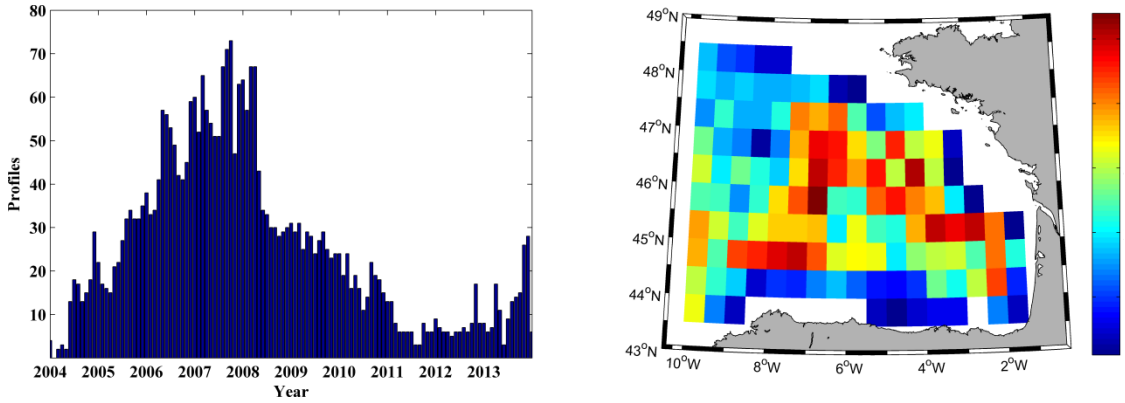

Figure 4.1. (a) Number of profiles for each month. (b) Number of profiles for each pixel on a 0.5° × 0.5° grid covering the Bay of Biscay.

To carry out this analysis a different approach from the one used in Chapter 3 was selected to identify the water masses. This approach follows the procedure described in Soto-Navarro et al. (2012). These authors also used Argo floats to analyzed changes in ENACW and MW in the western area of the Iberian Peninsula. They divided the upper 1200m of the water column in three water types: Surface water (SW, 0-100 dbar), ENACW (100-600 dbar) and MW (600-1200 dbar). These three types of water can be identified in the T–S diagram, which was obtained averaging all monthly profiles available for the Bay of Biscay over the period 2004–2013 (Figure 4.2). This diagram is similar to the one obtained by Soto-Navarro et al. (2012) for the Atlantic water and by González-Pola et al. (2005) for the southern part of the Bay of Biscay. It can be observed that most of the measures for ENACW (100-600 dbar) are in a potential density range between 27.0-27.2 kg m^{-3}, whilst MW measures (600-1200 dbar) are in a potential density range between 27.25-27.7 kg m^{-3}. These results are in good agreement with previous studies in the region (Boucher, 1985; Botas et al., 1989) and also with the information about water masses provided by the OSPAR Commission (2000) in the Bay of Biscay.

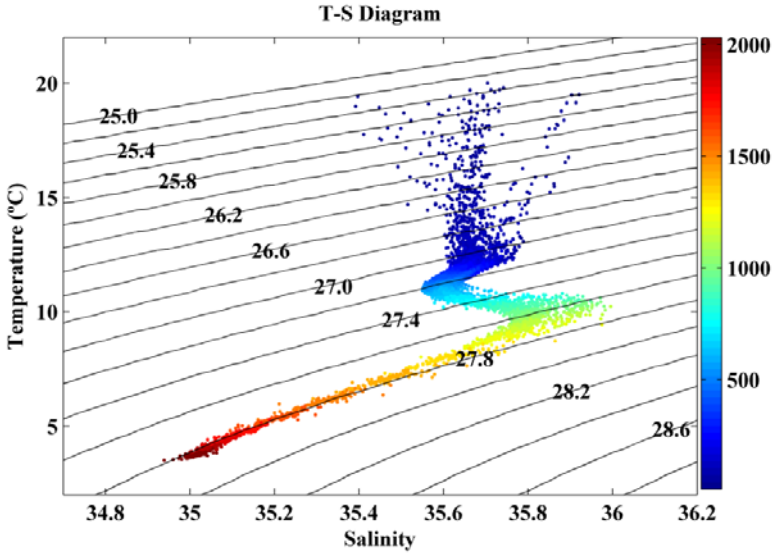

Figure 4.2. T–S diagram of all monthly profiles averaged for the whole area over the period 2004–2013. Superimposed lines in the diagram represent isopycnals (kg m^{-3}). Colors indicate the depth at which each T–S point was sampled.

Temperature and salinity changes along the water column can be interpreted using the model proposed by Bindoff and McDougall (1994). According to their methodology it is possible to know if changes in a scalar property detected along isobars are due to changes on isopycnals or vertical displacements of isopycnals. Changes on isopycnals are related to heat flux variability (pure warming) and freshwater flux variability (pure freshening) in the water formation area (Arbic and Owens, 2001; Jackett and McDougall, 1997). On the other hand, vertical displacements of isopycnals are related to the process that Bindoff and McDougall (1994) define as pure heaving. This process results in water masses sinking or floating without changing their intrinsic properties. These displacements are interpreted as wind stress variability or changes in the water

formation rates. Following the work developed by Bindoff and McDougall (1994), temporal changes of potential temperature and salinity along isobars can be decomposed through Eq. (1) for small displacements.

$$\left.\frac{d\varepsilon}{dt}\right|_p = \left.\frac{d\varepsilon}{dt}\right|_n - \left.\frac{dp}{dt}\right|_n \left(\frac{\delta\varepsilon}{\delta p}\right) \quad (1)$$

The left term accounts for a time variation of a scalar property (potential temperature or salinity) along isobars. The first term on the right-hand side accounts for the time variation of the scalar property along isopycnals. The latter term refers to the vertical displacement of isopycnals, taking in account the rate of change of isopycnal displacement and the vertical gradient of the scalar property. Vertical gradients of temperature are assumed to be constant in time.

4.2 Results and discussion

4.2.1 Water masses temperature and salinity trends

The results achieved by monthly averaging temperature and salinity profiles for SW, ENACW and MW for the whole area are shown in Figure 4.3. Over the upper 100 m (SW) the seasonal cycle is clearly reflected for temperature with values ranging from 11.5 °C to 16.5 °C (Figure 4.3a, green line). Salinity (Figure 4.3a, blue line) shows low values in 2007 (around 35.6) and a maximum peak in 2011 (around 35.8). Unlike temperature, no seasonal cycle was observed for salinity. Regarding ENACW (100–600 m), temperature ranges from 11.3 °C to 11.8 °C, while salinity shows values slightly higher over the period 2010–2012 (Figure 4.3b). MW shows temperature and salinity above average for 2004, 2005, 2011 and 2013 (Fig. 4.3c).

Temperature and salinity trends were calculated for each type of water (Table 4.1). All trends have a significance level higher than 95%, except the temperature trend for SW. Salinity shows a positive trend of 0.06 dec^{-1} for the first 100 m. This salinity trend is opposite to that detected for the upper 100 m by Llope et al. (2006) during the decade 1993–2003 in a sampling carried out close to Cape Peñas. They detected an important freshening for this layer, with values higher than 0.1 dec^{-1}. However, the salinity trend obtained in Chapter 3, which is around 0.08 dec^{-1} over the period 1975–2010 for the whole bay, is closer to the one observed in the present study.

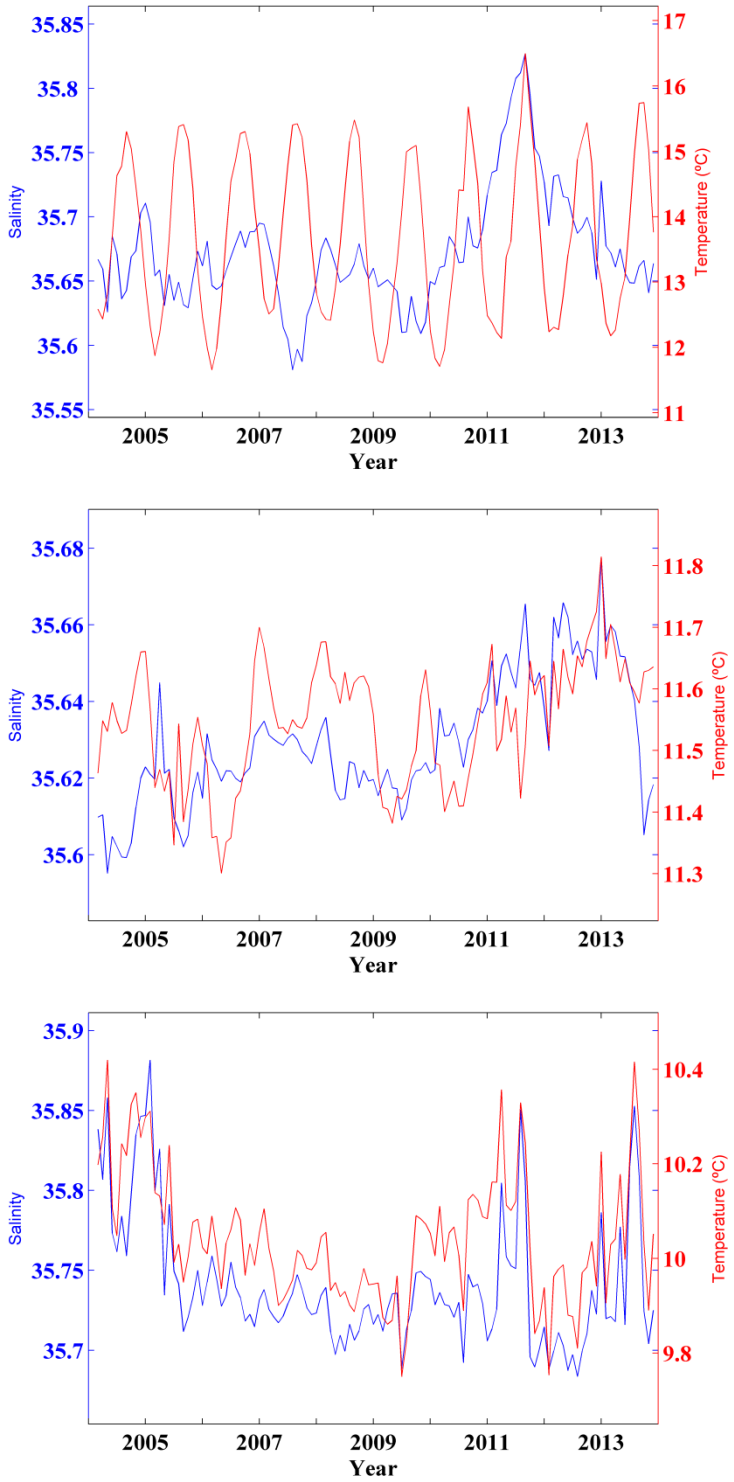

Figure 4.3. Temperature (red line) and salinity (blue line) variability for: (a) SW, (b) ENACW and (c) MW in the Bay of Biscay for the period 2004–2013.

A salinity increase (0.04 per decade) was observed for ENACW (Table 4.1). This salinity trend has a different sign when compared to the one obtained by González-Pola et al. (2005) for the southeastern Bay of Biscay during the previous decade (1993-2003). They found a freshening at 200-500 db ranging from 0.01 to 0.02 per decade. A

warming trend (0.32 ºC per decade) was found for ENACW by González-Pola et al. (2005), which is clearly higher than the one detected in our study (0.12 ºC per decade) for the decade 2004-2013 (Table 4.1). It is important to keep in mind the different spatial coverage of both studies, specially taking in account that different trends were found both for temperature and salinity depending on the region of the Bay of Biscay, as it was highlighted in the previous Chapter. It was observed that ENACW warms and salinificate in most of the bay at a rate of 0.05-0.11 ºC per decade and 0.01-0.03 per decade, respectively over the period 1975-2010. Therefore, the warming rate detected for the decade 2004-2013 is higher than noticed over the period 1975-2010, which is considered to be the strongest warming period in the North Atlantic (García-Soto et al., 2002; Intergovernmental Panel on Climate Change (IPCC), 2007; Gómez-Gesteira et al., 2008; deCastro et al., 2009; Gómez-Gesteira et al., 2011). On the other hand, ENACW seems to have suffered a higher salinification over the last decade compared to the results noticed in Chapter 3.

	T^a Trend (°C per decade)	***S Trend (per decade)***
SW	-0.05	0.06*
ENACW	0.12*	0.04*
MW	-0.11*	-0.05*

Table 4.1. Estimated linear trends for the Bay of Biscay over the decade 2004-2013. SW (0-100m), ENACW (100-600m), MW (600-1200m). The asterisk means a significance level higher than 95%.

The same water bodies were analyzed using Argo floats by Soto-Navarro et al. (2012) at the west of the Iberian Peninsula (38-42ºN, 24-8ºW), close to the Bay of Biscay, for the period 2002-2010. They found a warming (0.2 ºC per decade) and salinity (0.05 per decade) increase in ENACW. Although they noticed a higher warming, these trends agree with the results obtained for the Bay of Biscay. In addition, Soto-Navarro et al. (2012) found a higher salinity increase in SW (0.1 per decade) although they did not find any significant trend for temperature. They hypothesized that the increasing salinity detected in both SW and ENACW could be caused by an enhancement of the freshwater evaporative losses.

MW cooling and freshening was observed from 2004 to 2013, with a temperature trend of -0.11 ºC per decade and a salinity trend of -0.05 per decade (Table 4.1). Negative salinity and temperature trends were also detected for the MW by Soto-Navarro et al. (2012) at the west of the Iberian Peninsula over the period 2006-2010. These negative trends were preceded by warming and salinification from 2002 to 2006, which results in no significant trends for the MW when the whole period (2002-2010) is considered. Even, when their period 2006-2010 is considered, trends along the western Iberian Peninsula (-2 ±0.4 ºC per decade for temperature and -0.5±0.2 per decade for salinity) are not comparable with the ones observed in this study for the Bay of Biscay. In the case of Soto-Navarro et al. (2012) the periods with significant trends are much

shorter (just 4-5 years). The same authors did not find significant trends both in salinity and temperature in other close areas in the Eastern North Atlantic: zone 2 covering the Gulf of Cádiz and zone 3 covering the Canary region. Finally, as occurred for ENACW, opposite trends were found both for temperature (0.17 ºC per decade) and salinity (0.05 per decade) when compared with results obtained by González-Pola et al. (2005) at the southern Bay of Biscay. Once again, it is important to note that in this case the analysis was carried out at a single location inside the bay and that the period under study (1992-2003) does not overlap with the one considered in the present study (2004-2013).

4.2.2 Mechanisms controlling intermediate water masses variability

In order to know the mechanism that controls the changes detected along isobars the model proposed by Bindoff and McDougall (1994) was applied. Thus, the three components of the previously mentioned Eq. (1) were calculated and represented (Figure 4.4).

Temperature changes measured along isobars (Figure 4.4a, red line) do not show a clear positive or negative trend for the upper part of ENACW (100–350 m) as a consequence of the opposite contribution of isopycnal heave (green line) and changes in the intrinsic properties of the water mass (blue line). Changes on isopycnals have a positive contribution, with a maximum of 0.3 °C dec^{-1} at around 300 m. However the isopycnal heave term has a negative sign, which denotes an uplifting of isopycnals, with a maximum cooling rate of −0.3 °C dec^{-1} for the same depth (green line). As for the lower part of ENACW (350–600 m), both changes along isopycnals and changes due to vertical displacements decrease in absolute value although at a different rate. The unbalance between both terms results in a positive trend along isobars with a maximum (~0.25 °C dec^{-1}) at around 550 m. Salinity (Figure 4.4b) shows a similar behavior to the one observed for temperature although the influence of the intrinsic changes (blue line) was higher than the contribution of the isopycnal heave (green line). As a consequence, a positive salinity trend along isobars was found for ENACW at all depths with a maximum (0.06 dec^{-1}) at around 400 m.

Changes due to the vertical displacement of isopycnals play an important role to explain the changes observed along isobars. In order to quantify this contribution, the difference of depth at which each isopycnal was found at the beginning and at the end of the studied period was calculated (Figure 4.5). An important uplifting can be observed between 27.0 and 27.2 kg m^{-3} isopycnals, with a maximum (80 dbar) at about 27.15 kg m^{-3}, coinciding with the core of ENACW (González-Pola et al., 2005; Llope et al., 2006; Pérez et al., 2000). Taking into account that temperature and salinity decrease with depth along the first 500 dbar in the Bay of Biscay, the uplifting of isopycnals causes a decrease in temperature and salinity when measured along isobars. Therefore, isopycnal uplifting prevents a higher warming and salinification of ENACW that would be observed if only intrinsic changes influenced variations detected along isobars.

González-Pola et al. (2005) also found that the vertical displacement of isopycnals plays an important role in ENACW although they noticed that ENACW had warmed due to the sinking of isopycnals. However, they considered a different period (1993–2003) and local sampling in a shallow area in the southeast of the Bay of Biscay where ARGO measurements are not available.

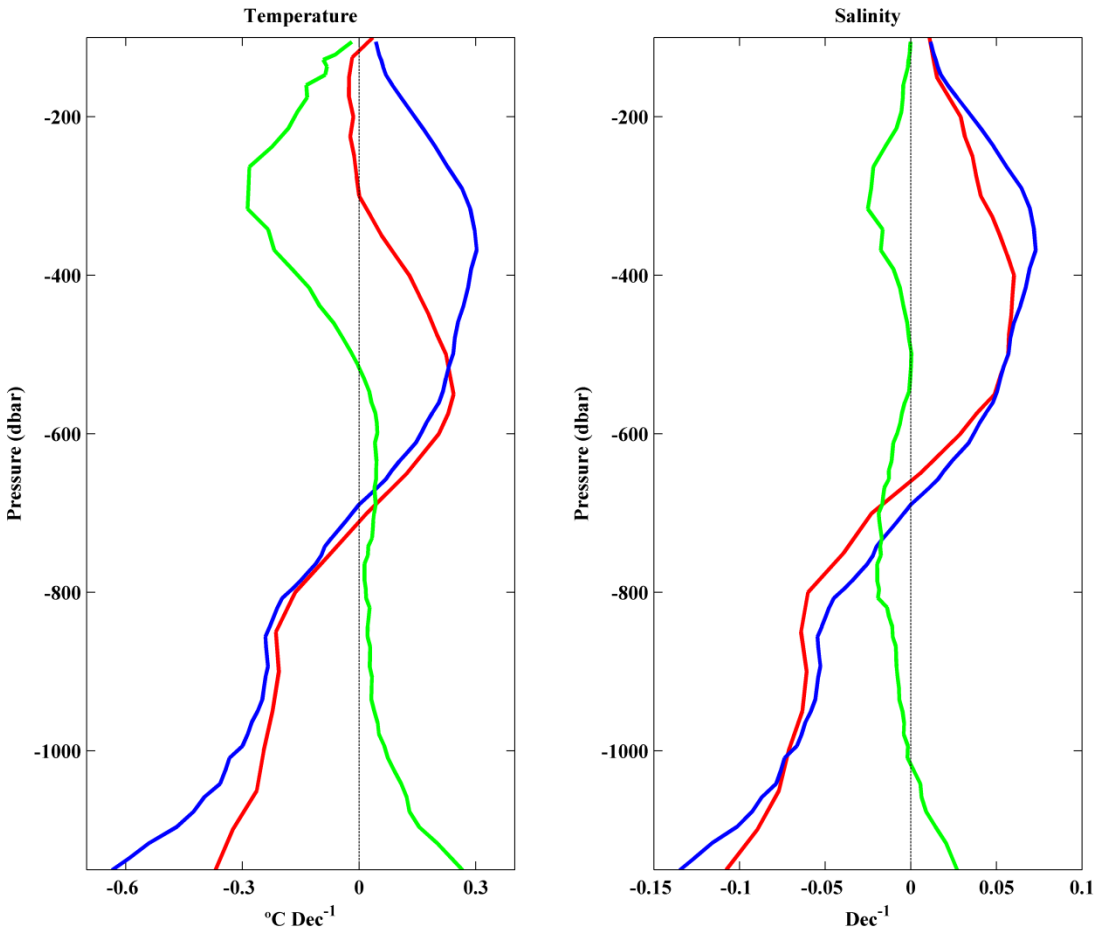

Figure 4.4. Decomposition of (a) temperature and (b) salinity changes along isobars (red line) as the sum of changes along isopycnals (blue line) and changes due to vertical displacement of isopycnals (green line).

Regarding the mechanisms that control changes in MW, a negative temperature trend was found along isobars from 700 m downward (Figure 4.4a), which becomes more negative with depth, mainly influenced by changes along isopycnals. The vertical displacement of isopycnals has also a contribution, which is especially patent from 900 m downward, reaching values close to 0.3 °C dec^{-1}. This is due to the moderate sinking (around 30 m) of isopycnals between 27.3 and 27.6 kg m^{-3} (Figure 4.5). Thus, the temperature decrease associated to intrinsic changes in water properties is partially compensated by vertical displacements. A similar decreasing trend was found for salinity (Figure 4.4b) along isobars. Moreover, the observed trend is mainly due to

intrinsic changes in water properties and not to isopycnal displacement, in accordance with results described by González-Pola et al. (2005) for MW.

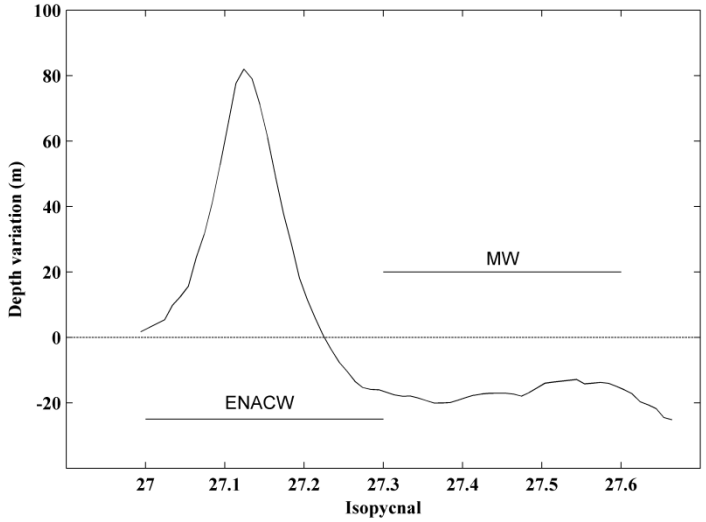

Figure 4.5. Vertical displacement of isopycnals for the period 2004–2013 in the Bay of Biscay

Overall, the trends and driving mechanisms observed for ENACW and MW in the Bay of Biscay (Figure 4.4) are similar to those analyzed by Soto-Navarro et al. (2012) for the area in front of the West Iberian Peninsula (38–42°N, 24–8°W). As we mentioned above, the Bay of Biscay depends both on local and remote forcing. Here, it seems that the origin of the changes observed for ENACW and MW is located outside the bay, in good agreement with results showed in Chapter 3. A completely different pattern is obtained for other close areas in the Eastern North Atlantic like, for example, zones 2 and 3 in Soto-Navarro et al. (2012), which covers the Azores and Canary currents respectively; or for the Canary region in Benítez-Barrios et al. (2008). The different trends observed for ENACW and MW at different locations are due to changes experienced by those water masses from their formation area. According to different authors (Baringer and Price, 1997; Daniault et al., 1994; González-Pola et al., 2005) the MW in the southern Bay of Biscay only contains about 12% of the water from the Mediterranean Sea. So, only a slight percentage of changes observed in the MW in the Bay of Biscay can be attributed to changes in the Mediterranean Sea. The greatest influence should be attributed to mixture processes during its displacement from the Strait of Gibraltar to the Bay of Biscay. This can explain why trends and driving mechanisms observed in the Bay of Biscay are more similar to those observed along the West Iberian Peninsula (zone 1 in Soto-Navarro et al., 2012) than to those observed in the Gulf of Cádiz or in the Canary region (zones 2 and 3 in Soto-Navarro et al., 2012).

4.3 Conclusions

Thermohaline variability was analyzed along the water column (0–1200 m) using Argo floats over the period 2004–2013. Trends were calculated for SW, ENACW and MW. The main conclusions are summarized as follows:

- A significant salinity increase was detected for SW, although a non-significant trend was found for near surface temperature.

- A significant increase was found both for ENACW salinity and temperature. This trend was mainly caused by changes in the intrinsic properties of this water mass, except for the upper part of ENACW, where the vertical displacement of isopycnals can balance intrinsic changes. Thus, the uplifting of isopycnals, which is related to cooling and freshening, compensates the contribution of changes along isopycnals.

- A significant cooling and freshening was observed for MW. In this case, changes due to isopycnal sinking cannot balance changes in the intrinsic properties of water.

Chapter 5: Mixed layer depth trends

The aim of this chapter is to analyze variations of the Mixed Layer Depth (MLD) during wintertime for the whole Bay of Biscay over the period 1975-2010. A comparison between Argo and SODA databases will be carried out in order to confirm the reliability of SODA dataset to calculate MLD. Two different approaches will be considered to calculate the wintertime MLD: the temperature criterion to define the isothermal layer depth (TLD) and the density criterion to define the isopycnal layer depth (PLD). In addition, two different wintertime parameters derived from the MLD (winter anomalies and annual maxima) will be calculated in order to give a complete view of the wintertime MLD trends.

5.1 Methods

The method used to determine the MLD was the threshold difference method that is based in the choice of a temperature or density threshold value. MLD is determined as the depth where the temperature or density exceeds the threshold value with respect to a reference depth located near the sea surface. The threshold difference method was shown to be more stable than the gradient method based on temperature or density gradients (Brainerd and Gregg, 1995). Hence, an important point is the choice of the threshold value. There is not a consensus about what are the best threshold values, which is related to the fact that MLD features change both in space and in time due to the different physical processes and hydrographic features that characterize the ocean all over the world (see Kara et al., 2000; deBoyer et al., 2004; Lorbacher et al., 2006; Holte and Talley, 2009 for recent discussions). Taking into account these studies, the most commonly used threshold values (ΔT=0.5ºC and $\Delta\sigma_\theta$=0.125 kg/m^3) were selected for potential temperature and density (e.g. Monterey and Levitus, 1997).

Therefore, a potential temperature threshold to define the iso-thermal layer depth (TLD) and a potential density threshold to define the iso-pycnal layer depth (PLD) were considered following the terminology applied by Hosoda et al. (2010) who analyzed different procedures to calculate MLDs using Argo floats. In this way, it is possible to detect possible biases derived of the salinity effect on the MLD that can produce important differences between TLD and PLD (e.g., deBoyer et al., 2004, Hosoda et al. 2010). Potential values were calculated to avoid pressure problems with increasing depth following the method describe in UNESCO (1983). Besides, a reference depth of 15 m was chosen to prevent the diurnal oscillations of temperature and the effect of precipitation and evaporation that takes place in the first meters beneath sea surface (Price et al., 1986). This choice was adopted because the first two levels in the SODA database are 5 m and 15 m.

The deepest MLDs occur during winter and early spring in the North Atlantic region (e.g. Monterey and Levitus, 1997; Kara et al., 2003). For this reason, the present study is focused on the analysis of winter MLD. Thus, annual maxima MLD and winter extended (December-March) anomalies were calculated. An annual maximum corresponds to the winter month when TLD/PLD attains the highest depth. TLD and PLD winter anomalies were calculated considering the available profiles for the December-March months and subtracting to each month, the mean value of that month for the whole period of time.

Argo and SODA datasets allow taking advantage of their salinity and temperature vertical resolution. Thus, both databases were selected to carry out this analysis. First of all, both databases were compared for the period 2003–2010 in order to know the reliability of SODA database. To carry out this comparison, all available data among

2003–2010 in the Bay of Biscay (43.25–48.25ºN//0.25–9.75ºW) were extracted (Figure 5.1). In this case, the domain was slightly enlarged, with respect to the rest of the study, in order to include a larger number of Argo profiles, especially during the years 2003 and 2004 when the number of profiles was limited. Thus, a better sampling was obtained ensuring better results in the comparison. Only profiles deeper than 1000m were selected in order to ensure that depth does not influence TLD/PLD calculations. A total of 101 points carried out the requirements in the SODA database, while a total of 3362 profiles, which corresponds to 58 floats, were extracted from the ARGO database. These 3362 profiles were submitted to the quality control specified in Chapter 2 that is enough to guarantee the quality of data. Argo and SODA profiles were interpolated for each meter following a linear interpolation in order to get the most accurate TLD/PLD value.

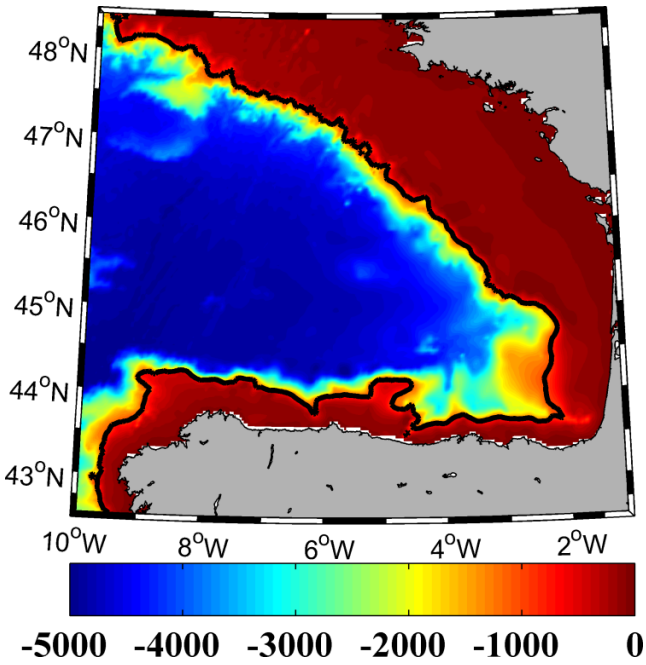

Figure 5.1. Bathymetry of the Bay of Biscay. Solid black line represents the−1000 m isobaths.

Data from the 101 points of SODA database and good quality profiles from ARGO database were horizontally averaged for the whole region and for each month over the period 2003–2010. Thus, an average profile was obtained for each month and for each database. Then, TLDs and PLDs were calculated based on each monthly averaged profile. Finally, annual maxima and winter anomalies were determined and correlated for both datasets.

The area between 43.75–47.25ºN and 2.25–8.25ºW was selected to analyze trends in wintertime MLD over the period 1975–2010. Only grid points deeper than 1000 m were considered, which includes 70 points from SODA database. The methodology was described above but TLDs/PLDs were calculated in this case for each of the 70 points in order to know if trends are similar in the whole bay. Trends were assumed to be linear

and obtained by fitting time series (TLDs and PLDs) to a straight line in a least-squares sense. The Spearman rank correlation coefficient was used to analyze the significance of trends and correlations. Finally, annual maxima and winter anomalies trends of TLD/PLD were correlated with atmospheric variables (air temperature, P-E balance and wind stress). Data from atmospheric variables were retrieved from the NCEP/NCAR database. Latent heat flux was used to calculate evaporation dividing the latent heat flux loss by the latent heat of water ($2.5x10^6$ J kg^{-1}) following González-Pola et al., (2005). Moreover, wind speed was used to calculate wind stress according to the formula: $\tau_{wind} = \rho_{air} C_D U_h^2$, where C_D is the wind-drag coefficient (0.0011), ρ_{air} is the air density (1.2250 kg m^{-3} at 15ºC) and U_h is the wind speed above sea surface (10 m).

5.2 Results and discussion

5.2.1 Argo and SODA correlation

The correlation between Argo and SODA databases using annual maxima and winter anomalies is shown in Table 5.1 over the period 2003–2010. Threshold values of ΔT=0.5ºC and $\Delta\sigma_\theta$=0.125kg/m^3 were used for potential temperature and for potential density, respectively. Correlation coefficients are slightly higher for winter anomalies (0.74 for PLD and 0.71 for TLD) than for annual maxima (0.66 for PLD and 0.64 for TLD). All these correlation coefficients are significant at a level higher than 90%.

	Annual Maxima	***Winter anomaly***
PLD	0.66 (0.074)	0.74 (0.037)
TLD	0.64 (0.089)	0.71 (0.046)

Table 5.1. Correlations between annual maxima and winter anomalies of PLD/TLD calculated from ARGO and SODA databases for the period 2003-2010. Statistical significance (p value) is showed in brackets.

In addition, monthly averaged PLDs and TLDs for both databases are shown in Figure 5.2. Overall, a good agreement was observed between both databases for the whole period. Nevertheless, SODA (red line) underestimates the MLD depth both for TLD (2003, 2006, 2008, 2009 and 2010) and PLD (all years except 2007). We should note that PLD depends both on temperature and salinity and so the sources on uncertainty are higher compared to TLD. The largest differences were observed in winter 2003. This fact seems to be related to the few Argo profiles available during that year. The Argo program was launched in 2002, which caused a less uniform sampling in the bay over the first years.

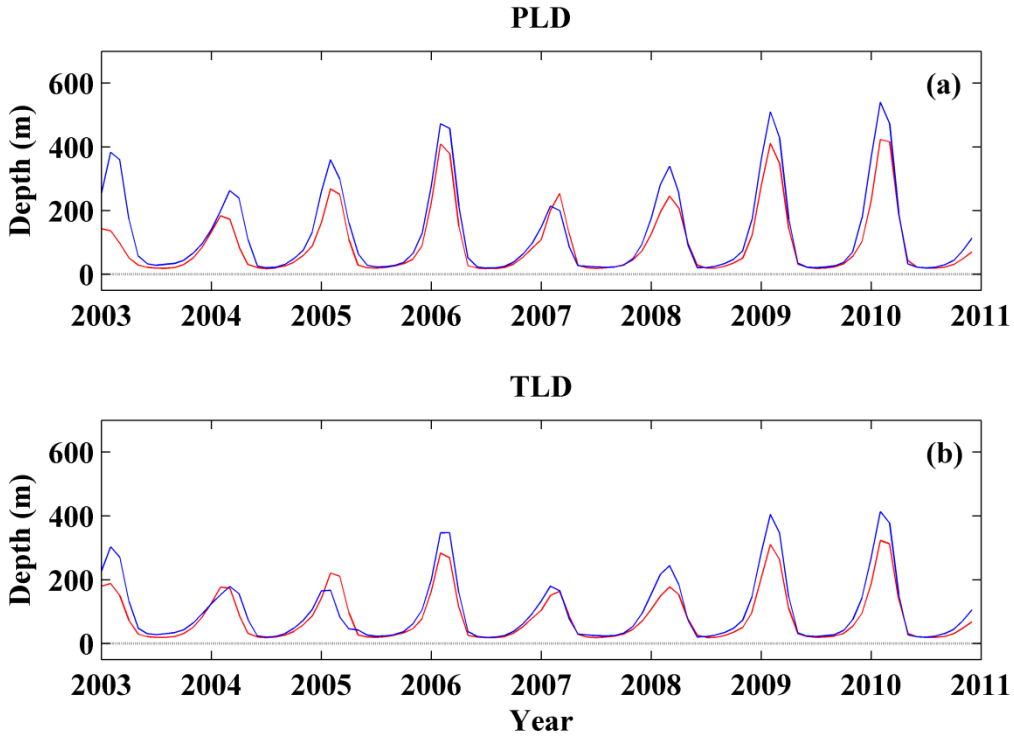

Figure 5.2. Comparison between Argo and SODA databases. (a) Isopycnal layer depth and (b) isothermal layer depth variability using Argo database (blue line) and SODA database (red line). A 1-2-1 filter was used to smooth signals only for visualization.

5.2.2 MLD variability

Once the reliability of SODA database was confirmed using in situ measurements, it was used to characterize the MLD in the bay over the period 1975–2010. Winter PLD/TLD means were calculated for each of the 70 grid points that constitute the bay (Figure 5.3). A remarkable southeast-northwest MLD gradient can be observed in both

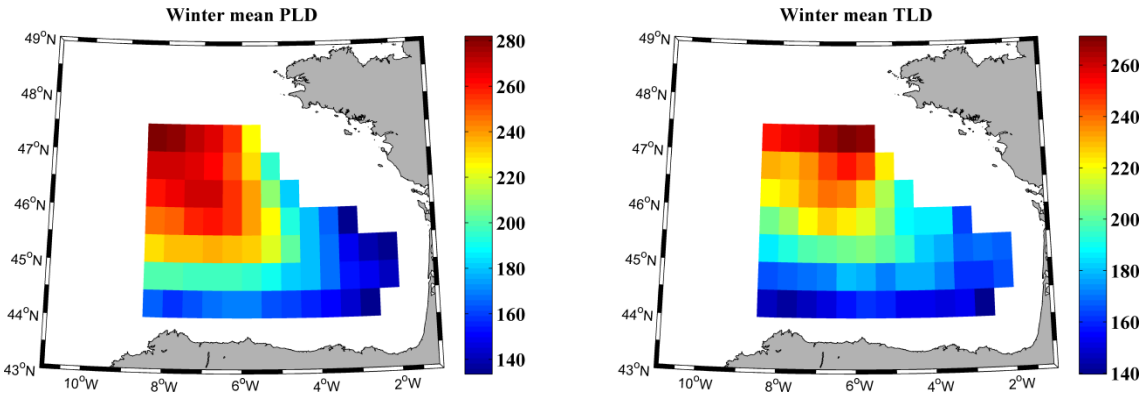

Figure 5.3. Mean values of winter mixed layer depth. (a) Winter mean isopycnal layer depth (m) and (b) winter mean isothermal layer depth (m) over the period 1975–2010.

frames. In this way, the deepest mean MLDs, around 270 m, were found near the northern boundary while the shallowest mean MLDs, around 140 m, were noticed at the

southeastern corner. Overall, not significant differences were found between winter mean PLD and winter mean TLD. The observed differences are related to haline forcing, which is a phenomenon produced by different oceanic processes such as surface freshwater fluxes or freshwater advection. These changes can produce that the halocline is located above the thermocline or vice versa. This effect on MLD has been previously described all over the world by different authors (deBoyer et al., 2007, Liu et al., 2009).

Long-term trends of annual maxima and winter anomalies of TLD and PLD for each grid point are shown in Figure 5.4. Black dots represent points with statistical significance higher than 90%. Negative (positive) trends mean that MLD tends to be shallower (deeper). In all cases, the most important feature is that points located at the southeastern corner of the Bay of Biscay show a significant positive trend. MLD deepens in this zone and shallows in the rest of the area, especially at the central part.

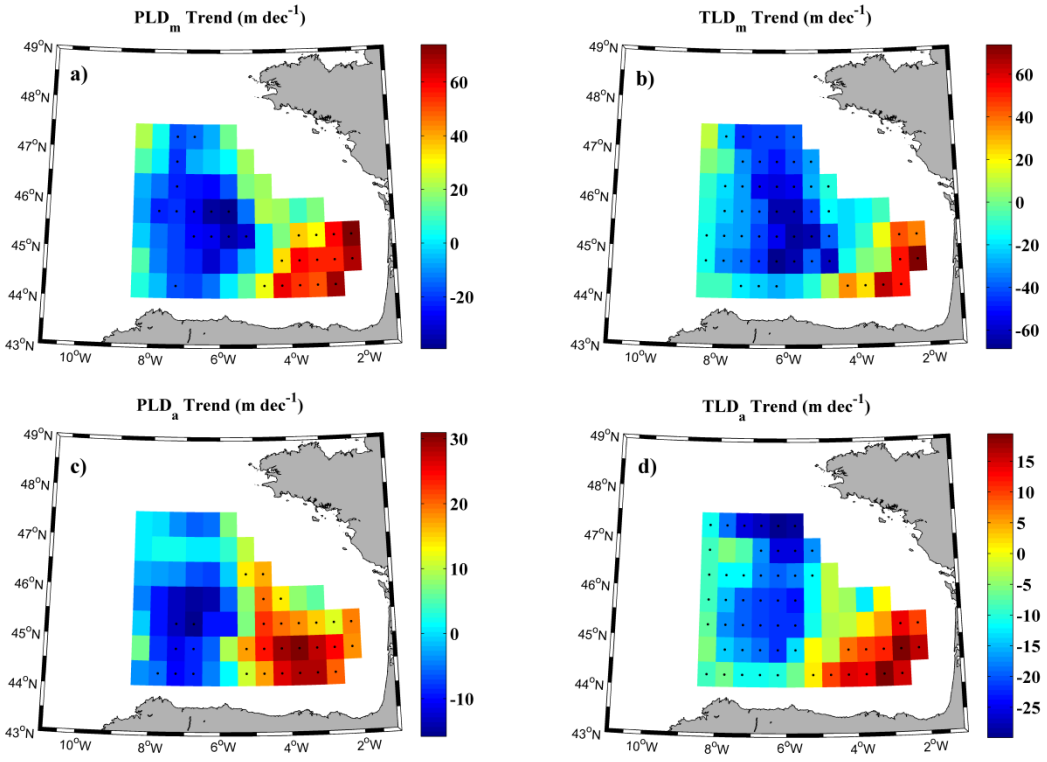

Figure 5.4. Trend values of mixed layer depth. (a) (b) Annual maxima trends and (m per decade) (c) (d) winter anomalies trends (m per decade) of PLD (left) and TLD (right) in the Bay of Biscay for the period 1975–2010. Black dots represent points with a significance level higher than 90%.

As it was previously mentioned, annual maxima correspond to the month when TLD/PLD attain their maximum, which corresponds to winter or early spring (commonly March) in the Bay of Biscay. First, trends in annual maxima of MLD (Figure 5.4a,b) will be analyzed. Trends at grid points with significant positive values are observed to range from 20 to 60 m per decade, being higher for PLD (Figure 5.4a) than for TLD (Figure 5.4b). In a similar way, trends at grid points with significant negative values range from -10 m to -60 m per decade for TLD and are around -25 m

per decade for PLD. The spatial distribution of significant positive and negative trends is similar for winter anomalies (Figure 5.4c,d). In this case, positive MLD trends range from 5 to 25 m per decade and negative trends from -5 to -25 m. Differences between TLD and PLD can also be observed for winter anomalies as previously noticed for annual maxima. The positive MLD trend described above for the southeastern of the bay is in good agreement with results obtained by Somavilla et al. (2011). They found that MLD was shallower during the 1970s and 1980s, becoming deeper from 1995 onwards.

5.2.3 Influence of atmospheric variables on MLD variability

In order to know the influence of the atmospheric forcing over the MLD trend, long-term trends calculated using the temperature and density criterion were correlated with different atmospheric variables (air temperature, P-E balance and wind stress) for the period 1975–2010. Trends, which were assumed to be linear, were calculated for these atmospheric variables following the same procedure used for PLDs and TLDs (Figure 5.5).

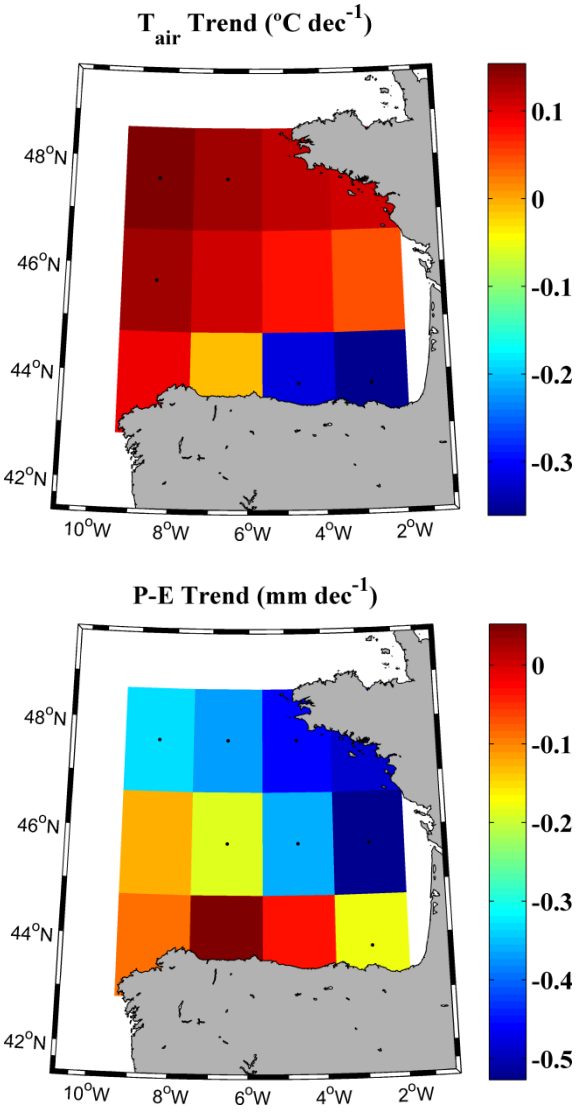

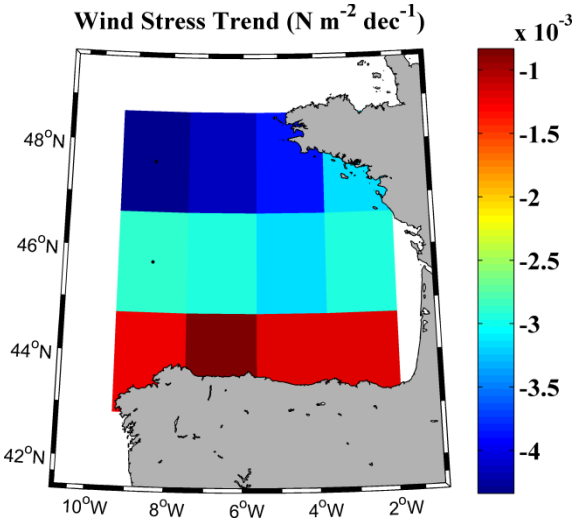

Figure 5.5. (a) Air temperature trend (ºC per decade), (b) P-E (precipitation minus evaporation) balance trend (mm per decade) and (c) wind stress trend (N m^{-2}per decade) calculated over the period 1975–2010. Black dots represent points with a significance level higher than 90%.

Only the air temperature trend shows a different sign depending on the area of the Bay of Biscay (Figure 5.5a), being positive over most of the bay, with values around 0.1ºC per decade. However, negative trends, with maximum values of -0.3ºC per decade, were detected at the southeastern corner. Dots represent trends with significance higher than 90%. Hence, the air temperature trend seems to be spatially consistent with annual maxima and winter anomalies TLD/PLD trends shown in Figure 5.4. P-E balance (Figure 5.5b) shows a significant negative trend, with differences between -0.5 mm per decade in the northeast boundary and around -0.15 mm per decade in central and southeastern boundary. Regarding wind stress (Figure 5.5c), grid points show negative trends for the whole area, being higher in the north (-0.004 N m^{-2} per decade) than in the south (-0.001 N m^{-2} per decade) of the bay.

As it was mentioned above, trends in air temperature seem to be correlated with trends in MLD (TLD and PLD). To analyze the significance of this resemblance between patterns we have proceeded as follows. Considering, for example, TLD as an ocean variable, it was spatially averaged for all grid points where the variable was observed to have significant positive trends (>90%). This resulted in a one-dimensional signal (TLD^{+}), where only a value is stored per month. The same protocol was followed for the grid points with significant decreasing trends (TLD^{-} signal). On the other hand, a similar signal was created for air temperature, in such a way that $Tair^{+}$ ($Tair^{-}$) was obtained by averaging the grid points with significant positive (negative) trends. The protocol previously described for TLD was also followed for PLD.

Table 5.2 shows the correlation between ocean variables (TLD and PLD) and Tair. As it previously mentioned the areas where air temperature decreases (increases) coincide macroscopically with the areas where MLD increases (decreases). Thus, only the comparisons among ocean and atmospheric variables with different sign were

considered. MLD^+ signals were only compared with $Tair^-$ signals and vice-versa. Significant negative correlations were obtained between air temperature and TLD/PLD.

	T_{air}^-
PLD^+_m	-0.45 (0.007)
TLD^+_m	-0.48 (0.004)
PLD^+_a	-0.39 (0.019)
TLD^+_a	-0.35 (0.035)

	T_{air}^+
PLD^-_m	-0.7 (0.001)
TLD^-_m	-0.83 (0)
PLD^-_a	-0.69 (0.001)
TLD^-_a	-0.8 (0)

Table 5.2. Left, correlations between points of negative air temperature trends ($Tair^-$) and points of positive annual maxima (PLDm/TLDm) and winter anomalies (PLDa/TLDa) trends. Right, correlations between points of positive air temperature trends ($Tair^+$) and points of negative annual maxima (PLDm/TLDm) and winter anomalies (PLDa/TLDa) trends. Statistical significance (p value) is showed in brackets).

This means that increasing air temperature results in the decrease of TLDs/PLDs depths. All correlations show a significance level higher than 95%. In particular, correlations between the $Tair^-$ and PLD^+/TLD^+ (both correspond to the southeast corner of the Bay of Biscay) range from -0.35 for winter anomalies of TLD to -0.48 for annual maxima. Higher correlation coefficients were found between $Tair^+$ and PLD^-/TLD^-, with values of -0.69 for winter anomalies of PLD and -0.83 for annual maxima. The significance of correlations proves the fact that could be foreseen by visual inspection, namely, decreasing MLD trends are related to increasing in air temperature and vice-versa. On the other hand, correlations with P-E and wind stress did not show significant results for any of the possible combinations.

The influence of air temperature on MLD was inferred previously at the southeastern Bay of Biscay by Somavilla et al. (2009). They analyzed an extreme mixing event, characterized for a deeper than normal MLD in 2005. They found that winter 2005 was characterized by a relatively high sensible heat flux (the highest since 1965) which is a variable where air temperature plays a crucial role. Air temperature decrease causes an increase in net heat loss and this is directly associated with MLD sinking. Moreover, Somavilla et al. (2011) indicated that winter net heat losses are also related to storminess activity. This fact agrees with results presented in Figure 5.5b since the balance between precipitation and evaporation (P-E) has a negative trend in most of the bay. On the other hand, wind stress does not play an important role in winter mixed layer formation in the Bay of Biscay according to these authors. Therefore, mixed layer development in the bay shows to be mostly conducted by convection processes than by wind stress.

Considering a global scale, this study shows that a relative small and semi-enclosed sea such as the Bay of Biscay may show opposite trends related to MLD variability. This fact is due to the high dependence of MLD on local atmospheric forcing and hydrographic conditions. For this reason, results shown in this study cannot be extrapolated to other regions. However, it seems that atmospheric forcing can play a

similar role to that described for the Bay of Biscay in neighboring areas. Thus, Carton et al. (2008) found that MLD variability is not closely related to variation in local wind speed in the North Atlantic (60W–30W, 35N–45N) for the period 1960–2004. However, these authors found that wind speed plays an important role to explain MLD variability in the North Pacific (180W–150W, 35N–45N) for the same period.

Winter temperature trend for the upper 700 m of the water column was also analyzed over the period 1975–2010 using SODA database (Figure 5.6). According to Levitus et al. (2005; 2009) the most important variations in the heat content during the last decades occurred in the upper 700 m. This was also shown for the Iberian Peninsula (Santos et al., 2012a) and the Bay of Biscay, as it was shown in Chapter 3. The whole area presents a positive trend but with different intensity. Warming is higher at the northwest corner and in the central part of the bay with values ranging from 0.1–0.15ºC per decade. However trends are almost negligible at the south and at the southeastern corner with values around 0.04ºC per decade. Macroscopically, the area of higher (negligible) warming coincides with the area where MLD has become shallower (deeper).

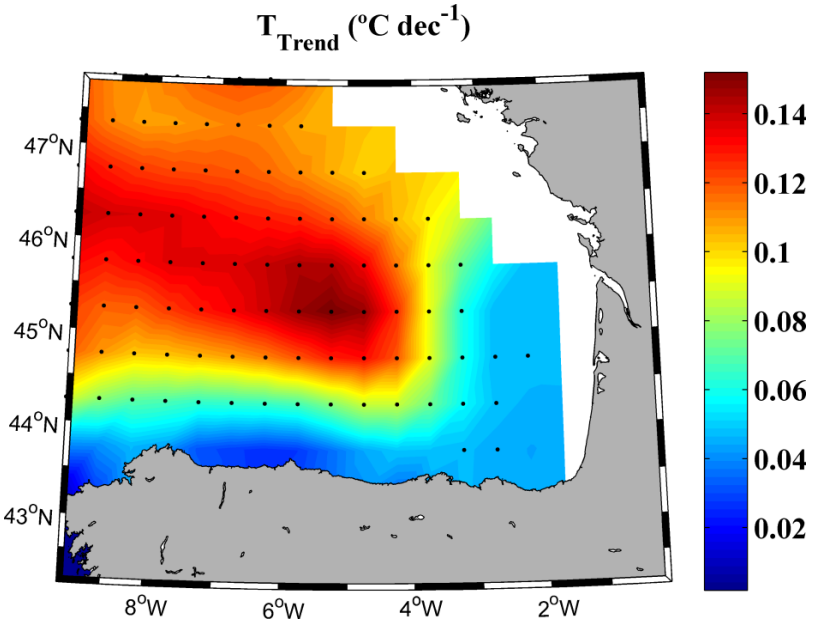

Figure 5.6. Winter ocean temperature trend for the upper 700 m over the period 1975–2010. Black dots represent grid points with a significance level higher than 95%.

5.3. Conclusions

MLD trends were analyzed in the Bay of Biscay over the period 1975–2010. MLD was calculated using a potential temperature criterion to define the TLD and a potential density criterion to define the PLD. Time evolution of MLD was analyzed in

terms of trends in winter anomalies and in annual maxima. Some of the main findings are outlined below:

- MLD tended to deepen at the southeastern corner and shallow at the rest of the bay.

- Correlations carried out between atmospheric variables and MLD trends evidence that air temperature plays a key role in regulating the MLD variability. In this way, negative air temperature trends, localized in the southeastern part of the bay, are related with MLD deepening at this area and positive air temperature trends observed for the rest of the bay are related to MLD shoaling.

- MLD evolution did not show significant correlations with wind stress and precipitation minus evaporation.

- Warming calculated for the upper 700 m is observed to be more intense at the area where MLD became shallower and negligible at the area where MLD deepened.

- The MLD analysis carried out in this study highlights that mesoscale features can play an important role even in small semi-enclosed areas like the Bay of Biscay, where the observed behavior is far from being spatially homogeneous.

Chapter 6: Changes in sea surface temperature seasonality

The aim of this chapter is to analyze SST variability in the Bay of Biscay over the period 1982–2014. Changes will be analysed for each month in order to detect if SST variability was homogenous or not throughout the year. In addition, the calculation of monthly trends will help us to detect changes in the duration of the warm season which influences biodiversity both at ecosystem and population levels. Finally, trends in the number of extreme hot SST days will also be analyzed.

6.1 Methods

Daily SST values and their associated errors were obtained from $OISST_{1/4}$ database. All available data files for the Bay of Biscay (1–8°W, 43–48°N) over the period 1982-2014 were extracted. As a result, a grid with a total of 457 pixels was considered to carry out this study.

6.1.1 SST trends

SST trends were calculated from daily SST averaged on a monthly scale. Trends were calculated as the slope of monthly SST versus time for every pixel individually. SST OI estimates are affected by random, sampling and bias errors (Reynolds et al., 2007). With the aim of reducing the influence of these errors, weighted least squares with weights proportional to the inverse of the variance of SST OI were used in the regression procedure. Moreover, daily SST series are affected by problems of autocorrelation. The Quenouille procedure (Quenouille, 1952) was applied in order to solve this problem. Thus, the degrees of freedom were recalculated using this procedure for every pixel following Lima and Wethey (2012) and deCastro et al. (2014). The Quenouille procedure is based on the expression $N_{eff}=N\ (1-r_1)/(1+r_1)$, where N is the sample size and r_1 represents the lag−1 autocorrelation coefficient of detrended series.

6.1.2 Duration of the warm season

The onset of the warm season was calculated for each pixel and year as the day when the 75th percentile of the entire SST dataset was exceeded. In order to ensure a higher confidence in the results, the first three days that exceeded the 75th percentile were selected and averaged. In the same way, the end of the warm season was the mean of the last three days for which the SST was higher than the 75th percentile. Thus, the onset and end day of the warm season was obtained for each pixel and year. The total duration was calculated by taking into account both dates. Trends in dates of beginning and end of warm season and its duration were calculated as the linear regression using the value obtained for each year.

6.1.3 Extreme SST trends

An extreme hot SST day was defined as a day with a SST anomaly over the 95th percentile considering the entire dataset. Trends in the number of extreme hot days for every pixel (i, j) were calculated following the procedure developed by Lima and Wethey (2012) and also applied by deCastro et al. (2014). First of all, daily SST anomalies were calculated to remove the seasonal cycle. This was achieved by subtracting from the SST of a certain day (e.g. January 1, 1982) the mean temperature of that day (January 1) over the period 1982–2014. Then, the number of extreme hot

SST days ($^{95}N_{i,j}$) was calculated as the number of days per month with extremely high SST anomaly (over the 95th percentile). Therefore, an extreme day can occur at any time of the year. After that, the monthly trends were calculated as the slope of the linear regression of $^{95}N_{i,j}$ versus time. Finally, trends in the number of extreme hot SST days for each pixel were obtained from spatially averaging the trend value with the closest neighborhood of every pixel.

6.2 Results

6.2.1 Mean SST and SST trends

First of all, mean values and trends were calculated at annual scale to be compared with previous research (Table 6.1). Trends found in previous studies were recalculated (when possible) using the database considered in the present study (NOAA OI ¼ degree daily SST) for comparisons purposes. Results in last column showed to be in good agreement with previous research, highlighting the robustness of the trends in spite of the heterogeneity of the data sets.

Author/s	Period	Area	Database	SST trend (ºC dec^{-1})	SST trend recalculated (ºC dec^{-1})
Koutsikopoulos et al., (1998)	1972-1993	Global	Meteo-France	0.64	
Planque et al., (2003)	1971-1998	SE	Meteo-France	0.5	
Llope et al., (2006)	1993-2003	43º36';6º10'	CTD sampling	0.55	
Gómez-Gesteira et al., (2008)	1985-2005	Coast	AVHRR	0.24±0.04	0.27±0.05
deCastro et al., (2009)	1985-2006	Global	AVHRR	0.33±0.05	0.35±0.04
	1974-2006	Global	ERSST	0.22	
Goikoetxea et al., (2009)	1977-2007	SE (San Sebastian)	Aquarium of San Sebastian	0.26	
Michel et al., (2009a)	1985-2003	BB & close areas	Pathfinder v5.0	0.37	0.33±0.09
	1985-2003	BB & close areas	ORCA model	0.22	0.33±0.09
	1985-2003	BB & close areas	WOD	0.3	0.33±0.09
Michel et al., (2009b)	1986-2005	BB & close areas	BoByClim	0.30	0.33±0.09
Lima & Wethey (2012)	1982-2010	Coast	$OISST_{1/4}$	0.25	0.24±0.03

Table 6.1. Annual SST trends within the Bay of Biscay according to different authors, periods, locations and databases. The associated standard deviation is also included.

Annual mean SST values were calculated for the whole Bay of Biscay from 1982 to 2014 (Figure 6.1a). Mean SST decreases with increasing latitude from 16.5ºC at the south of the bay to 13ºC at the northern part. The highest SST values were found at the southeastern corner, probably due to the continental influence (Valencia et al., 2003; 2004). The annual warming trend detected for the whole area (Figure 6.1b) ranges from 0.15 ºC per decade to 0.35 ºC per decade with maximum values at the western part, over

the French shelves, and the lowest ones along the French coast, around 46ºN, and also in the north-western corner of the bay.

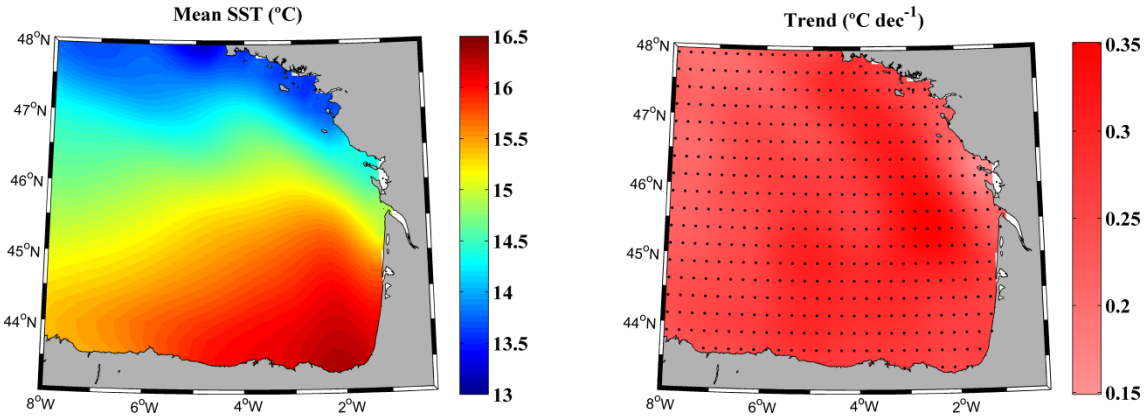

Figure 6.1. (a) Annual mean SST (°C) and (b) decadal SST trends (°C dec^{-1}) in the Bay of Biscay from 1982 to 2014. Black dots represent the grid points with a significance level higher than 95%.

SST mean (Figure 6.2) and trends (Figure 6.3) were analyzed at monthly scale. With regard to the mean SST values, it is possible to group them into three different kinds of patterns. Thus, from December to March the mean SST increases gradually from the northeast to the southwest of the bay. The lowest SST was found along the French coast in the area where the two main rivers of the bay (Loire and Gironde) flow into the shelf. This pattern changes drastically from May to August when the lowest SST values were found at the northwestern and north area, being the highest SST values detected at the southeastern corner of the bay. This fact, as noted when annual means were analyzed, is related with an intense continental influence due to the concavity of this area (Valencia et al., 2003; 2004). April represents the transition between both patterns. Finally, from September to November, mean SST increases from north to south in a similar way to those observed at open ocean areas (far from continents) due to the different insolation with latitude.

SST trends can also be grouped (Figure 6.3) although the chosen months do not necessarily correspond with those chosen for mean values. From December to March warming was detected for most of the bay with values ranging from 0.1 to 0.3 ºC per decade. An exception should be made along the French coast, in particular north of 45ºN, where lower SST trends were observed and even cooling (~ -0.1°C per decade) was found at some particular areas. Higher warming trends were found from April to June with significant positive trends ranging from 0.3 to 0.5 ºC per decade for most of the bay. However, SST trends were clearly lower during July and August, months with the highest mean SST. This warming is especially lower in the oceanic part of the bay where even a cooling was observed at some points. In this case, warming was only significant along the coast during August probably related to the continental influence. Finally, a strong warming was also observed from September to November, being the highest increase measured in October with significant values that exceeds 0.5 ºC per decade. Mean SST values and trends are summarized in Table 6.2.

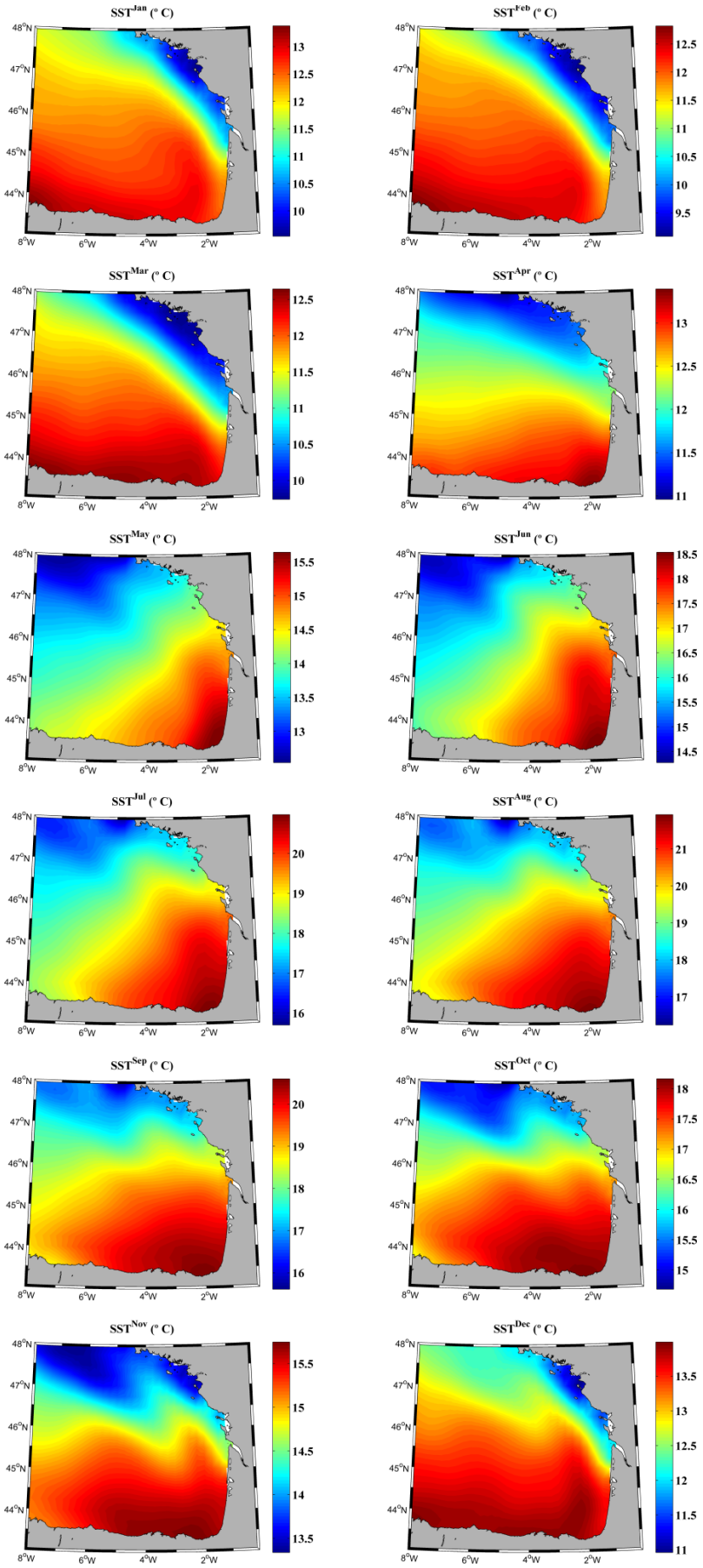

Figure 6.2. Monthly mean SST (°C) in the Bay of Biscay over the period 1982–2014.

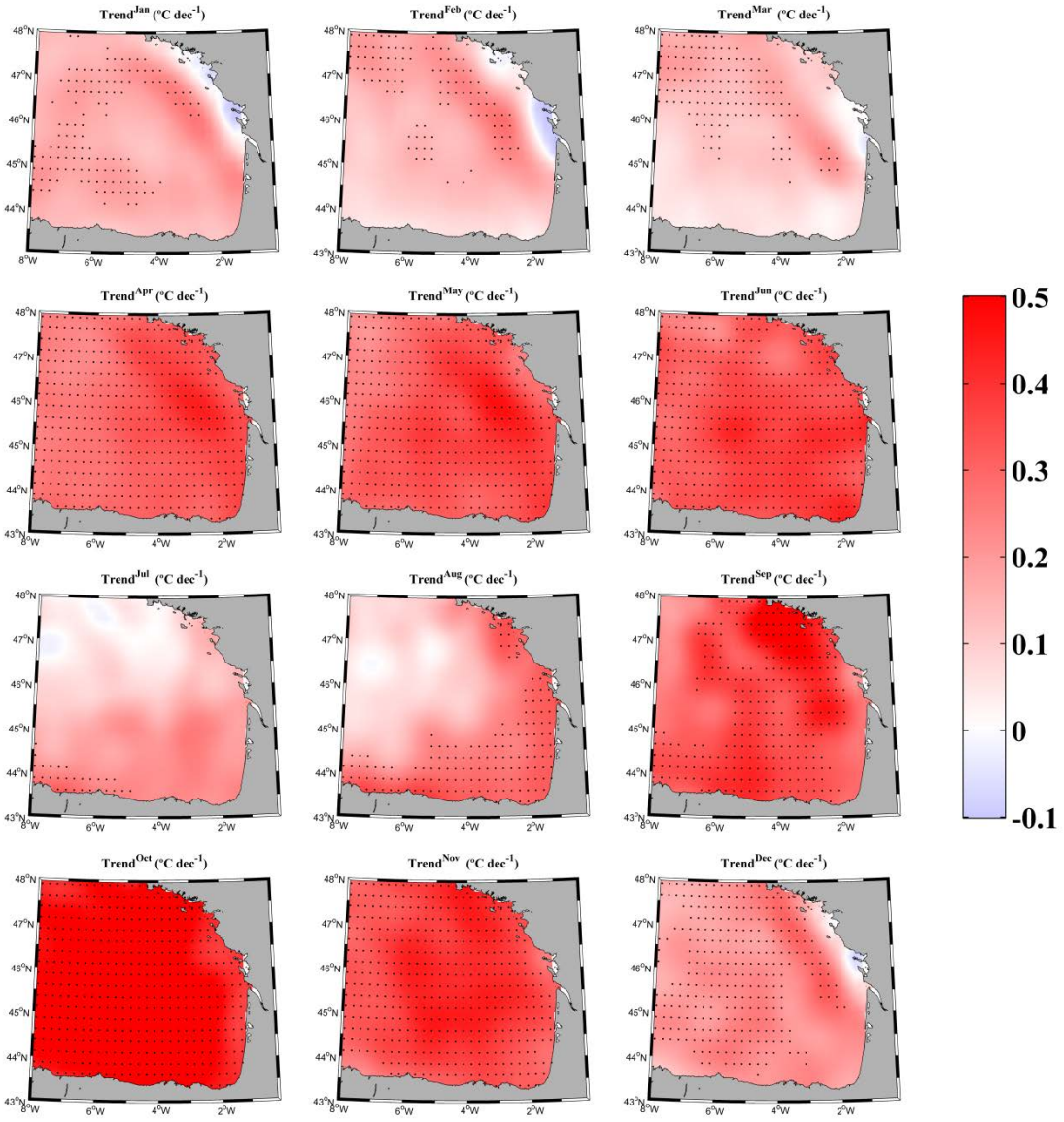

Figure 6.3. Monthly SST trends (°C per decade) in the Bay of Biscay over the period 1982–2014. Black dots represent the grid points with a significance level higher than 95%.

	SST Mean (ºC)	Trend (ºC per decade)		SST Mean (ºC)	Trend (ºC per decade)
Jan	12.2±0.7	0.14 ± 0.06	**Jul**	18.6±1.2	0.14 ± 0.09
Feb	11.7±0.8	0.12 ± 0.07	**Aug**	19.6±1.2	0.19 ± 0.11
Mar	11.7±0.7	0.10 ± 0.05	**Sep**	18.7±1.1	0.35 ± 0.08
Apr	12.3±0.6	0.31 ± 0.05	**Oct**	16.8±0.9	0.53 ± 0.08
May	14.0±0.7	0.33 ± 0.05	**Nov**	14.8±0.7	0.36 ± 0.06
Jun	16.4±1.0	0.34 ± 0.04	**Dec**	13.2±0.6	0.20 ± 0.06

Table 6.2. Monthly mean SST (ºC) and trend (ºC per decade) values with their associated standard deviation for the whole Bay of Biscay over the period 1982-2014. Values were obtained by means of a spatial average of figures 6.2 and 6.3, respectively.

6.2.2. Duration of the warm season

Previous results (Figure 6.3 and Table 6.2) show that the observed annual trends are due to changes in spring and autumn more than to warmer summers or milder winters. This can affect the duration of the warm season, which was calculated following the procedure described in section 6.1.2.

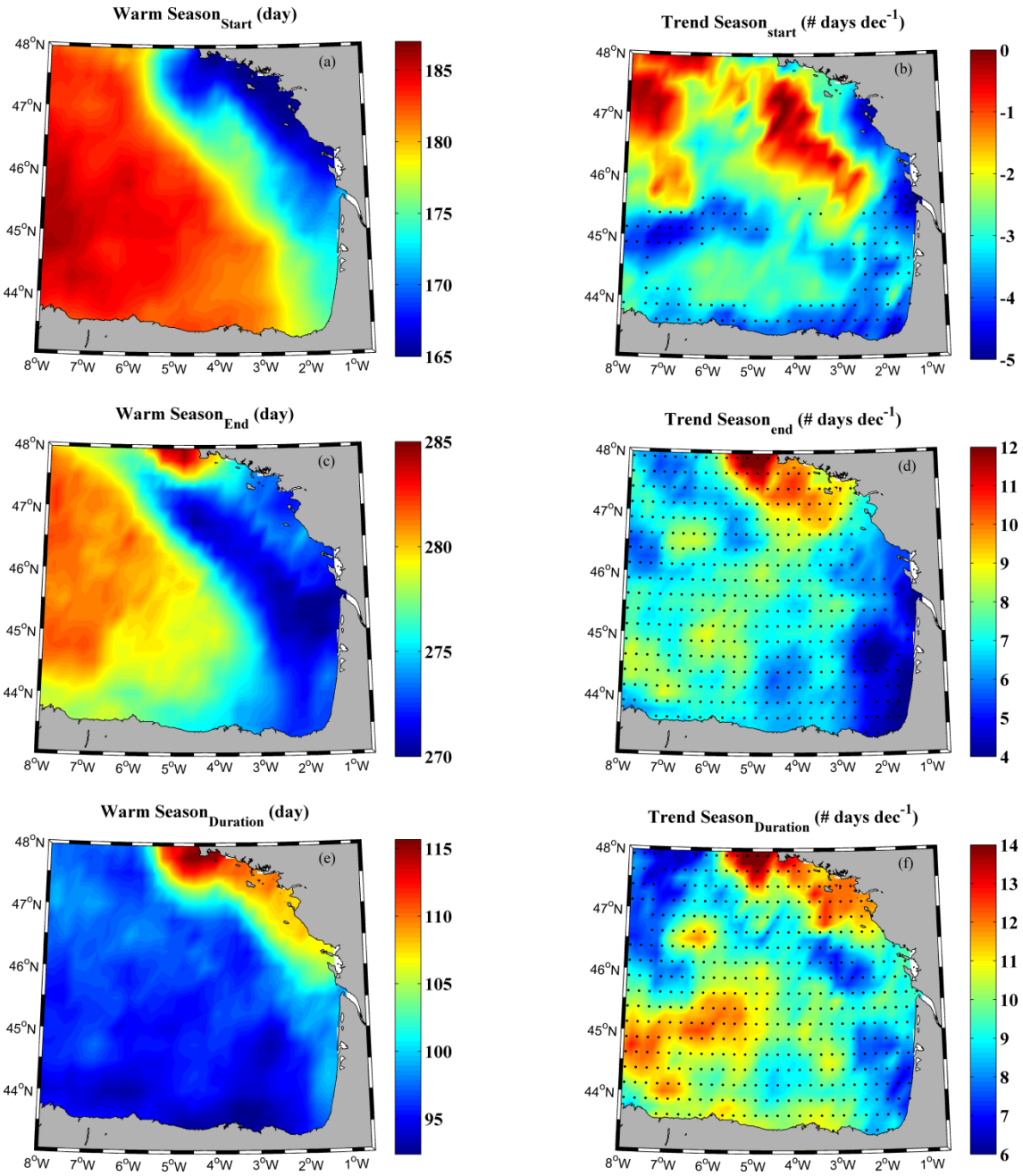

Figure 6.4. Day when the warm season starts (a) and ends (c) in the Bay of Biscay averaged over the period 1982–2014. (b) Trend (# days dec^{-1}) in the beginning of the warm season and (d) in the end of the warm season. (e) Mean duration of the warm season and (f) trend (# days dec^{-1}) of the warm season duration. Black dots represent the grid points with a significance level higher than 95%. Negative trends indicate an advance and positive trends account for a delay.

The warm season started between mid-June (day 165) and the beginning of July (day 185) (Figure 6.4a). It starts earlier in the south and eastern part of the bay especially over the continental shelf. Trends in the start of the warm season (Figure 6.4b) are negative for the whole area (the warm season starts earlier) although they are not spatially homogenous. In general, changes are more intense at shelf area reaching values up to -5 days per decade. The warm season ends between the end of September (day 270) in the eastern part and the beginning of October (day 280) in the western part (Figure 5.4c). The warm season is observed to finish later (Figure 5.4d) with a lower increase in the southeastern corner (~4 days per decade) and maximum ones in the northeastern area (~12 days per decade). As a consequence, the mean duration of the warm season was between 95 and 105 days with the exception of the coastal strip north of 46ºN where the duration is slightly higher (105-115 days) (Figure 6.4e). The total duration of the warm season, considering the whole period under study, has been expanded in around one month for more than 65% of the area, although this increment was not spatially homogeneous (Figure 6.4f). The highest increase (~14 days per decade) is observed at the northeastern corner of the area.

6.2.3. Trends in the number of extreme hot SST events

The increase in extreme hot SST days was analyzed during months with the highest SST warming trends (from April to June in Figure 6.5a and from September to November in Figure 6.5c) and during the month with the highest SST mean (August, Figure 6.5b). Taking into account that Figures 6.5a and 6.5b accounts for more than one month, values were normalized in order to show changes in the number of extreme hot SST days per month. A significant increase in the number of extreme hot days was observed between April and June (Figure 6.5a) with a mean excess of 1.16±0.23 days per decade. This is especially patent in the central part of the bay, where values higher than 1.5 days per decade are attained. Regarding the warmest month (August) a slight increase (~ 1.0 days per decade) was observed near shore and a decrease (~ -1.0 days per decade) for the oceanic part (Figure 6.5b). Finally, a significant increase in extreme hot SST days was also detected over the period September-November (Figure 6.5c) with a mean excess of 1.81±0.42 days per decade. The highest values (>2.5 days per decade) are attained at the southwestern part of the bay.

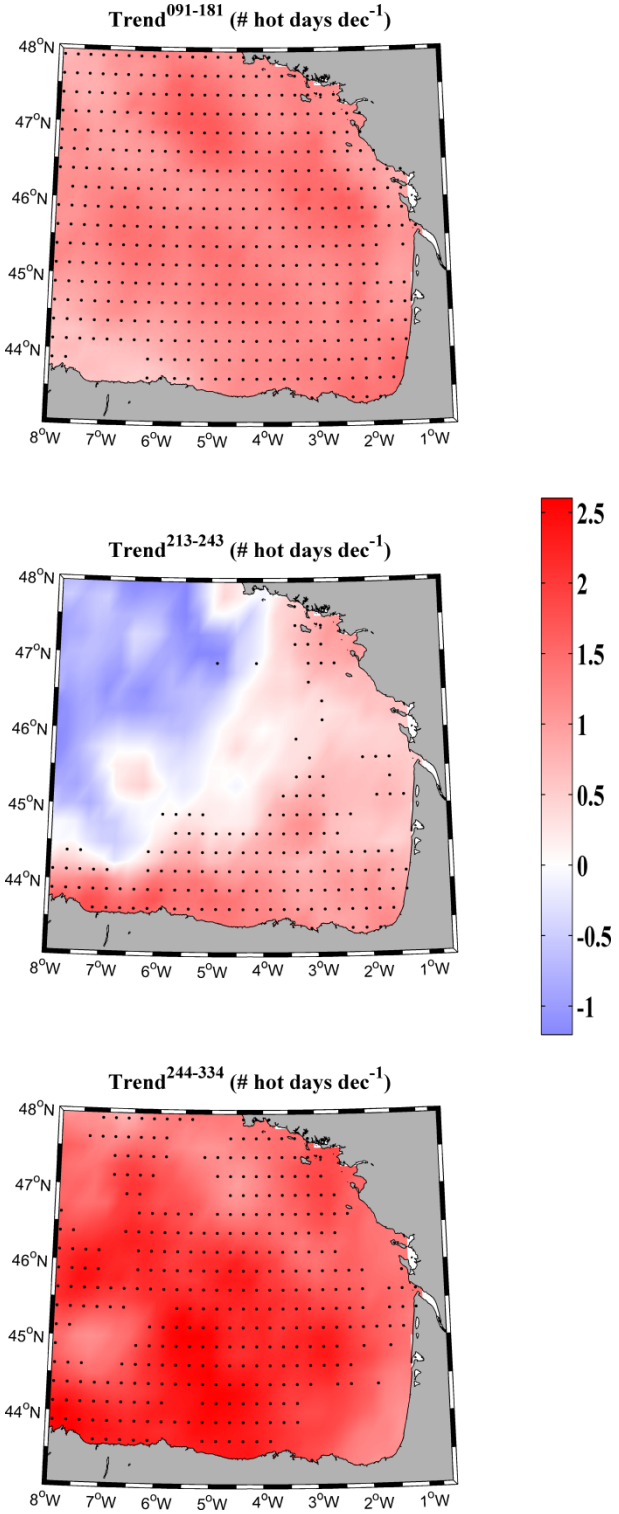

Figure 6.5. (a) April–June, (b) August and (c) September–November trend in the number of extreme hot SST days (# days dec^{-1}). Trend values in (a) and (c) were normalized at monthly values. Black dots represent the grid points with a significance level higher than 95%.

6.3 Discussion

Annual SST trends measured for the Bay of Biscay over the period 1982-2014 (0.26±0.03 ºC per decade averaging pixels shown in Figure 6.1b) are similar to the ones obtained in previous studies carried out in the area. In general, SST trends are highly dependent upon spatial and temporal scales, as well as the database used, as shown Table 6.1.

Thus, deCastro et al. (2009) observed an annual SST warming between 0.15-0.45 ºC per decade from 1985 to 2006 that agrees with the values shown in this study. However, these authors detected a higher warming over the north and northwest area of the bay being the lowest values observed in the southwestern area. Michel et al. (2009b) analyzed annual SST trends in the Bay of Biscay and their surrounding area over the period 1986-2005. They detected the highest warming over the Armorican shelf (roughly 0.5ºC per decade) north of 47ºN, so, their results partially agree with those presented in Figure 6.1b. Michel et al. (2009a) also analyzed annual SST from simulations and satellite data in the bay and it surrounded area from 1985 to 2003. They notified a warming trend ranging from 0.22 to 0.37 ºC per decade depending on the used method. In addition, Koutsikopoulos et al. (1998) found that the southeastern corner showed a stronger warming trend and they did not find statistically significant trends in the northern area over the period 1972-1993. Lima and Wethey (2012) studied coastal SST trends all over the world from 1982 to 2010 by means of the database used in this study. They obtained a SST trend of ~ 0.25 ºC per decade along the coast of the Bay of Biscay which is similar to the one observed in the present study. In addition, Gómez-Gesteira et al. (2008) also showed the same coastal SST warming using data from the AVHRR database. Studies carried out with data from punctual sampling in the southeastern part of the bay showed different warming rates, probably due to the different time periods and databases considered. Thus, Planque et al. (2003) and Llope et al. (2006) detected higher warming trends, whilst Goikoetxea et al. (2009) found a lower SST warming that fits better the results shown in the present study.

The observed annual warming rates are in good agreement with those observed in the North Atlantic. In this sense, Taboada and Anadón (2012) analyzed annual SST trends over the period 1982-2010 using data derived from the AVHRR sensors. They detected an overall warming pattern which rate depends on the location. Thus, for example, a warming trend of 0.2-0.3 ºC per decade can be observed for the Bay of Biscay. In addition, Levitus et al. (2009) observed an annual warming rate of 0.41 ºC per decade for the whole North Atlantic considering the first 700 meters of the water column over the period 1969-2008.

A seasonal analysis of the evolution of the SST for the whole Bay of Biscay has been conducted for a similar period of time. Spring and summer trends were analyzed

by deCastro et al. (2009) using SST satellite data over the period 1985-2006. They also found strong warming rates during spring (0.48 ± 0.13 ºC per decade for April-June), although considerably higher than observed in the present study. In addition, they also detected a high increase during summer (0.54 ± 0.10 ºC per decade for July-September), which is much higher than observed here for those months. Their spatial pattern affects most of the area, especially the northern part. This pattern contrasts with the significant SST trends shown, in the present study, only at coastal areas in July and August. The reason for these discrepancies is twofold. On the one hand, the present study also considers the last decade, when the warming rate has been considerably lower than in previous decades as it was shown in Chapter 4 for the surface water using Argo floats. On the other hand, the behaviour observed for the three months under study is not homogeneous (September is clearly different from the rest) (Figure 6.3; Table 6.2) which suggest that calculating trends at seasonal scale is not the best strategy. This shows the importance of carrying out the analysis at monthly scale to better understand SST variability.

SST cooling observed along the French coast during winter months (from December to March, Figure 6.3) is linked to the particular features of that area. The area is under the influence of Gironde and Loire rivers, whose plume can originate a thermal inversion due to the presence of colder and less-saline water during the months with high discharges (Koutsikopoulos and Le Cann, 1996; Puillat et al., 2004). Winter wind can also play an important role (Lazure and Jegou, 1998) since it pushes and confines the plume in the near-shore area, which is partially isolated from the rest of the bay. Some studies have shown that river discharge increases the stratification since freshwater decreases near surface density creating a layer (usually called “barrier layer”) that difficulties the vertical mixing (e.g: Vizy and Cook, 2010; Park et al., 2011; Materia et al., 2012). As a consequence, water at this nearshore area warms at a different rate than adjacent shelf water. A detailed analysis of the different warming pattern detected along this nearshore strip will be carried out in the last chapter of this thesis.

The strongest SST warming occurred during April-June and September-November (Figure 6.3) whilst a more moderate warming was observed during summer (July-August). These results contrast with those developed by Koutsikopoulos et al. (1998), who suggested that the warming trends observed from 1972 to 1993 were due to mild winter more than to warm summers. Monthly SST trends obtained in the present study suggest that warming is due to changes in the extent of the warm season more than to warmer summers or milder winters. This hypothesis is corroborated by Figure 6.4 that shows a remarkable increase in the extent of the warm season (6-14 days per decade). This fact only coincides partially with the idea of a “deseasonality” suggested by Fontán et al. (2008) and Goikoetxea et al. (2009). These authors describe the prevalence of long warm summers and cold winters that modify the classical seasonal cycle at mid-latitudes. Here, summers are longer and only slightly warmer but winters

are not colder in most of the area. We should mention that both works analyze the southeastern part of the bay, where our results (Figure 6.3) show a strong warming in August and a negligible warming during winter months. As it was mentioned previously, the highest increase in the duration of the warm season (~14 days per decade) was observed at the northeastern corner of the area. These high values can also be observed at the English Channel but not in the rest of the Bay of Biscay.

The increase in the frequency of extreme hot SST events (Figure 6.5) in the Bay of Biscay in spring (1.16±0.23 days per decade) and autumn (1.81±0.42 days per decade) can be compared with the observed by other authors. Lima and Wethey (2012) analyzed the variability of extreme hot days in coastal SST for the same area and detected an increase in the number of hot days on the order of 10-15 days per decade. Nevertheless, the considered annual scale does not allow identifying whether the increase was continuous throughout the year or concentrated on particular periods. Actually, deCastro et al. (2014) found important intra-annual variations in adjacent areas like the western Iberian Peninsula.

As it was pointed out in the introduction section, changes in the timing of the warm season along with the excess of extreme hot SST days can drive important changes in marine ecosystems. Thus, Wethey et al. (2011) showed the importance of extreme events in the context of long term climate change to determine the biogeographic distribution of different intertidal populations in the Bay of Biscay. Similarly, Fernández (2011) and Voerman et al. (2013) related the loss in kelp abundance and diversity to the increase in summer mean SST and in the number of extreme SST values (over >20ºC) along the Spanish coast of the bay. In addition, different studies analyzed the influence of changes in SST over pelagic species, some of which constitute important fisheries in the Bay of Biscay. In this way, Planque et al. (2007) and Bellier et al. (2007) analyzed the potential spawning habitat of sardine (*Sardina pilchardus*) and anchovy (*Engraulis encrasicolus*) and the fluctuations in spawning locations. These authors detected that the anchovy spawning region was displaced northward probably due to warmer temperatures during the 90s over the French continental shelf. Dufour et al. (2010) studied changes in migration phenology and spatial distribution of albacore (*Thunnus alalunga*) and bluefin (*Thunnus thynnus*) tunas. They detected that albacore and bluefin had advanced their arrival at the bay at a rate of 2 and 5.6 days per decade, respectively. In addition, they observed that the latitude at which catches occurred inside the bay drifted northward. Sagarminaga and Arrizabalaga (2010) also detected an earlier arrival of albacore juveniles to the bay. Both studies linked these changes in the migration phenology with interannual variability in spring warming. On the other hand, changes mentioned above, influence the biological activity over the whole Bay in a different way since changes in the SST force variations in the mixed layer depth (e.g: Somavilla et al., 2009; Taboada and Anadon, 2012). Thus, Somavilla et al. (2009) associated a deeper mixed layer depth, as a consequence of colder winter, with higher surface concentrations of nutrients, which

in turn, favour an enhancement of the spring bloom in the Bay of Biscay. So, an increase in the duration of the warm season and an increase in the number of extreme hot SST days favour a higher stratification of the water column. This fact complicates the supply of nutrients from deeper layers to the mixed layer and therefore the availability of nutrients.

Therefore, changes in the timing of seasonal warming and changes in the frequency of extreme hot SST days are important to understand changes in marine ecosystems and to determine scenarios and policies to mitigate those changes. Likewise, results obtained in the present study evidence the importance of regional studies since SST changes show a high spatial and temporal variability.

6.4 Conclusions

SST variability was analyzed for the Bay of Biscay over the period 1982-2014 using the NOAA OI ¼ degree daily SST database. SST trends at monthly scale, the duration of the warm season and changes in the number of extreme hot SST days were considered to better understand the SST variability of the area. The main findings of the present study can be summarized as follows:

- The observed warming, which is the prevalent trend in the bay, is more related to the increase in the duration of the warm season than to the existence of warmer summers or milder winters.

- The warm season has expanded in approximately one month during the last three decades due both to the advance in the beginning of the season as to the delay in its finalisation.

- Warming in SST is linked to an increase in the number of extreme hot events. A significant increase in the number of extreme hot SST days has occurred during the months affected by the increase of the warm season (April-June and September-November).

- These results prove that analysing trends at annual or even seasonal scale can be insufficient to understand the complexity of climate changes. Analysis at monthly or daily scale and focusing on changes in seasons and extreme events seems to be an alternative to understand the real extent of the changes under progress and its impact on marine ecosystems.

Chapter 7: Warming modulation by Loire and Gironde river discharges

The influence of the turbid plume formed by Loire and Gironde River discharges over the SST in the eastern Bay of Biscay (0.6º-36.6ºW, 44.2-47.8ºW) will be studied in this chapter. This analysis will be carried out during months of maximum plume extension by means of two complementary databases (MODIS and $OISST_{1/4}$). SST trends will be related with changes in river runoff and the direction and intensity of winds. In addition, correlations between SST variations and both NAO and AMO indexes will be calculated.

7.1 Methods

7.1.1 River plume detection

Normalized water-leaving radiance (nLw) was retrieved from MODIS database over the period 2002-2014. MODIS allows selecting several values of normalized water-leaving radiance. Some nLw bands (412, 443, 469) were discarded because their high depth of penetration. The characterization of the river plume formed by Loire and Gironde Rivers was carried out by means of two nLw values (555, 645) obtaining a similar behavior. Although the 555 nm band provides one of the strongest turbid signals to determine river plumes (Nezlin and DiGiacomo, 2005; Nezlin et al., 2005; Saldias et al., 2012), the 645nm band was selected because it has a lower penetration that allows analyzing shallow areas preventing bottom influence. A turbid threshold of 0.2 $mWcm^{-2}\mu m^{-1}sr^{-1}$ was obtained to delimit the turbid river plume for this band following the methodology described in Fernández-Nóvoa et al. (2015). Daily nLw 645 from MODIS-Aqua and MODIS-Terra were merged following Mendes et al. (2014). This allows obtaining a larger number of available pixels increasing the consistency of the study. These merged images were then interpolated into a regular mesh (0.01º × 0.01º). Monthly SST trends were calculated assuming linear regression.

7.1.2 SST trend calculation

SST values were retrieved from MODIS and $OISST_{1/4}$ over the periods 2002-2014 and 1982-2014, respectively. SST data from MODIS was obtained using 11-12 µm channels since these bands are located close to the maximum of the Earth's emission and have larger bandwidth than other available channels (Reinart and Reinhold, 2008). This SST product has been shown to be suitable to analyze water surface temperatures in previous studies (Barré et al., 2006; Reinart and Reinhold, 2008; Chavula et al., 2009). SST images from MODIS-Aqua and MODIS-Terra were also merged following Mendes et al. (2014). SST values from both databases were averaged at monthly scale. Then, monthly SST anomalies were calculated and, finally, linear trends were calculated using monthly SST anomalies.

7.1.3 Wind and heat fluxes

Wind and heat fluxes data were retrieved from the CFSR database. CFSR wind data was chosen because it presents a great correlation with buoy measurements (Álvarez et al., 2014). Wind data at a reference height of 10 m were daily averaged for two locations near Gironde and Loire mouth (Figure 7.1, red dots).

Heat fluxes (shortwave, longwave, latent heat and sensible heat) were also obtained from the CFSR database at monthly scale. The net heat flux (Q_T) through the ocean surface was calculated following equation 1:

$$Q_T = Q_{SW} + Q_{LW} + Q_S + Q_L \quad (1)$$

where Q_{SW} is the shortwave flux, Q_{LW} is the longwave flux, Q_S is the sensible heat flux and Q_L is the latent heat flux. A negative (positive) heat flux implies that ocean is losing (gaining) heat.

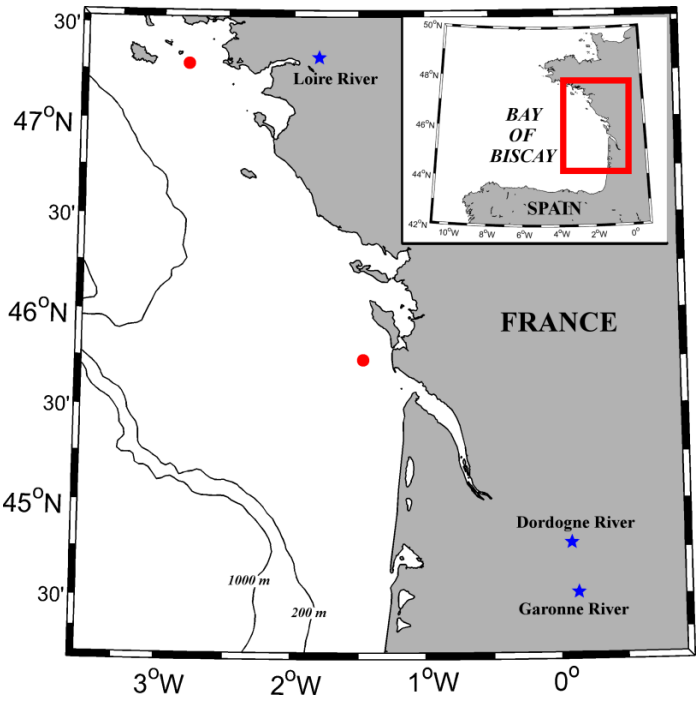

Figure 7.1. Bathymetry of the region under study. Contour lines represent, 200 and 1000 m isobaths. Red dots mark the location where wind was obtained. Blue asterisks mark the location where river discharge was sampled.

7.1.4 River discharge data

Daily runoff data for Loire and Gironde Rivers were obtained from the Banque Hydro French Database (http://www.hydro.eaufrance.fr/). River runoff is available over the period 1997-2014 for the Gironde and 1982-2014 for the Loire. The Gironde discharge was obtained as the sum of Dordogne and Garonne Rivers discharge. Daily data were averaged at monthly scale. River discharge data were sampled at positions marked with blue asterisks in Figure 7.1.

7.2 Results

The monthly area occupied by the turbid plume generated by Loire and Gironde Rivers (averaged from 2002 to 2014) is shown in Figure 7.2. River plume extension is

higher from December to February with values over 25,000 km^2. In general, those months are characterized by high river discharges (surpassing 1000 m^3s^{-1} for both rivers) as shown in Figure 7.3. However, there are other months (especially spring months) characterized by high river discharges where the river plume is considerably smaller. This fact implies that other factors besides the river discharge can also modulate the river plume.

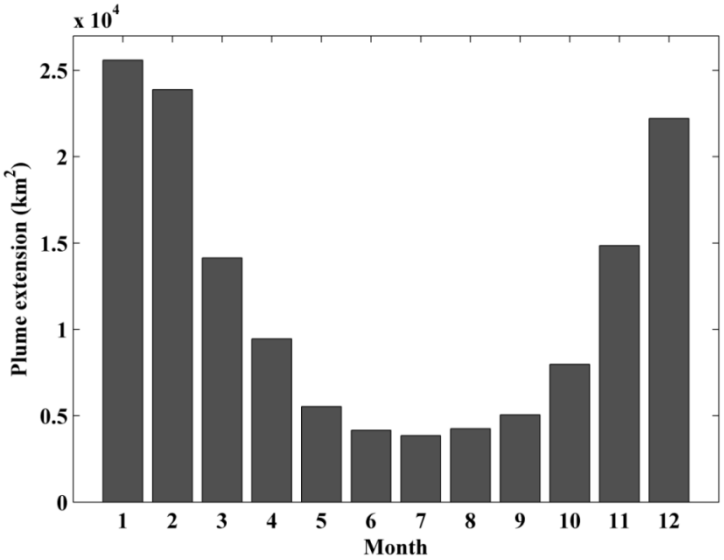

Figure 7.2. Monthly mean area (km^2) occupied by the turbid plume formed by Loire and Gironde Rivers discharges over the period 2002-2014.

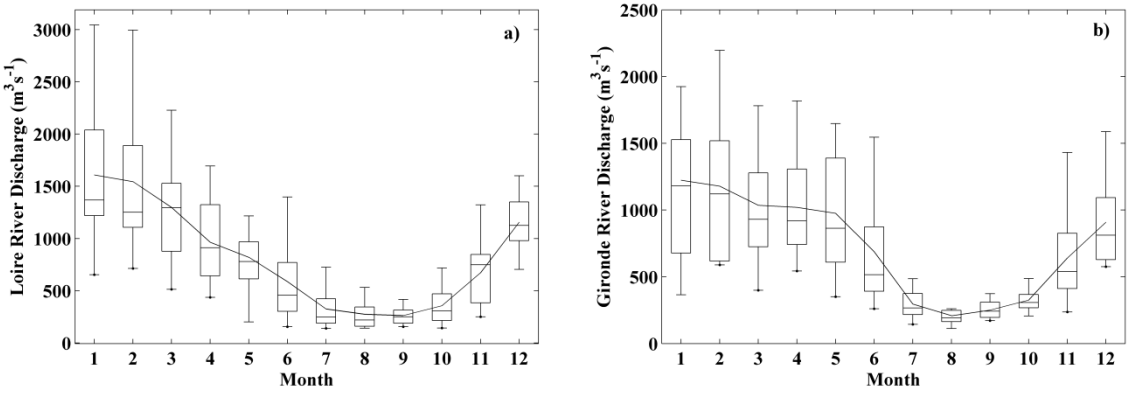

Figure 7.3. Annual hydrologic cycle variability (m^3s^{-1}) for (a) Loire and (b) Gironde runoff over the period 2002-2014. Solid black line represents the monthly average flow and the line inside each box represents the median for each month. Lower and upper whiskers show minimum and maximum river flow, respective, whilst lower and upper box indicate first and third quartiles, respectively.

The second main factor that conditions the extension of the river plume is wind (Mendes et al., 2014; Fernández-Nóvoa et al., 2015). Wind direction is mainly southwesterly from December to February as shown in Figure 7.4. Taking into account the coast orientation, southwesterly winds tends to accumulate material provided by river discharge near coast and to decrease cross-shore transport and dilution (Chao, 1988; Mendes et al., 2014). This behavior favors the retention and maintenance of the

plume on a large area. Due to this fact, the further analysis will be focus on December-February (DJF) period when the extent of the plume attains the highest values.

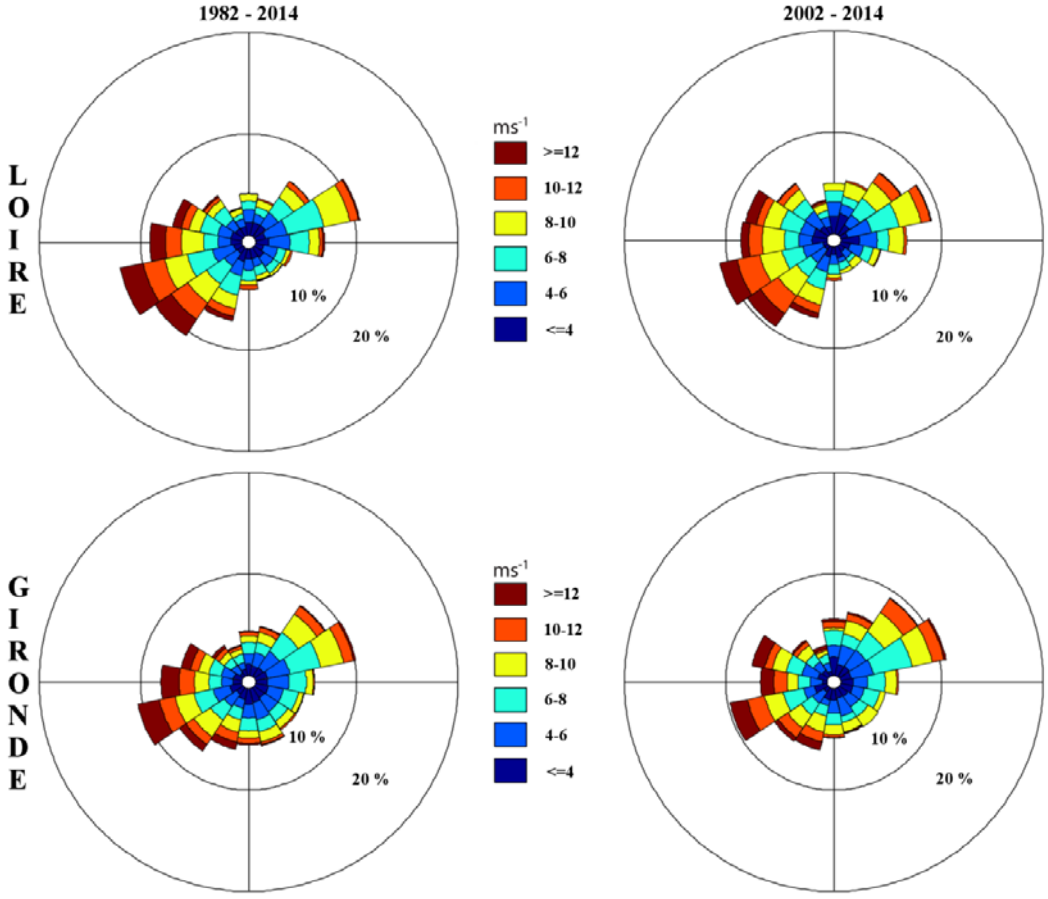

Figure 7.4. Wind rose (ms−1) representing DJF winds near Loire (upper panels) and Gironde (lower panels) over the periods 1982-2004 (left) and 2002–2014 (right).

The mean DJF plume averaged over the period 2002-2014 is shown in Figure 7.5. It has an offshore extension of 100 km and maximum turbid values on the order of 2 $mWcm^{-2}\mu m^{-1}sr^{-1}$ near Loire and Gironde estuaries. In addition, a band of high turbid values (exceeding $1mWcm^{-2}\mu m^{-1}sr^{-1}$) can be observed near coast between Loire and Gironde Rivers. Dark solid line corresponds to the threshold of 0.2 $mWcm^{-2}\mu m^{-1}sr^{-1}$ mentioned above.

The mean DJF SST field calculated from $OISST_{1/4}$ data and averaged over the period 2002-2014 is shown in Figure 7.6a. Minimum values (close to 9.5ºC) are located near the mouth of both rivers. In addition, a band with low temperatures (below 10.5ºC) can also be observed near coast between Loire and Gironde estuaries. This fringe of low temperature is very similar to the fringe of high turbid values in the area occupied by the plume (Figure 7.5), which suggest that the coldest SST values are related to the distribution of the turbid plume. In fact, there is a considerable difference (greater than 3ºC) between the area more influenced by the turbid plume, with values below 10ºC,

and the area outside the plume influence, with values above 13ºC. The mean DJF SST field calculated from MODIS data over the same period (Figure 7.6b) is very similar to the one calculated from $OISST_{1/4}$ data.

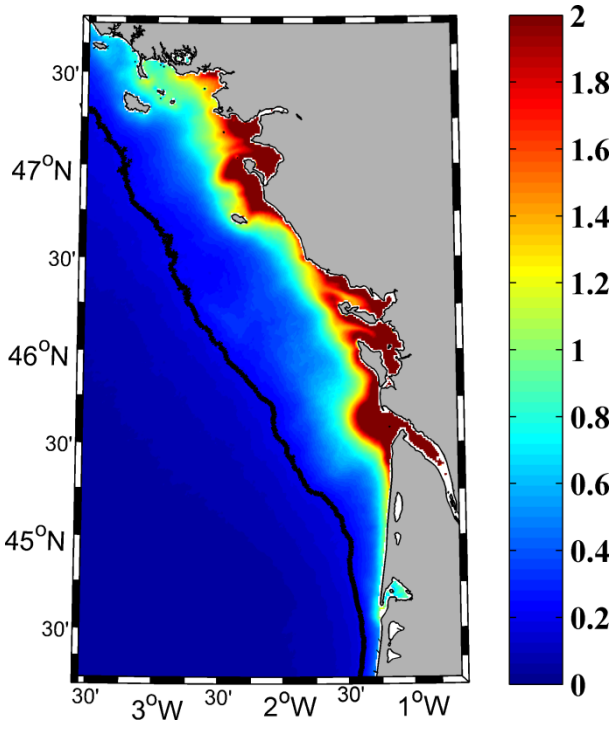

Figure 7.5. Mean DJF turbid plume ($mWcm^{-2}\mu m^{-1}sr^{-1}$) calculated over the period 2002-2014. The contour line corresponds to the turbid threshold 0.2 $mWcm^{-2}\mu m^{-1}sr^{-1}$).

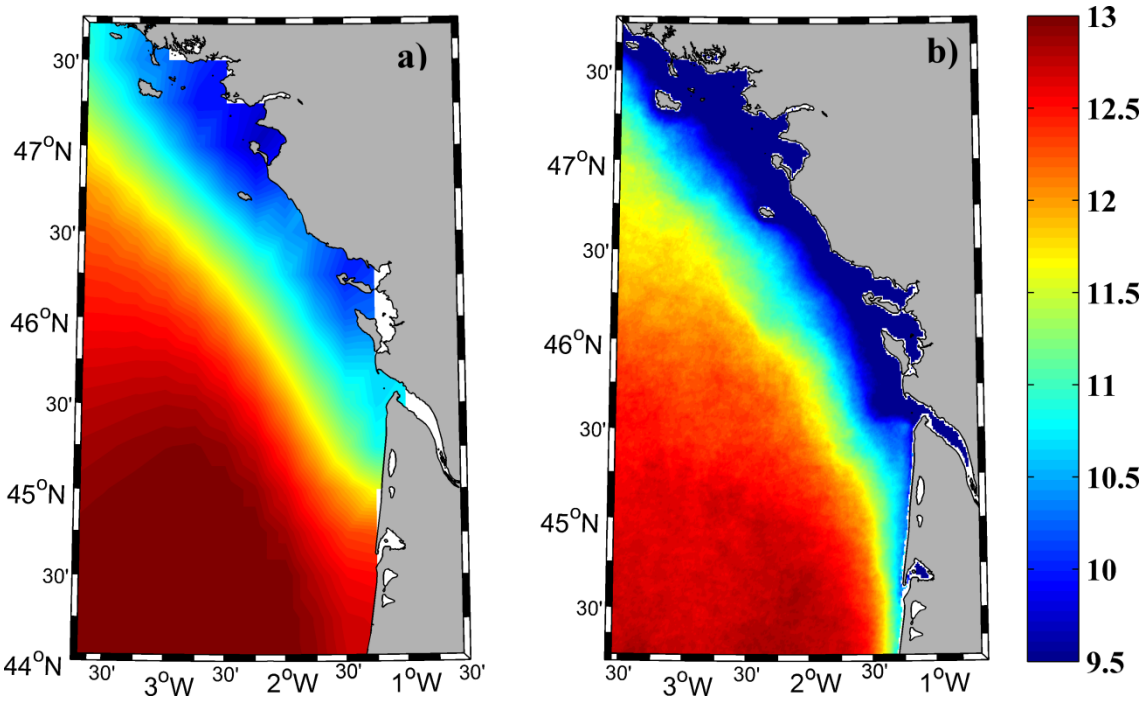

Figure 7.6. Mean DJF SST (ºC) calculated over the period 2002-2014; (a) $OISST_{1/4}$ (b) MODIS.

DJF SST trends were calculated over the period 2002-2014 using $OISSST_{1/4}$ (Figure 7.7a) and MODIS (Figure 7.7b) data. DJF SST trends calculated using the $OISST_{1/4}$ show a continuous cooling along the French coast north of 45ºN. This cooling was previously observed in some winter months in Chapter 6. The highest cooling (~ -0.5ºC per decade) was observed close to Loire estuary and north of Gironde estuary. This cooling strip contrasts with the warming observed for the rest of the area. In spite of the limited length of the series (only the period with available MODIS data was considered), trends are observed to be significant at 90%. DJF SST trends calculated from MODIS data (Figure 7.7b) show a similar pattern with a moderate cooling in most of the area influenced by the plume and a warming, reaching values close 0.5ºC per decade, outside the river plume area. Obviously, the signal is noisier than the one calculated with $OISST_{1/4}$. We should note that MODIS data are obtained at a much finer resolution (~0.01º instead of 0.25º) and have not been interpolated in such a way that voids due to cloud coverage or satellite malfunction can limit the number of available data at some grid point and bias trends at those locations.

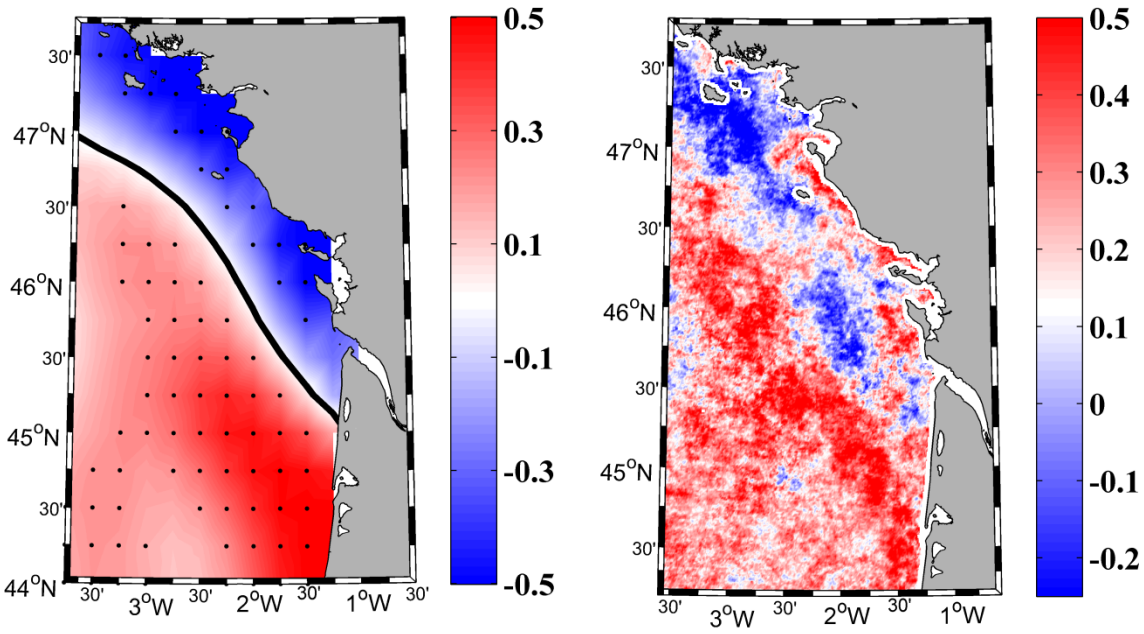

Figure 7.7. DJF SST trends (ºC per decade) calculated over the period 2002-2014; (a) $OISST_{1/4}$. (b) MODIS. Contour line corresponds to null trend. Black dots represent grid points with significance higher than 90%.

Both databases have shown similar mean and trend patterns (Figures 7.6 and 7.7). This allows extending back the period of study to the total length of $OISST_{1/4}$ database (1982-2014). The pattern depicted in Figure 7.8 is similar to the one described in Figure 7.7 but covering a longer period. Overall, warming (~0.3 ºC per decade) was observed in most of the area under scope, with the exception of small nearshore zones close to the mouths of Gironde and Loire, where a maximum cooling rate of approximately -0.15 ºC per decade was observed. In summary, coastal cooling is maintained even when the period under study is extended to the last 30 years. This

phenomenon is not a particular event that occurs only during the short period of time covered by MODIS data.

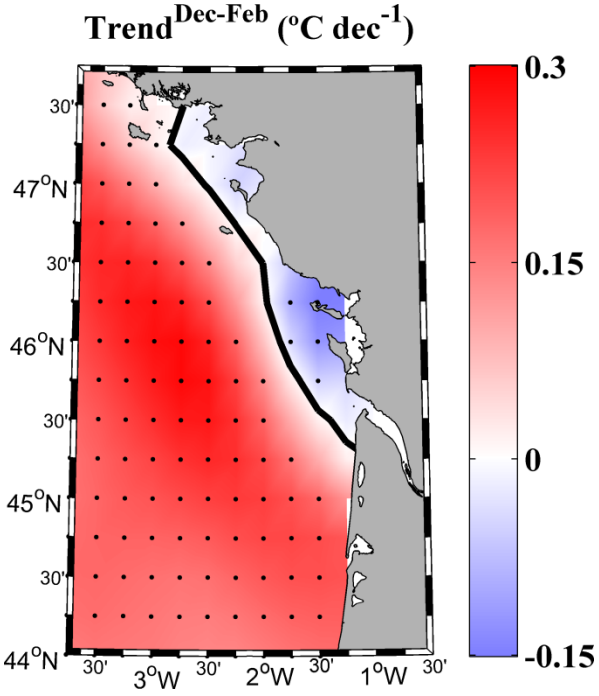

Figure 7.8. DJF SST trends (ºC per decade) calculated over the period 1982-2014 with $OISST_{1/4}$ data. Contour line corresponds to null trend. Black dots represent grid points with significance higher than 90%.

DJF trends in total heat flux (Figure 7.9a) calculated over the period 1982-2014 show a similar pattern to the one observed for DJF SST trends (Figure 7.8). Ocean trends range from -7 to -11 W m^{-2} per decade whilst the trend in the nearshore strip ranges from -3 to -5 W m^{-2} per decade. Note that ocean loses heat during DJF, so a negative trend means that the loss rate has increased. So, ocean is losing heat now at a higher rate than three decades ago. Following Somavilla et al. (2009) the radiative term can be neglected in DJF because shortwave and longwave fluxes balance each other. In this sense, changes in the total heat flux are mainly due to changes in the turbulent term (latent and sensible fluxes). In addition, Somavilla et al. (2009) also state that DJF sensible heat flux is close to zero being negligible when compared with the latent heat flux. Thus, the pattern depicted in Figure 7.9b, where only latent heat flux has been considered, is very similar to the one depicted in Figure 7.9a for the total heat fluxes. In both cases (total heat and latent heat), only ocean trends are statistically significant at 95%.

Differences between ocean and coastal areas can be analyzed in terms of oceanic (AMO) and atmospheric (NAO) indices. The influence of AMO on SST anomaly was studied (Figure 7.10a) for DJF over the period 1982-2014. The correlation between both signals is close to zero in the area affected by the river plume whilst it is significantly positive for the rest of the region. This fact evidences that the nearshore strip influenced by Loire and Gironde discharges follows a different SST behavior when compared to the oceanic part of the bay. We should note that AMO represents the SST anomaly of

the North Atlantic. The lack of correlation with the coastal zone close to Loire and Gironde Rivers proves that the SST at that particular area is more dependent on coastal than on oceanic features. The influence of NAO index on SST anomaly over the area under scope was also considered under the temporary conditions described above. Figure 7.10b shows significant positive correlation (>0.4) between SST NAO index for the months under study only in the area influenced by the river plume, which evidences its influence on coastal SST. It is a well-known fact that winter NAO is positively correlated with surface temperature over most of the Northern part of the European Continent (http://www.cpc.ncep.noaa.gov/). That influence is reflected here only for the part of the bay close to the rivers.

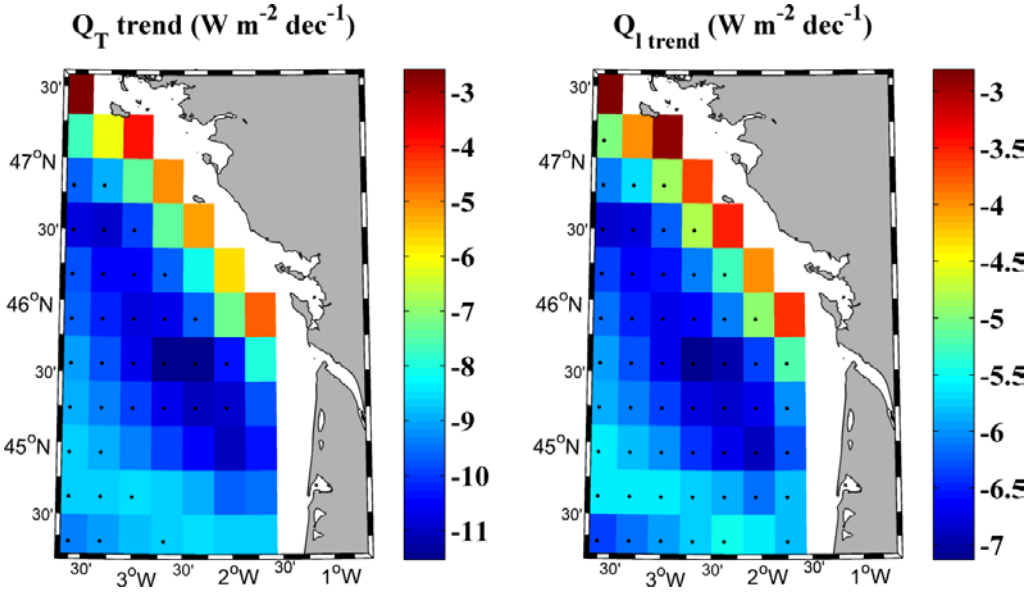

Figure 7.9. DJF trends in heat fluxes (W m^{-2} per decade) calculated over the period 1982-2014 with CFSR data. (a) Total heat; (b) Latent heat.

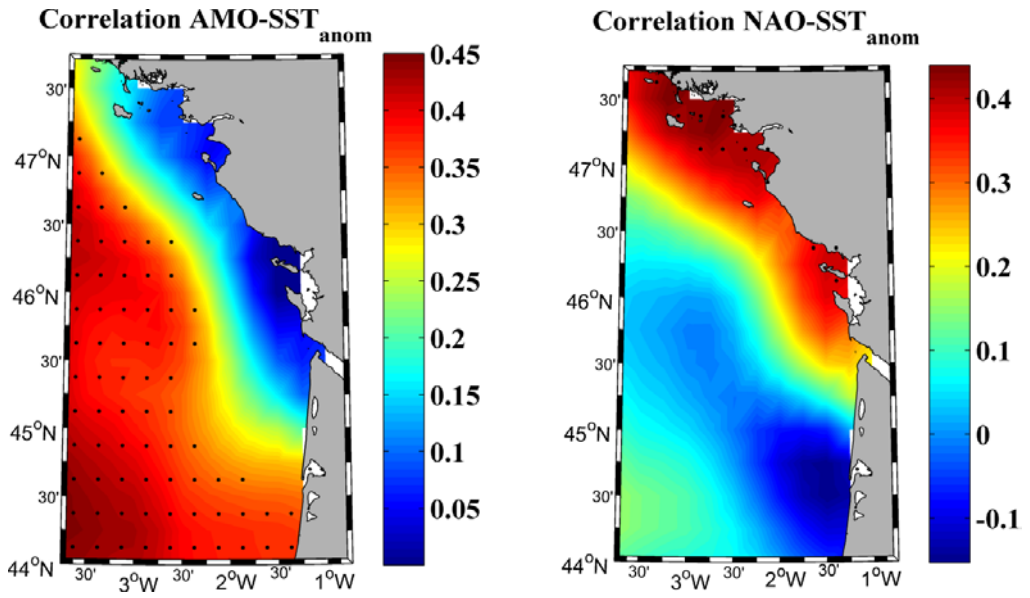

Figure 7.10. Correlation between DJF NAO (a), DJF AMO (b) indices and DJF SST anomaly over the period 1982-2014. Black dots represent grid points with significance higher than 95%.

7.3 Discussion

The area affected by Gironde and Loire Rivers has shown different winter SST trends when compared with the adjacent oceanic part of the Bay of Biscay. Overall, SST tends to warm at the oceanic part and to cool slightly at the part influenced by rivers (Figure 7.8). This fact is corroborated by heat flux patterns and by the dependence on atmospheric and oceanic indices. Thus, the coastal area where both rivers flow into the ocean is the only part of the Bay where SST depends on NAO but not on the SST of the North Atlantic represented by AMO. In the same way, figures 7.7 and 7.8 show that coastal cooling is limited to the north of 45º. Previous studies that analyzed wintertime SST trends in this coastal area over a similar period are not conclusive. Gómez-Gesteira et al. (2008) mentioned that coastal warming is negligible along the French coast over the period 1985-2005 during winter and fall, whilst they observed a high increase during spring and summer. However, Planque et al. (2003) showed that warming was greater in the southeastern corner of the Bay during winter.

In a wider context, there are several drivers that can cause different coastal SST trends when compared with the ones observed at adjacent oceanic areas. Possibly, coastal upwelling is the most studied cause (Relvas et al., 2009; Santos et al., 2011; 2012a; 2012b; 2012c; deCastro et al., 2014). Nevertheless, upwelling is not a key phenomenon in the area, especially in winter. The southeastern corner of the Bay is characterized by a high continental influence during summer due to the concavity of this area (Valencia et al., 2003; 2004). However, advection from land to ocean was also discarded in the area following Cattiaux et al. (2011). Different authors have identified the presence of large rivers as the main cause of unusual cooling (Howden and Murtugudde, 2001) or warming (Belkin, 2009; Vizy and Cook; 2010; Park et al., 2011; Materia et al., 2012). The importance of the river discharge can be put into context for the particular case under study since the combined discharge of both rivers (~2500 m^3s^{-1}) is higher than the flow per kilometer of coast of upwelled water observed for the main upwelling system over the world (Patti et al., 2008).

The mechanism proposed by different authors (Belkin, 2009; Vizy and Cook, 2010; Park et al., 2011; Materia et al., 2012) to explain the especially intense surface warming observed at certain areas affected by large rivers is based on the development of a buoyant surface layer that traps solar radiation and enhances vertical stratification. The mechanism is strengthened by positive feedback since the partially isolated surface layer is warmed by solar radiation that increases surface temperature which results in density decrease and hence reinforcement of stratification. These previous studies are focused on spring-summer periods when riverine water is warmer than offshore water. A similar mechanism can be invoked in the present study. The river plume is much fresher and colder (Figure 7.6) than the surrounding water. In spite of the possible existence of a thermal inversion near surface (Koutsikopoulos and Le Cann, 1996), the

stability of the water column is kept due to the continuous supply of freshwater. Overall, the surface water near coast is cooled by the atmosphere but vertical mixing is inhibited by density differences produced by near surface fresh water. Thus, in a context of global warming, offshore water warms at a much higher rate than near shore water. Here, the positive feedback mechanism mentioned for other areas is no longer valid since surface water tends to cool and surface density to increase. In addition, the combined discharge of both rivers is rather moderate when compared to the rivers considered in the studies mentioned above (Congo, Amazonas or Yangtze). Thus, in spite of the shallowness of the area, the zone affected by the river plume is much smaller than observed for those large rivers.

Previous research carried out at other locations (Mendes et al., 2014; Fernández-Nóvoa et al., 2015) has proved that the extension of the plume is strongly dependent on river runoff and prevailing winds. The role of winds in the area is also corroborated by different works (Lazure and Jegou, 1998; Puillat et al., 2004; 2006). In the present case, changes in DJF river runoff over the period 1982-2014 can be considered negligible for Loire River (on the order of -40 m^3s^{-1}per decade). Actually, the observed trends are not statistically significant and strongly dependent on the length of the series. To remove or add a single year can drive the trend from positive to negative (or vice-versa). River runoff increases at a rate on the order of 120 m^3s^{-1}per decade (still not significant) when considering the last period (2002-2014), which coincides with a stronger coastal cooling as shown in Figure 7.7. As we mentioned above, the area affected by the plume has little horizontal mixing with the rest of the area due to the prevailing winds that tend to compress the plume decreasing the cross-shore transport and dilution (Chao, 1988; Mendes et al., 2014). This behavior favors the retention and maintenance of the plume on a large area, partially isolated from the rest of the bay. Changes in the duration and intensity of prevailing DJF southwesterly winds were also analyzed at the stations located close to the mouth of Gironde and Loire Rivers (Table 7.1). Null trends were observed for duration and intensity of these winds over the period 1982 to 2014. Nevertheless, trends are positive and significant (Table 7.1) when considering the short period 2002-2014. SW winds tend to intensify and be more frequent during this period. This results in a higher compression and retention of the plume near coast which, in turns, results in a more marked cooling in that area as depicted in Figure 7.7.

		Area	**2002-2014**	**1982-2014**
SW winds	**Duration (days dec^{-1})**	Loire	11	--
		Gironde	13*	--
	Intensity ($ms^{-1}dec^{-1}$)	Loire	1.6**	--
		Gironde	1.6**	--
River	**Runoff ($m^3s^{-1}dec^{-1}$)**	Loire	126	-40
		Gironde	122	n/a

Table 7.1. Trends in wind intensity and duration and in river discharge. Values with null trends are marked with --. Statistical significance at 95% || 99% is marked with * || **.

7.4 Conclusions

The influence of Loire and Gironde discharges on SST changes was analyzed in the eastern part of the bay. The main conclusions of this study were the following:

- The ocean area warms while the coastal area suffers a light cooling with low significance over the period 1982-2014.

- Differences between coastal and oceanic warming are reinforced during periods when river discharge and SW winds are over their mean values (e.g. 2002-2014). This results in a significant cooling in the area influenced by freshwater inputs.

- The mere presence of a freshwater layer is able to modulate the warming observed at the adjacent ocean locations even in absence of significant changes in the properties of the plume like its extent or freshwater content.

General conclusions

This thesis was conceived as an attempt to determine changes in thermohaline variables, as well as to analyze their causes and physical implications, for the whole Bay of Biscay over the last decades. The main results obtained were the following:

- The two main upper water masses in the bay have experienced significant changes. ENACW has been observed to warm and salinificate over the period 1975-2010 and also during the decade 2004-2013. On the contrary, a significant cooling and freshening was detected for MW over the period 2004-2013. The main cause of these variations was changes in the regions where the water masses are originated each year.

- Mixed layer depth tended to sink at the southeastern corner of the bay and to be shallower at the rest of the bay over the period 1975-2010. Air temperature plays a key role in regulating the MLD variability. In this way, negative air temperature trends, localized in the southeastern part of the bay, were related with MLD deepening at this area and positive air temperature trends observed for the rest of the bay were related to MLD shoaling.

- A surface warming was detected for the whole bay since 1982 (0.26 ºC per decade). Warming is more related to the increase in the duration of the warm season than to the existence of warmer summers or milder winters. In addition, months affected by the increase of the warm season (April-June and September-October) also suffered a significant increase in the number of extreme hot SST days.

- In the present warming context of the bay, the only area where a cooling was observed since eighties is the coastal strip under the influence of the river plume formed by Loire and Gironde Rivers during winter months. Cooling was more intense during periods when river discharge and Southwesterly winds are over their mean values (e.g. 2002-2014).

Acronym and abbreviation list

- **AABW**: Antartic Bottom Water.
- **AMO**: Atlantic Multidecadal Oscillation.
- **AMSR:** Advanced Microwave Scanning Radiometer.
- **AO**: Artic Oscillation.
- **AVHRR**: Advanced Very High Resolution Radiometer.
- **CFSR**: Climate Forecast System Reanalysis.
- **CTDs**: Conductivity, temperature, depth sensors.
- **Dec^{-1}:** Per decade
- **EA**: East Atlantic pattern.
- **ENACW**: Eastern North Atlantic Central Water.
- **$ENACW_{sp}$**: Eastern North Atlantic Central Water subpolar branch.
- **$ENACW_{st}$**: Eastern North Atlantic Central Water subtropical branch.
- **GCOS**: Global Climate Observing System.
- **IPC**: Iberian Poleward Current.
- **IPCC**: Intergovernmental Panel on Climate Change.
- **LSW**: Labrador Sea Water.
- **MBTs**: Mechanical bathythermograph
- **MLD**: Mixed layer depth.
- **MODIS**: Moderate Resolution Imaging Spectroradiometer.
- **MOW**: Mediterranean Outflow Water.
- **MW**: Mediterranean Water.
- **NADW**: North Atlantic Deep Water.
- **NAO**: North Atlantic Oscillation.
- **NCAR**: National Center for Atmospheric Research.
- **NCEP**: National Center for Environmental Prediction.
- **nLw**: Normalized water-leaving radiance.
- **NOAA**: National Oceanic and Atmospheric Administration.
- **NSW**: Norwegian Sea Water.
- **OI**: Optimum Interpolation.
- **$OISST_{1/4}$**: NOAA ¼º Optimum Interpolation sea surface temperature database.
- **P-E**: Precipitation minus Evaporation.
- **PLD**: Isopycnal Layer Depth.
- **PSD**: Physical Sciences Division.
- **RAOB**: Radiosonde observations.
- **SODA**: Simple Ocean Data Assimilation.
- **SSS**: Sea surface salinity.
- **SST**: Sea surface temperature.
- **SW**: Surface water.

- **Tair**: Air temperature.
- **TLD**: Isothermal layer depth.
- **USGODAE**: United States Global Ocean Data Assimilation Experiment.
- **WOD**: World Ocean Database.
- **XBTs**: Expendable Bathythermograph.

List of figures

Figure 1.1. Average annual surface air temperature anomalies from 1880 to 2014 analyzed using independent methods by four different institutions. Source: NASA Earth Observatory **6**

Figure 1.2. Sea surface salinity change from 1950 to 2008. Seasonal and El Niño-Southern Oscillation signals were removed. Salinity values are expressed on the Practical Salinity Scale 1978 (Fofonoff and Lewis, 1979). Source: IPCC (2013) based on Durack and Wijffels (2010). **8**

Figure 1.3. Bathymetry of the Bay of Biscay. Contour lines represent 200, 1000 and 4000 m isobaths. Location of the Bay of Biscay (marked with a red square) in the upper left figure. **11**

Figure 1.4. Annual hydrologic cycle variability (m^3s^{-1}) for Loire runoff over the period 1982-2014. Solid red line represents the monthly average flow and the line inside each box represents the median for each month. Lower and upper whiskers show minimum and maximum river flow, respective, whilst lower and upper box indicate first and third quartiles, respectively. **12**

Figure 1.5. Schematic illustration of circulation in the Bay of Biscay. Source: Reproduced from Koutsikopoulos and Le Cann (1996) modified by OSPAR Commission (2000). **13**

Figure 1.6. Diagram that summarizes the thermohaline properties of the water masses present in the Bay of Biscay in six hydrographic stations (its position can be seen in the small plot on the bottom right). Superimposed lines in the diagram represent isopycnals (kg m^{-3}) Source: Lavín et al. (2006), it was produced with data from ICES and IEO databank. **14**

Figure 1.7. Surface circulation in the Northeastern Atlantic. **15**

Figure 1.8. Annual cycle of the heat fluxes averaged for the whole Bay of Biscay (W m^{-2} per decade) over the period 1982-2014. Data retrieved from the Climate Forecast System Reanalysis database. **16**

Figure 1.9. Sea surface salinity averaged over the period 2003-2011. Data retrieved from the Physical IBI reanalysis product (Copernicus project, http://marine.copernicus.eu/) **18**

Figure 2.1. Process followed by an Argo float to generate each profile. Source: http://www.argo.ucsd.edu/..... **24**

Figure 2.2. Flowchart followed to process the data contained in the OISST ¼. Source: NOAA's National Centers for Environmental Information website..... **26**

Figure 2.3. Monthly values for the AMO index over the period 1950-2014 (A ± 1 month running average was considered). **29**

Figure 2.4. Effects of the positive and negative phases of NAO over the North Atlantic. Source: www.climate.gov..... **30**

Figure 2.5. Monthly values for the EA index over the period 1950-2014 (A ± 1 month running average was considered). **30**

Figure 3.1. Bay of Biscay bathymetry. Dots represent the 0.5ºx0.5º grid of data. The marked isobaths corresponds to −50, −200, −1000 and −4000 m..... **34**

Figure 3.2. Vertical profile of (a) temperature trends (ºC per decade) and (b) salinity trends (per decade) for the entire Bay of Biscay from 1975 to 2010. Circles represent trends with a significance level greater than 95%. **36**

Figure 3.3. T-S diagram of the water masses present in the Bay of Biscay at 3.25ºW and 44.75ºN from 1975 to 2010 till a depth of 700m calculated using SODA database. ENACW is highlighted by means of gray dots. **37**

Figure 3.4. (a) Annual temperature trends (ºC per decade) and (b) annual salinity trends (per decade) corresponding to ENACW in the Bay of Biscay from 1975 to 2010. Black dots represent the grid points where trends with a significance level greater than 99% were obtained. The blanks represent points where ENACW was scarcely detected. **37**

Figure 3.5. (a) Annual temperature trends (°C per decade) and (b) annual salinity trends (per decade) of ENACW mass in the North Atlantic area (0–22.25°W and 41.75–54.25°N) from 1975 to 2010. Black dots represent the grid points where trends with a significance level greater than 99% were obtained. The blanks represent points where ENACW was scarcely detected..... **38**

Figure 3.6. Mean depth of ENACW (m) in the North Atlantic area for the period 1975-2010. The blanks represent points where ENACW was scarcely detected. Dotted line represents the 500 m isobath. **39**

Figure 3.7. (a) Time evolution of temperature (black dotted line) and salinity (solid gray line) of ENACW and NAO index (black solid line) over the period 1975-2010. (b) Time evolution of temperature (black dotted line) and salinity (solid gray line) of ENACW and EA index (black solid line) over the period 1975-2010. The atmospheric indices were calculated for the extended winter (DJFM). Signals were normalized to be represented together. The mean temperature and salinity were calculated using only the grid points with significant trends (>99%) in Figure 3.5, respectively. Shaded areas represent the trends observed for NAO and EA indices..... **41**

Figure 3.8. Air temperature trend (ºC per decade) calculated over the North Atlantic region from 1975 to 2010. Black dots represent the grid points with significant trends (>95%)..... **42**

Figure 3.9. P-E (precipitation minus evaporation) balance trend (mm mo^{-1} per decade) calculated over the North Atlantic from 1975 to 2010. Black dots represent the grid points with significant trends (>95%) **42**

Figure 4.1. (a) Number of profiles for each month. (b) Number of profiles for each pixel on a 0.5° × 0.5° grid covering the Bay of Biscay. **46**

Figure 4.2. T–S diagram of all monthly profiles averaged for the whole area over the period 2004–2013. Superimposed lines in the diagram represent isopycnals (kg m^{-3}). Colors indicate the depth at which each T–S point was sampled..... **47**

Figure 4.3. Temperature (red line) and salinity (blue line) variability for: (a) SW, (b) ENACW and (c) MW in the Bay of Biscay for the period 2004–2013. ..... **49**

Figure 4.4. Decomposition of (a) temperature and (b) salinity changes along isobars (red line) as the sum of changes along isopycnals (blue line) and changes due to vertical displacement of isopycnals (green line). **52**

Figure 4.5. Vertical displacement of isopycnals for the period 2004–2013 in the Bay of Biscay **53**

Figure 5.1. Bathymetry of the Bay of Biscay. Solid black line represents the −1000 m isobaths. **57**

Figure 5.2. Comparison between Argo and SODA databases. (a) Isopycnal layer depth and (b) isothermal layer depth variability using Argo database (blue line) and SODA database (red line). A 1-2-1 filter was used to smooth signals only for visualization.... **59**

Figure 5.3. Mean values of winter mixed layer depth. (a) Winter mean isopycnal layer depth (m) and (b) winter mean isothermal layer depth (m) over the period 1975–2010.**59**

Figure 5.4. Trend values of mixed layer depth. (a) (b) Annual maxima trends and (m per decade) (c) (d) winter anomalies trends (m per decade) of PLD (left) and TLD (right) in the Bay of Biscay for the period 1975–2010. Black dots represent points with a significance level higher than 90%. **60**

Figure 5.5. (a) Air temperature trend (ºC per decade), (b) P-E (precipitation minus evaporation) balance trend (mm per decade) and (c) wind stress trend (N m^{-2} per decade) calculated over the period 1975–2010. Black dots represent points with a significance level higher than 90%. **62**

Figure 5.6. Winter ocean temperature trend for the upper 700 m over the period 1975–2010. Black dots represent grid points with a significance level higher than 95%. **64**

Figure 6.1. (a) Annual mean SST (°C) and (b) decadal SST trends (°C per decade) in the Bay of Biscay from 1982 to 2014. Black dots represent the grid points with a significance level higher than 95%. **70**

Figure 6.2. Monthly mean SST (°C) in the Bay of Biscay over the period 1982–2014.**71**

Figure 6.3. Monthly SST trends (°C per decade) in the Bay of Biscay over the period 1982–2014. Black dots represent the grid points with a significance level higher than 95%. **72**

Figure 6.4. Day when the warm season starts (a) and ends (c) in the Bay of Biscay averaged over the period 1982–2014. (b) Trend (# days per decade) in the beginning of the warm season and (d) in the end of the warm season. (e) Mean duration of the warm season and (f) trend (# days per decade) of the warm season duration. Black dots represent the grid points with a significance level higher than 95%. Negative trends indicate an advance and positive trends account for a delay. **73**

Figure 6.5. (a) April–June, (b) August and (c) September–November trend in the number of extreme hot SST days (# days per decade). Trend values in (a) and (c) were normalized at monthly values. Black dots represent the grid points with a significance level higher than 95%. **75**

Figure 7.1. Bathymetry of the region under study. Contour lines represent, 200 and 1000 m isobaths. Red dots mark the location where wind was obtained. Blue asterisks mark the location where river discharge was sampled. **83**

Figure 7.2. Monthly mean area (km^2) occupied by the turbid plume formed by Loire and Gironde Rivers discharges over the period 2002-2014. ..... **84**

Figure 7.3. Annual hydrologic cycle variability (m^3s^{-1}) for (a) Loire and (b) Gironde runoff over the period 2002-2014. Solid black line represents the monthly average flow and the line inside each box represents the median for each month. Lower and upper whiskers show minimum and maximum river flow, respective, whilst lower and upper box indicate first and third quartiles, respectively..... **84**

Figure 7.4. Wind rose (ms^{-1}) representing DJF winds near Loire (upper panels) and Gironde (lower panels) over the periods 1982-2004 (left) and 2002–2014 (right)..... **85**

Figure 7.5. Mean DJF turbid plume ($mWcm^{-2}\mu m^{-1}sr^{-1}$) calculated over the period 2002-2014. The contour line corresponds to the turbid threshold 0.2 $mWcm^{-2}\mu m^{-1}sr^{-1}$)..... **86**

Figure 7.6. Mean DJF SST (ºC) calculated over the period 2002-2014; (a) $OISST_{1/4}$ (b) MODIS. **86**

Figure 7.7. DJF SST trends (ºC per decade) calculated over the period 2002-2014; (a) OISST1/4. (b) MODIS. Contour line corresponds to null trend. Black dots represent grid points with significance higher than 90%. **87**

Figure 7.8. DJF SST trends (ºC per decade) calculated over the period 1982-2014 with $OISST_{1/4}$ data. Contour line corresponds to null trend. Black dots represent grid points with significance higher than 90%. **88**

Figure 7.9. DJF trends in heat fluxes (W m^{-2} per decade) calculated over the period 1982-2014 with CFSR data. (a) Total heat; (b) Latent heat. **89**

Figure 7.10. Correlation between DJF NAO (a), DJF AMO (b) indices and DJF SST anomaly over the period 1982-2014. Black dots represent grid points with significance higher than 95%..... **89**

List of tables

Table 1.1. Change in ocean heat content (10^{22} J per decade) and change in mean temperature (ºC per decade) for the upper 700 m for the World Ocean and individual basins calculated using linear trends over the period 1955-2010. Source: Data from Levitus et al. (2012). **7**

Table 2.1. Oceanographic and atmospheric databases used in this thesis. **28**

Table 4.1. Estimated linear trends for the Bay of Biscay over the decade 2004-2013. SW (0-100 m), ENACW (100-600 m), MW (600-1200 m). The asterisk means a significance level higher than 95%. **50**

Table 5.1. Correlations between annual maxima and winter anomalies of PLD/TLD calculated from ARGO and SODA databases for the period 2003-2010. Statistical significance (p value) is showed in brackets. **58**

Table 5.2. Left, correlations between points of negative air temperature trends ($Tair^-$) and points of positive annual maxima (PLDm/TLDm) and winter anomalies (PLDa/TLDa) trends. Right, correlations between points of positive air temperature trends ($Tair^+$) and points of negative annual maxima (PLDm/TLDm) and winter anomalies (PLDa/TLDa) trends. Statistical significance (p value) is showed in brackets). **63**

Table 6.1. Annual SST trends within the Bay of Biscay according to different authors, periods, locations and databases. The associated standard deviation is also included... **69**

Table 6.2. Monthly mean SST (ºC) and trend (ºC per decade) values with their associated standard deviation for the whole Bay of Biscay over the period 1982-2014. Values were obtained by means of a spatial average of figures 6.2 and 6.3, respectively. **72**

Table 7.1. Trends in wind intensity and duration and in river discharge. Values with null trends are marked with --. Statistical significance at 95% || 99% is marked with * || **. **91**

Bibliography

[Alexander et al., 2006] Alexander, L.V., Zhang, X., Peterson, T.C., Caesar, J., Gleason, B., Klein Tank, A.M.G., Haylock, M., Collins, D., Trewin, B., Rahimzadeh, F., Tagipour, A., Rupa Kumar, K., Revadekar, J., Griffiths, G., Vincent, L., Stephenson, D.B., Burn, J., Aguilar, E., Brunet, M., Taylor, M., New, M., Amd, M., Rusticucci, P.Z., Vazquez-Aguirre, J.L., 2006. Global observed changes in daily extremes of temperature and precipitation. Journal of Geophysical Research-Atmosphere 111, doi:10.1029/2005JD006290.

[Álvarez et al., 2010] Álvarez, I., Gomez-Gesteira, M., Gomez-Gesteira, J. L., Dias, J. M., 2010. Summer upwelling frequency along the western Cantabrian coast from 1967 to 2007. Journal of Marine Systems 79(1), 218-226.

[Álvarez et al., 2011] Álvarez, I., Gomez-Gesteira, M., Lorenzo, M. N., Crespo, A. J. C., Dias, J. M., 2011. Comparative analysis of upwelling influence between the western and northern coast of the Iberian Peninsula. Continental Shelf Research 31(5), 388-399.

[Álvarez et al., 2014] Álvarez, I., Gómez-Gesteira, M., deCastro, M., Carvalho, D., 2014. Comparison of different wind products and buoy wind data with seasonality and interannual climate variability in the southern Bay of Biscay (2000-2009). Deep-Sea Research II 106, 38-48, doi:10.1016/j.dsr2.2013.09.028.

[Arbic and Owens, 2001] Arbic, B.K., Owens,W.B., 2001. Climatic warming of the Atlantic intermediate waters. Journal of Climate 14, 4091–4108 doi:10.1175/1520-0442(2001)014b4091:CWOAIWN2.0.CO;2.

[Argo Science Team, 2001] Argo Science Team 2001. Argo: the global array of profiling floats. In: Koblinsky, C.J., Smith, N.R. (Eds.), Observing the Oceans in the 21st Century. GODAE Project Office and Bureau of Meteorology, Melbourne.

[Bardey et al., 1999] Bardey, P., Garnesson, P., Moussu, G., Wald, L., 1999. Joint analysis of temperature and ocean colour satellite images for mesoscale activities in the Gulf of Biscay. International Journal of Remote Sensing 20(7), 1329-1341.

[Baringer and Price, 1997] Baringer, M.O., Price, J.F., 1997. Mixing and spreading of the Mediterranean outflow. Journal of Physical Oceanography 27, 1654–1677.

[Barnston and Livezey, 1987] Barnston, A.G., Livezey, R.E. 1987. Classification, seasonality and persistence of low-frequency atmospheric circulation patterns. Monthly Weather Review, 115, 1083–1126.

[Barré et al., 2006] Barré, N., Provost, C., Saraceno, M. 2006. Spatial and temporal scales of the Brazil-Malvinas Current confluence documented by simultaneous MODIS Aqua 1.1-km resolution SST and color images. Advances in Space Research, 37, 770-786, doi:10.1016/j.asr.2005.09.026.

[Belkin, 2009] Belkin, I.M., 2009. Rapid warming of Large Marine Ecosystems. Progress in Oceanography 81, 207-213, doi:10.1016/j.pocean.2009.04.011.

[Bellier et al., 2007] Bellier, E., Planque, B., Petitgas, P., 2007. Historical fluctuations in spawning location of anchovy (Engraulis encrasicolus) and sardine (Sardina pilchardus) in the Bay of Biscay during 1967-1973 and 2000-2004. Fisheries Oceanography 16 (1), 1–15, doi:10.1111/j.1365-2419.2006.00410.x.

[Benítez-Barrios et al., 2008] Benítez-Barrios, V.M., Hernández-Guerra, A., Vélez-Belchí, P., Machín, F., Fraile-Nuez, E., 2008. Recent changes in the subsurface temperature and salinity in the Canary region. Geophysical Research Letters 35, doi:10.1029/2008GL033329 (L07603).

[Bindoff and McDougall, 1994] Bindoff, N.L., McDougall, T.J., 1994. Diagnosing climate change and ocean ventilation using hydrographic data. Journal of Physical Oceanography 24, 1137–1152, doi:10.1175/1520-0485(1994)024b1137:DCCAOVN2.0.CO;2.

[Borja and Collins, 2009] Borja, A., Collins, M., 2009. Regional Seas integrative studies, as a basis for an ecosystem-based approach to management: The case of the Bay of Biscay. Continental Shelf Research 29(8), 951-956.

[Borja et al., 2000] Borja, A., Egaña, J., Valencia, V., Franco, J., Castro, R., 2000. 1947-1997, Estudio y validación de una serie de datos diarios de temperatura del agua del mar en San Sebastián, procedente de su Aquarium. Ozeanografika 3, 139-152.

[Borja et al., 2008] Borja, A., Fontan, A., Sáenz, J. O. N., Valencia, V., 2008. Climate, oceanography, and recruitment: the case of the Bay of Biscay anchovy (Engraulis encrasicolus). Fisheries Oceanography 17(6), 477-493.

[Botas et al., 1989] Botas, J.A., Fernández, E., Bode, A., Anadón, R., 1989. Water masses off the Central Cantabrian Coasts. Scientia Marina 53 (4), 755–761.

[Botas et al., 1990] Botas, J. A., Fernández, E., Bode, A., Anadón, R., 1990. A persistent upwelling off the central Cantabrian coast (Bay of Biscay). Estuarine, Coastal and Shelf Science 30(2), 185-199.

[Boucher, 1985] Boucher, J., 1985. Caractéristiques physiques et biologiques. In: Laubier, L., Monniot, C. (Eds.), Peuplements profonds du golfe de Gascogne. IFREMER, Brest, pp. 25–42.

[Boyer et al., 2005] Boyer, T.P., Levitus, S., Antonov, J.I., Locarnini, R.A., Garcia, H.E., 2005. Linear trends in salinity for the World Ocean, 1955–1998. Geophysical Research Letters 32, L01604, doi:10.1029/2004GL021791.

[Boyer et al., 2007] Boyer, T., Levitus, S., Antonov, J., Locarnini, R., Mishonov, A., Garcia, H., Josey, S. A., 2007. Changes in freshwater content in the North Atlantic Ocean 1955–2006. Geophysical Research Letters 34(16).

[Boyer et al., 2009] Boyer, T. P., Antonov, J. I., Baranova, O. K., Garcia, H. E., Johnson, D. R., Locarnini, R. A., Mishonov, A.V., O'Brien, T.D., Seidov, D., Smolyar, I.V., Zweng, M. M., 2009. Chapter 1: Introduction. World Ocean Database 2009, NOAA Atlas NESDIS 66, DVD ed., S. Levitus, Ed., U.S. Gov. Printing Office, Wash., D.C., USA, pp. 216.

[Bozec et al., 2011] Bozec, A., Lozier, M. S., Chassignet, E. P., Halliwell, G. R., 2011. On the variability of the Mediterranean Outflow Water in the North Atlantic from 1948 to 2006. Journal of Geophysical Research: Oceans (1978–2012) 116(C9).

[Brainerd and Gregg, 1995] Brainerd, K. E., Gregg, M. C., 1995. Surface mixed and mixing layer depths. Deep Sea Research Part I: Oceanographic Research Papers 42(9), 1521-1543.

[Brown and Minnett, 1999] Brown, O.B., Minnett, P., J. 1999. MODIS Infrared Sea Surface Temperature Algorithm Theoretical Basis Document, Ver 2.0, http://modis.gsfc.nasa.gov/data/atbd/atbd_mod25.pdf.

[Carton and Giese, 2008] Carton, J. A. and Giese, B.S. 2008. A Reanalysis of Ocean Climate Using Simple Ocean Data Assimilation (SODA). Monthly Weather Review, 136(8), 2999-3017.

[Carton et al., 2005] Carton, J. A., Giese, B. S., Grodsky, S. A., 2005. Sea level rise and the warming of the oceans in the Simple Ocean Data Assimilation (SODA) ocean reanalysis. Journal of Geophysical Research: Oceans 110(C9).

[Carton et al., 2008] Carton, J. A., Grodsky, S. A., Liu, H., 2008. Variability of the oceanic mixed layer, 1960-2004. Journal of Climate 21(5), 1029-1047.

[Casey and Cornillon, 2001] Casey, K.S., Cornillon, P., 2001. Global and regional sea-surface temperature trends. Journal of Climate 14, 3801–3818.

[Casey et al., 2010] Casey, K.S., Brandon, T.B., Cornillon, P., Evans, R., 2010. The past, present and future of the AVHRR Pathfinder SST Program. In: Barale, V., Gower, J.F.R., Alberotanza, L. (Eds.), Oceanography from Space. Springer, doi:10.1007/978-90-481-8681-5_16.

[Cattiaux et al., 2011] Cattiaux, J., Vautard, R., Yiou, P., 2011. North-Atlantic SST amplified recent wintertime European land temperature extremes and trends. Climate dynamics, 36(11-12), 2113-2128, doi:10.1007/s00382-010-0869-0.

[Cayan, 1992] Cayan, D.R., 1992. Latent and sensible heat flux anomalies over the Northern Oceans: the connection to monthly atmospheric circulation. Journal of Climate 5:354–369.

[Chao, 1988] Chao, S.Y., 1988. Wind-driven motion of estuarine plumes. Journal of Physical Oceanography 18, 1144-1166.

[Charria et al., 2013] Charria, G., Lazure, P., Le Cann, B., Serpette, A., Reverdin, G., Louazel, S., Batifoulier, F., Dumas, F., Pichon, A., Morel, Y., 2013. Surface layer circulation derived from Lagrangian drifters in the Bay of Biscay. Journal of Marine Systems 109, S60-S76.

[Chavula et al., 2009] Chavula, G., Brezonik, P., Thenkabail, P., Johnson, T., Bauer, M., 2009. Estimating the surface temperature of Lake Malawi using AVHRR and MODIS satellite imagery. Physics and Chemistry of the Earth 34, 749-754, doi:10.1016/j.pce.2009.08.001.

[Church et al., 2011] Church, J.A., White, N.J., Konikow, L.F., Domingues, C.M., Cogley, J.G., Rignot, E., Gregory, J.M., van den Broeke, M.R., Monaghan, A.J., Velicogna, I., 2011. Revisiting the Earth's sea-level and energy budgets from 1961 to 2008. Geophysical Research Letters 38(18).

[Chylek et al., 2006] Chylek, P., Dubey, M., Lesins, G. 2006. Greenland warming of 1920–1930 and 1995–2005. Geophysical Research Letters, 33, L11707, doi:10.1029/2006GL026510.

[Chylek et al., 2014] Chylek, P., Dubey, M. K., Lesins, G., Li, J., Hengartner, N. 2014. Imprint of Atlantic Multi-decadal Oscillation and Pacific Decadal Oscillation on southwestern US climate: Past, present and future. Climate Dynamics, 43(1-2), 119-129, doi:10.1007/s00382-013-1933-3.

[Curry and McCartney, 2001] Curry, R.G., McCartney, M.S. 2001. Ocean gyre circulation changes associated with the North Atlantic Oscillation. Journal of Physical Oceanography 31, 3374–3400.

[Daniault et al., 1994] Daniault, J.P., Maze, J.P., Arhan, M., 1994. Circulation and mixing of Mediterranean Water west of the Iberian Peninsula. Deep Sea Research I 41, 1685–1714.

[deBoyer et al., 2004] de Boyer Montégut, C., Madec, G., Fischer, A. S., Lazar, A., Iudicone, D., 2004. Mixed layer depth over the global ocean: An examination of profile data and a profile-based climatology. Journal of Geophysical Research: Oceans 109(C12), doi:10.1029/2004JC002378.

[deBoyer et al., 2007] de Boyer Montégut, C., Mignot, J., Lazar, A., Cravatte, S., 2007. Control of salinity on the mixed layer depth in the world ocean: 1. General description. Journal of Geophysical Research: Oceans 112(C6), doi:10.1029/2006JC003953.

[deCastro et al., 2006] deCastro, M., Lorenzo, N., Taboada, J.J., Sarmiento, M., Álvarez, I., Gómez-Gesteira, M. 2006. Teleconnection patterns influence on precipitation variability and on river flow regimes in the Miño river basin (NW Spain). Climate Research 32, 63–73.

[deCastro et al., 2008a] deCastro, M., Gómez-Gesteira, M., Álvarez, I., Lorenzo, M., Cabanas, J.M., Prego, R., Crespo, A.J.C. 2008a. Characterization of fall–winter upwelling recurrence along the Galician western coast (NW Spain) from 2000 to 2005: dependence on atmospheric forcing. Journal of Marine Systems 72, 145-158, doi:10.1016/j.jmarsys.2007.04.005.

[deCastro et al., 2008b] deCastro, M., Gómez-Gesteira, M., Lorenzo, M.N., Alvarez, I., Crespo, A.J.C. 2008b. Influence of atmospheric modes on coastal upwelling along the western coast of the Iberian Peninsula, 1985 to 2005. Climate Research 36, 169–179, doi:10.3354/cr00742.

[deCastro et al., 2009] deCastro, M., Gómez-Gesteira, M., Álvarez, I., Gesteira, J.L.G., 2009. Present warming within the context of cooling–warming cycles observed since 1854 in the Bay of Biscay. Continental Shelf Research 29, 1053–1059.

[deCastro et al., 2011a] deCastro, M., Gómez-Gesteira, M., Álvarez, I., Crespo, A.J.C, 2011. Atmospheric modes influence on the Iberian Poleward Current variability. Continental Shelf Research 31, 425–432.

[deCastro et al., 2011b] deCastro, M., Gomez-Gesteira, M., Ramos, A. M., Alvarez, I., deCastro, P., 2011. Effects of heat waves on human mortality, Galicia, Spain. Climate Research *48*(2-3), 333-341.

[deCastro et al., 2014] deCastro, M., Gómez-Gesteira, M., Costoya, X., Santos, F., 2014. Upwelling influence on the number of extreme hot SST days along the Canary upwelling ecosystem. Journal of Geophysical Research: Oceans 119, 3029–3040, doi:10.1002/2013JC009745.

[del Río et al., 1998] del Río, G. D., González, N., Marcote, D., 1998. The intermediate Mediterranean water inflow along the northern slope of the Iberian Peninsula. Oceanologica acta 21(2), 157-163.

[Dessay, 2002] Dessai, S., 2002. Heat stress and mortality in Lisbon part I. Model construction and validation. International Journal of Biometeorology 47(1), 6-12.

[Dima and Lohmann, 2007] Dima, M., Lohmann, G. 2007. A hemispheric mechanism for the Atlantic Multidecadal Oscillation. Journal of Climate, 20(11), 2706-2719.

[Domingues et al., 2008] Domingues, C.M., Church, J.A., White, N.J., Gleckler, P.J., Wijffels, S.E., Barker, P.M., Dunn, J.R., 2008. Improved estimates of upper-ocean warming and multidecadal sea-level rise. Nature 453, 1090–1093.

[Dufour et al., 2010] Dufour, F., Arrizabalaga, H., Irigoien, X., Santiago, J., 2010. Climate impacts on albacore and bluefin tunas migrations phenology and spatial distribution. Progress in Oceanography 86, 283–290, doi:10.1016/j.pocean.2010.04.007.

[Durack and Wijffels, 2010] Durack, P. J., Wijffels, S. E., 2010. Fifty-year trends in global ocean salinities and their relationship to broad-scale warming. Journal of Climate 23(16), 4342-4362.

[Enfield et al., 2001] Enfield, D.B., Mestas-Nuñez, A.M., Trimble, P.J. 2001. The Atlantic multidecadal oscillation and its relation to rainfall and river flows in the continental U.S. Geophysical Research Letters, 28 (10), 2077–2080.

[Fernández, 2011] Fernández, C., 2011. The retreat of large Brown seaweeds on the north coast of Spain: the case of Saccorhiza polyschides. European Journal of Phycology 46 (4), 352–360, doi:10.1080/09670262.2011.617840.

[Fernández-Nóvoa et al., 2015] Fernández-Nóvoa, D., Mendes, R., deCastro, M., Dias, J.M., Sánchez-Arcilla, A., Gómez-Gesteira, M., 2015. Analysis of the influence of river discharge and wind on the Ebro turbid plume using MODIS-Aqua and MODIS-Terra data. Journal of Marine Systems 142, 40-46, doi:10.1016/j.jmarsys.2014.09.009.

[Ferrer et al., 2009] Ferrer, L., Fontán, A., Mader, J., Chust, G., González, M., Valencia, V., Uriarte, A., Collins, M. B., 2009. Low-salinity plumes in the oceanic region of the Basque Country. Continental Shelf Research 29(8), 970-984.

[Fofonoff and Lewis, 1979] Fofonoff, N. P., Lewis, E. L., 1979. A practical salinity scale. Journal of Oceanography 35(1), 63-64.

[Fontán et al., 2008] Fontán, A., Valencia, V., Borja, Á., Goikoetxea, N., 2008. Oceano-meteorological conditions in the SE Bay of Biscay for the period 2001–2005. A comparison with the last two decades. Journal of Marine Systems 72, 167–177.

[Fraga et al., 1982] Fraga, F., Mouriño, C., Manríquez, M., 1982. Las masas de agua en la costa de Galicia: junio-octubre.

[Fraga, 1981] Fraga, F., 1981. Upwelling off the Galician coast, northwest Spain. Coastal upwelling 176-182.

[Froidefond et al., 1996] Froidefond, J. M., Castaing, P., Jouanneau, J. M., 1996. Distribution of suspended matter in a coastal upwelling area. Satellite data and in situ measurements. Journal of Marine systems 8(1), 91-105.

[Fusco et al., 2008] Fusco, G., Artale, V., Cotroneo, Y., & Sannino, G., 2008. Thermohaline variability of Mediterranean Water in the Gulf of Cadiz, 1948–1999. Deep Sea Research Part I: Oceanographic Research Papers 55(12), 1624-1638.

[García-Soto and Pingree, 2009] García-Soto, C., Pingree R.D., 2009. Spring and summer blooms of phytoplankton (SeaWiFS/MODIS) along a ferry line in the Bay of Biscay and western English Channel. Continental Shelf Research 29, 1111–1122.

[García-Soto and Pingree, 2012] Garcia-Soto, C., Pingree, R. D., 2012. Atlantic Multidecadal Oscillation (AMO) and sea surface temperature in the Bay of

Biscay and adjacent regions. Journal of the Marine Biological Association of the United Kingdom 92(02), 213-234.

[García-Soto et al., 2002] García-Soto, C., Pingree, R.D., Valdés, L. 2002. Navidad Development in the Southern Bay of Biscay: climate change and Swoddy structure from remote sensing and in situ measurements. Journal of Geophysical Research 107, C83118.

[GCOS, 2009] GCOS, 2009: Progress Report on the Implementation of the Global Observing System for Climate in Support of the UNFCCC 2004–2008, GCOS-129 (WMO/TD-No.1489; GOOS-173; GTOS-70) , Geneva, Switzerland.

[Giménez, 2011] Giménez, L., 2011. Exploring mechanisms linking temperature increase and larval phenology: the importance of variance effects. Journal of Experimental Marine Biology and Ecology 400(1), 227-235.

[Ginzburg et al., 2004] Ginzburg, A.I., Kostianoy, A.G., Sheremet, N.A., 2004. Seasonal and interannual variability of the Black Sea surface temperature as revealed from satellite data (1982-2000). Journal of Marine Systems 52, 33–50.

[Goikoetxea et al., 2009] Goikoetxea, N., Borja, A., Fontán, A., González, M., Valencia, V. 2009. Trends and anomalies of the sea surface temperature during the last 60 years within the southeastern Bay of Biscay. Continental Shelf Research 29, 1060–1069.

[Gómez-Ballesteros et al., 2014] Gómez-Ballesteros, M., Druet, M., Muñoz, A., Arrese, B., Rivera, J., Sánchez, F., Cristobo, J., Parra, S., García-Alegre, A., González-Pola, C., Gallastegui, J., Acosta, J., 2014. Geomorphology of the Avilés canyon system, Cantabrian Sea (Bay of Biscay). Deep Sea Research Part II: Topical Studies in Oceanography 106, 99-117.

[Gómez-Gesteira et al., 2008] Gómez-Gesteira, M., deCastro, M., Alvarez, I., Gesteira, J.L.G., 2008. Coastal sea surface temperature warming trend along the continental part of the Atlantic Arc (1985–2005). Journal of Geophysical Research: Oceans 113, C04010, doi:10.1029/2007JC004315.

[Gómez-Gesteira et al., 2011] Gómez-Gesteira, M., Gimeno, L., deCastro, M., Álvarez, I., Nieto, R., Taboada, J.J., Ramos, A.M., Iglesias, I., Gómez-Gesteira, J.L., Lorenzo, M.N., Crespo, A.J.C., Santo, F.E., Barriopedro, D., Trigo, I.F., 2011. The state of climate in NW Iberia. Climate Research 48, 109–144.

[González et al., 2013] González, M., Fontán, A., Esnaola, G., Collins, M., 2013. Abrupt changes, multidecadal variability and long-term trends in sea surface

temperature and sea level datasets within the southeastern Bay of Biscay. Journal of Marine Systems 109, S144-S152.

[González-Nuevo and Nogueira, 2014] González-Nuevo, G., Nogueira, E. 2014. Temporal and spatial variability of river plumes in the NW and N Iberian shelf (1987–2007). Continental Shelf Research 91, 95-108.

[González-Pola et al., 2005] González-Pola, C., Lavín, A., Vargas-Yáñez, M. 2005. Intense warming and salinity modification of intermediate water masses in the southeastern corner of the Bay of Biscay for the period 1992–2003. Journal of Geophysical Research: Oceans, 110, doi:10.1029/2004JC002367.

[González-Pola et al., 2007] González-Pola, C., Fernández-Díaz, J. M., Lavín, A., 2007. Vertical structure of the upper ocean from profiles fitted to physically consistent functional forms. Deep Sea Research Part I: Oceanographic Research Papers 54(11), 1985-2004.

[Goreau et al., 2005] Goreau, T.J., Hayes, R.L., McAllister, D., 2005. Regional patterns of sea surface temperature rise: Implications for global ocean circulation change and the future of coral reefs and fisheries. World Resource Review 17 (3), 350–374.

[Gouretski et al., 2012] Gouretski, V., Kennedy, J., Boyer, T., Kohl, A., 2012. Consistent near-surface ocean warming since 1900 in two largely independent observing networks. Geophysical Research Letters 39, L19606.

[Halpern et al., 2008] Halpern, B.S., Walbridge, S., Selkoe, K.A., Kappel, C.V., Micheli, F., D'Agrosa, C., Bruno, J.F., Casey, K.S., Ebert, C., Fox, H.E., Fujita, R., Heinemann, D., Lenihan, H.S., Madin, E.M.P., Perry, M.T., Selig, E.R., Spalding, M., Steneck, R., Watson, R., 2008. A global map of human impact on marine ecosystems. Science 319, 948–952, doi:10.1126/science.1149345.

[Halpert and Bell, 1997] Halpert, M.S., Bell, G.D. 1997. Climate assessment for 1996. Bulletin of the American Meteorological Society 78, S1–S49.

[Hartman et al., 2014] Hartman, S. E., Hartman, M. C., Hydes, D. J., Jiang, Z. P., Smythe-Wright, D., González-Pola, C., 2014. Seasonal and inter-annual variability in nutrient supply in relation to mixing in the Bay of Biscay. Deep Sea Research Part II: Topical Studies in Oceanography 106, 68-75.

[Harvey, 1982] Harvey, J., 1982. θ-S relationships and water masses in the eastern North Atlantic. Deep Sea Research Part A. Oceanographic Research Papers 29(8), 1021-1033.

[Holte and Talley, 2009] Holte, J., Talley, L., 2009. A new algorithm for finding mixed layer depths with applications to Argo data and subantarctic Mode Water formation. Journal of Atmospheric and Oceanic Technology 26(9), 1920-1939.

[Hosoda et al., 2009] Hosoda, S., Suga, T., Shikama, N., Mizuno, K., 2009. Global surface layer salinity change detected by Argo and its implication for hydrological cycle intensification. Journal of oceanography 65(4), 579-586.

[Hosoda et al., 2010] Hosoda, S., Ohira, T., Sato, K., Suga, T., 2010. Improved description of global mixed-layer depth using Argo profiling floats. Journal of oceanography 66(6), 773-787.

[Houghton, 2009] Houghton, J., 2009. Global Warming: The Complete Briefing. Fourth edition. Cambridge University Press (438 pp.).

[Howden and Murtugude, 2001] Howden, S.D., Murtugudde, R., 2001. Effects of river inputs into the Bay of Bengal. Journal of Geophysical Research 106(C9), 825-19843.

[Hurrel, 1995] Hurrell, J.W. 1995. Decadal trends in the North Atlantic Oscillation: regional temperatures and precipitation. Science, 269(5224), 676-679.

[Huthnance et al., 2002] Huthnance, J. M., Van Aken, H. M., White, M., Barton, E. D., Le Cann, B., Coelho, E. F., Álvarez-Fanjul, E., Miller, P., Vitorino, J., 2002. Ocean margin exchange—water flux estimates. Journal of Marine Systems 32(1), 107-137.

[IHO, 1971] International Hydrographic Organizations, 1971. Limits of oceans and seas, 3rd Ed, page 42.

[Iorga and Lozier, 1999] Iorga, M. C., Lozier, M. S., 1999. Signatures of the Mediterranean outflow from a North Atlantic climatology: 1. Salinity and density fields. Journal of Geophysical Research: Oceans (1978–2012) 104(C11), 25985-26009.

[IPCC, 2007] Intergovernmental Panel on Climate Change, 2007. Climate change 2007: the physical science basis. Contribution of Working Group 1 to the Fourth Assessment Report of the Intergovernmental Panel on Climate Change. Cambridge University Press, Cambridge, UK.

[IPCC, 2013] Climate Change 2013: The Physical Science Basis. Contribution of Working Group I to the Fifth Assessment Report of the Intergovernmental Panel

on Climate Change. In: Stocker, T.F., Qin, D., Plattner, G.K., Tignor, M., Allen, S.K., Boschung, J., Nauels, A., Xia, Y., Bex, V., Midgley, P.M. (Eds.). Cambridge University Press,Cambridge, United Kingdom and New York, NY, USA (1535 pp.).

[Ishii and Kimoto, 2009] Ishii, M., Kimoto, M., 2009: Reevaluation of historical ocean heat content variations with time-varying XBT and MBT depth bias corrections. Journal of Oceanography 65, 287–299.

[Jackett and McDougall, 1997] Jackett, D.R., McDougall, T.J., 1997. A neutral density variable for the world's oceans. Journal of Physical Oceanography 27, 237–263.

[Johnson and Gruber, 2007] Johnson, G.C., Gruber, N. 2007. Decadal water mass variations along 20 ºW in the northeastern Atlantic Ocean. Progress in Oceanography 73, 277–295.

[Kalnay et al., 1996] Kalnay, E., Kanamitsu, M., Kistler, R., Collins, W., Deaven, D., Gandin, L., Iredell, M., Saha, S., White, G., Woollen, J., Zhu, Y., Leetmaa, A., Reynold, R., Chelliah, M., Ebisuzaki, W., Higgins, W., Janowiack, J., Mo, C.K., Ropelewski, C., Wang, J., Jenne, R., Joseph, D. 1996. The NCEP/NCAR 40-year reanalysis project. Bulletin of the American meteorological Society, 77(3), 437-471, doi:10.1175/1520-0477(1996)077<0437:TNYRP>2.0.CO;2.

[Kara et al., 2000] Kara, A. B., Rochford, P. A., Hurlburt, H. E., 2000. An optimal definition for ocean mixed layer depth. Journal of Geophysical Research: Oceans 105(C7), 16803-16821.

[Kara et al., 2003] Kara, A. B., Rochford, P. A., Hurlburt, H. E., 2003. Mixed layer depth variability over the global ocean. Journal of Geophysical Research: Oceans 108(C3), doi:10.1029/2000JC000736.

[Kavvada et al., 2013] Kavvada, A., Ruiz-Barradas, A., Nigam, S. 2013. AMO's structure and climate footprint in observations and IPCC AR5 climate simulations. Climate Dynamics, 41, 1345–1364, doi:10.1007/s00382-013-1712-1.

[Kelly-Gerreyn et al., 2006] Kelly-Gerreyn, B. A., Hydes, D. J., Jegou, A. M., Lazure, P., Fernand, L. J., Puillat, I., Garcia-Soto, C., 2006. Low salinity intrusions in the western English Channel. Continental Shelf Research 26(11), 1241-1257.

[Kerr, 2000] Kerr, R. A. 2000. A North Atlantic climate pacemaker for the centuries. Science, 288(5473), 1984-1985.

[Kilpatrick et al., 2001] Kilpatrick, K. A., Podesta, G. P., Evans, R., 2001. Overview of the NOAA/NASA advanced very high resolution radiometer Pathfinder algorithm for sea surface temperature and associated matchup database. Journal of Geophysical Research: Oceans 106(C5), 9179-9197.

[Koutsikopoulos and Le Cann, 1996] Koutsikopoulos, C., Le Cann, B., 1996. Physical processes and hydrological structures related to the Bay of Biscay anchovy. Scientia Marina 60, 9–19.

[Koutsikopoulos et al., 1998] Koutsikopoulos, C., Beillois, P., Leroy, C., Taillefer, F. 1998. Temporal trends and spatial structures of the sea surface temperature in the Bay of Biscay. Oceanologica Acta 21, 335–344.

[Lavín et al., 1998] Lavín, A., Valdés, L., Gil, J., Moral, M., 1998. Seasonal and inter-annual variability in properties of surface water off Santander, Bay of Biscay, 1991–1995. Oceanologica Acta 21(2), 179-190.

[Lavín et al., 2006] Lavín, A., Valdes, L., Sanchez, F., Abaunza, P., Forest, A., Boucher, J., Lazure, P., Jegou, A. M., 2006. The Bay of Biscay: the encountering of the ocean and the shelf, In: The sea 14(24), 933-1001.

[Lavín et al., 2007] Lavín, A., Moreno-Ventas, X., de Zárate, V. O., Abaunza, P., Cabanas, J. M., 2007. Environmental variability in the North Atlantic and Iberian waters and its influence on horse mackerel (*Trachurus trachurus*) and albacore (*Thunnus alalunga*) dynamics. ICES Journal of Marine Science: Journal du Conseil, 64(3) 425-438.

[Lazure and Jegou, 1998] Lazure, P., Jegou, A.M., 1998. 3D modelling of seasonal evolution of Loire and Gironde plumes on Biscay Bay continental shelf. Oceanologica Acta 21 (2), 165–177.

[Le Boyer et al., 2013] Le Boyer, A., Charria, G., Le Cann, B., Lazure, P., Marié, L., 2013. Circulation on the shelf and the upper slope of the Bay of Biscay. Continental Shelf Research 55, 97-107.

[Le Quéré et al., 2010] Le Quéré, C., Takahashi, T., Buitenhuis, E.T., Rödenbeck, C., Sutherland, S.C., 2010. Impact of climate change and variability on the global oceanic sink of CO2. Global Biogeochemical Cycles 24(4).

[Levitus and Boyer, 1994] Levitus, S. Boyer, T., 1994. World Ocean Atlas 1994. vol. 4: Temperature. NESDIS Atlas series. NOAA, Washington, DC 117 pp.

[Levitus et al., 2005] Levitus, S., Antonov, J., Boyer, T., 2005. Warming of the world ocean, 1955–2003. Geophysical Research Letters 32(2).

[Levitus et al., 2009] Levitus, S., Antonov, J. I., Boyer, T. P., Locarnini, R. A., Garcia, H. E., Mishonov, A. V., 2009. Global ocean heat content 1955–2008 in light of recently revealed instrumentation problems. Geophysical Research Letters 36(7), doi:10.1029/2008GL037155.

[Levitus et al., 2012] Levitus, S., Antonov, J.I., Boyer, T.P., Baranova, O.K., García, H.E., Locarnini, R.A., Mishonov, A.V., Reagan, J.R., Seidov, D., Yarosh, E.S., Zweng, M.M., 2012. World ocean heat content and thermosteric sea level change (0–2000 m) 1955–2010. Geophysical Research Letters 39, L10603.

[Lima and Wethey, 2012] Lima, F.P., Wethey, D.S., 2012. Three decades of high-resolution coastal sea surface temperatures reveal more than warming. Nature Communications 3, 704, doi:10.1038/ncomms1713.

[Liu et al., 2009] Liu, H., Grodsky, S. A., Carton, J. A., 2009. Observed subseasonal variability of oceanic barrier and compensated layers. Journal of Climate 22(22), 6104-6119, doi:10.1175/2009JCLI2974.1.

[Llope et al., 2006] Llope, M., Anadón, R., Viesca, L., Quevedo, M., González-Quiros, R., Stenseth, N.C. 2006. Hydrography of the Southern Bay of Biscay shelf-break region:interacting the multiscale physical variability over the period 1993–2003. Journal of Geophysical Research 111, C09021, doi:10.1029/2005JC002963.

[Lorbacher et al., 2006] Lorbacher, K., Dommenget, D., Niiler, P. P., Köhl, A., 2006. Ocean mixed layer depth: A subsurface proxy of ocean-atmosphere variability. Journal of Geophysical Research: Oceans 111(C7), doi:10.1029/2003JC002157.

[Materia et al., 2012] Materia, S., Gualdi, S., Navarra, A., Terray, L., 2012. The effect of Congo River freshwater discharge on Eastern Equatorial Atlantic climate variability. Climate dynamics 39, 2109-2015, doi:10.1007/s00382-012-1514-x.

[Mauritzen et al., 2001] Mauritzen, C., Morel, Y., Paillet, J., 2001. On the influence of Mediterranean water on the central waters of the North Atlantic Ocean. Deep Sea Research Part I: Oceanographic Research Papers 48(2), 347-381.

[Mazé et al., 1997] Mazé, J. P., Arhan, M., Mercier, H., 1997. Volume budget of the eastern boundary layer off the Iberian Peninsula. Deep Sea Research Part I: Oceanographic Research Papers 44(9), 1543-1574.

[MEECE, 2013] MEECE report, 2013. Deliverable D3.4 Synthesis report on climate simulations. Bay of Biscay, http://www.meece.eu/documents/deliverables/WP3/D3%204_Part6_Biscay.pdf.

[Mendes et al., 2014] Mendes, R., Vaz, N., Fernández-Nóvoa, D., da Silva, J.C.B., deCastro, M., Gómez-Gesteira, M., Dias, J.M. 2014. Observation of a turbid plume using MODIS imagery: The case of Douro estuary (Portugal). Remote Sensing of Environment, 154, 127-138, doi:10.1016/j.rse.2014.08.003.

[Michel et al., 2009a] Michel, S., Treguier, A.M., Vandermeirsch, F. 2009a. Temperature variability in the Bay of Biscay during the past 40 years, from an in situ analysis and a 3D global simulation. Continental Shelf Research 29, 1070–1087.

[Michel et al., 2009b] Michel, S., Vandermeirsch, F., Lorance, P., 2009b. Evolution of upper layer temperature in the Bay of Biscay during the last 40 years. Aquatic Living Resources 22, 447–461, doi:10.1051/alr/29009054.

[Mikaloff-Fletcher et al., 2006] Mikaloff-Fletcher, S.E., Gruber, N., Jacobson, A.R., Doney, S.C., Dutkiewicz, S., Gerber, M., Follows, M., Joos, F., Lindsay, K., Menemenlis, D., Mouchet, A., Müller, S.A., Sarmiento, J.L., 2006. Inverse estimates of anthropogenic CO2 uptake, transport, and storage by the ocean. Global Biogeochemical Cycles 20(2).

[Monterrey and Levitus, 1997] Monterey, G. I., Levitus, S., 1997. Seasonal variability of mixed layer depth for the world ocean. US Department of Commerce, National Oceanic and Atmospheric Administration, National Environmental Satellite, Data, and Information Service.

[Motos et al., 1996] Motos, L., Uriarte, A. and Valencia, V., 1996. The spawning environment of the Bay of Biscay anchovy (*Engraulis encrasicolus* L.). Scientia Marina 60 (Suppl. 2), 117–140.

[Muller et al., 2013] Muller, R.A., Curry, J., Groom, D., Jacobsen, R., Perlmutter, S., Rohde, R., Rosenfeld, A., Wickham, C., Wurtele, J. 2013. Decadal variations in the global atmospheric land temperatures. Journal of Geophysical Research: Atmospheres, 118(11), 5280-5286, doi:10.1002/jgrd.50458.

[NASA, 2015] NASA, 2015. MODIS. Retrieved 19/06/2015, from: http://modis.gsfc.nasa.gov/.

[Nezlin and DiGiacomo, 2005] Nezlin, N.P., DiGiacomo, P.M., 2005. Satellite ocean color observations of stormwater runoff plumes along the San Pedro Shelf

(southern California) during 1997-2003. Continental Shelf Research 25(4), 1692-1711, doi:10.1016/j.csr.2005.05.001.

[Nezlin et al., 2005] Nezlin, N.P., DiGiacomo, P.M., Stein, E.D., Ackerman, D., 2005. Stormwater runoff plumes observed by SeaWiFS radiometer in the Southern California Bight. Remote Sensing of Environment 98, 494-510, doi:10.1016/j.rse.2005.08.008.

[NOAA, 2008], NOAA, 2008. Northern Hemisphere Teleconnection Patterns, Easter Atlantic (EA). (http://www.cpc.ncep.noaa.gov/data/teledoc/ea.shtml).

[NOAA, 2009] NOAA KLM User's Guide, 2009, available online from http://ncdc.noaa.gov/oa/pod-guide/ncdc/docs/klm.

[Occhipinti-Ambrogi, 2007] Occhipinti-Ambrogi, A., 2007. Global change and marine communities: alien species and climate change. Marine pollution bulletin 55(7), 342-352.

[OSPAR Commission, 2000] OSPAR Commission, 2000. Quality Status Report 2000: Region IV — Bay of Biscay and Iberian Coast. OSPAR Commission, London, (134 + xiii pp.).

[Palmer et al., 2007] Palmer, M., Haines, K., Tett, S., Ansell T., 2007. Isolating the signal of ocean global warming. Geophysical Research Letters 34, L23610.

[Park et al., 2011] Park, T., Jand, C.J., Jungclaus, J.H., Haak, H., Park, W., Oh, I.S., 2011. Effects of the Changjiang River discharge on sea surface warming in the Yellowand East China Seas in summer. Continental Shelf Research 31, 15–22, doi:10.1016/j.csr.2010.10.012.

[Pascual et al., 2004] Pascual, A., Cearreta, A., Rodríguez-Lázaro, J., Uriarte, A., 2004. Geology and Palaeoceanography. Elsevier Oceanography Series. In: Borja, Á., Collins, M. (Eds.), Oceanography and Marine Environment of the Basque Country. Elsevier, pp. 53-73.

[Patti et al., 2008] Patti, B., Guisande, C., Vergara, A.R., Riveiro, I., Maneiro, I., Barreiro, A., Bonanno, A., Buscaino, G., Cuttitta, A., Basilone, G., Mazzola, S., 2008. Factors responsible for the differences in satellite-based chlorophyll a concentration between the major global upwelling areas. Estuarine, Coastal and Shelf Science 76(4), 775-786, doi:10.1016/j.ecss.2007.08.005.

[Pérez et al., 1995] Pérez, F. F., Ríos, A. F., King, B. A., Pollard, R. T., 1995. Decadal changes of the θ− S relationship of the Eastern North Atlantic Central Water. Deep Sea Research Part I: Oceanographic Research Papers 42(11), 1849-1864.

[Pérez et al., 2000] Pérez, F.F., Pollard, R.T., Read, J.F., Valencia, V., Cabanas, J.M., Ríos, A.F., 2000. Climatological coupling of the thermohaline decadal changes in Central Water of the Eastern North Atlantic. Scientia Marina 64, 347–353.

[Petus et al., 2010] Petus, C., Chust, G., Gohin, F., Doxaran, D., Froidefond, J. M., Sagarminaga, Y., 2010. Estimating turbidity and total suspended matter in the Adour River plume (South Bay of Biscay) using MODIS 250-m imagery. Continental shelf research 30(5), 379-392.

[Petus et al., 2014] Petus, C., Marieu, V., Novoa, S., Chust, G., Bruneau, N., Froidefond, J. M., 2014. Monitoring spatio-temporal variability of the Adour River turbid plume (Bay of Biscay, France) with MODIS 250-m imagery. Continental Shelf Research, 74, 35-49.

[Pingree and Le Cann, 1989] Pingree, R. D., Le Cann, B., 1989. Celtic and Armorican slope and shelf residual currents. Progress in Oceanography 23(4), 303-338.

[Pingree and LeCann, 1992] Pingree, R. D., Le Cann, B., 1992. Three anticyclonic Slope Water Oceanic eDDIES (SWODDIES) in the southern Bay of Biscay in 1990. Deep Sea Research Part A. Oceanographic Research Papers 39(7), 1147-1175.

[Pingree, 1993] Pingree, R. D., 1993. Flow of surface waters to the west of the British Isles and in the Bay of Biscay. Deep Sea Research Part II: Topical Studies in Oceanography 40(1), 369-388.

[Planque et al., 2003] Planque, B., Beillois, P., Jegou, A.M., Lazure, P., Petitgas, P., Puillat, I. 2003. Large- scale hydroclimatic variability in the Bay of Biscay: The 1900s in the context of interdecadal changes. ICES Marine Science. Symposium 219, 61–70.

[Planque et al., 2007] Planque, B., Bellier, E., Lazure, P., 2007. Modelling potential spawning habitat of sardine (Sardina pilchardus) and anchovy (Engraulis encrasicolus) in the Bay of Biscay. Fisheries Oceanography 16 (1), 16–30, doi:10.1111/j.1365-2419.2006.00411.x.

[Pollar and Pu, 1985] Pollard, R. T., Pu, S., 1985. Structure and circulation of the upper Atlantic Ocean northeast of the Azores. Progress in Oceanography 14, 443-462.

[Pollard et al., 2006] Pollard, R.T., Griffiths, M.J., Cunningham, S.A., Read, J.F., Perez, F.F., Rios, A.F. 1996. Vivaldi 1991—a study of the formation, circulation and ventilation of the eastern North Atlantic Central Water. Progress in Oceanography 37, 167–192.

[Polyakov and Johnson, 2000] Polyakov, I., Johnson, M. 2000. Arctic decadal and interdecadal variability. Geophysical Research Letters, 27, 4097–4100.

[Price et al., 1986] Price, J. F., Weller, R. A., Pinkel, R., 1986. Diurnal cycling: observations and models of the upper-ocean response to diurnal heating, cooling, and wind mixing. Technical report. Woods Hole Oceanographic Institution, MA (USA).

[Puillat et al., 2003] Puillat, I., Lazure, P., Jégou, A. M., Planque, B., Lampert, L., 2003. Mesoscale, interannual, and seasonal hydrological variability over the French continental shelf of the Bay of Biscay during the 1990s. In ICES Marine Science Symposia 219, pp. 333-336.

[Puillat et al., 2004] Puillat, I., Lazure, P., Jégou, A.M., Lampert, L., Miller, P.I., 2004. Hydrographical variability on the French continental shelf in the Bay of Biscay, during the 1990s. Continental Shelf Research 24, 1143-1163, doi:10.1016/j.csr.2004.02.008.

[Puillat et al., 2006] Puillat, I., Lazure, P., Jégou, A.M., Lampert, L., Miller, P., 2006. Mesoscale hydrological variability induced by northwesterly wind on the French continental shelf of the Bay of Biscay. Scientia Marina 70(S1), 15-26.

[Purkey and Johnson, 2010] Purkey, S. G., Johnson, G. C., 2010. Warming of global abyssal and deep Southern Ocean waters between the 1990s and 2000s: Contributions to global heat and sea level rise budgets. Journal of Climate 23, 6336–6351.

[Quenouille, 1952] Quenouille, M.H., 1952. Associated Measurements, 242 pp. Butterworths, London, U.K.

[Quero et al., 1998] Quero, J. C., Du Buit, M. H., Vayne, J. J., 1998. Les observations de poissons tropicaux et le réchauffement des eaux dans l'Atlantique européen. Oceanologica Acta 21(2), 345-351.

[Rallo and Borja, 2004] Rallo, A., Borja, A., 2004. Marine research in the Basque Country: an historical perspective. In: Borja, A., Collins, M. (Eds.), Oceanography and Marine Environment of the Basque Country, Elsevier Oceanography Series, Vol. 70. Elsevier, Amsterdam, pp. 3–25.

[Reinart and Reinhold, 2008] Reinart, A., Reinhold, M. 2008. Mapping surface temperature in large lakes with MODIS data. Remote Sensing of Environment, 112, 603-611, doi:10.1016/j.rse.2007.05.015.

[Relvas et al., 2009] Relvas, P., Luis, J., Santos, A.M.P., 2009. Importance of the mesoscale in the decadal changes observed in the northern Canary upwelling system. Geophysical Research Letters 36, L22601, doi:10.1029/2009GL040504.

[Reverdin et al., 2013] Reverdin, G., Marié, L., Lazure, P., d'Ovidio, F., Boutin, J., Testor, P., Martin, N., Lourenco, A., Gaillard, F., Lavín, A., Rodríguez, C., Somavilla, R., Mader, J., Rubio, A., Blouch, P., Rolland, J., Bozec, Y., Charria, G., Batifoulier, F., Dumas, F., Louazel, S., Chanut, J., 2013. Freshwater from the Bay of Biscay shelves in 2009. Journal of Marine Systems 109, S134-S143.

[Reynolds and Smith, 1994] Reynolds, R.W., Smith, T.M. 1994. Improved global sea surface temperature analysis using optimum interpolation. Journal of Climate, 7, 929–948.

[Reynolds et al., 2007] Reynolds, R. W., Smith, T. M., Liu, C., Chelton D. B., Casey, K. S., Schlax M. G. 2007. Daily high-resolution-blended analyses for sea surface temperature. Journal of Climate, 20, 5473-5496, doi:10.1175/2007JCLI1824.1.

[Reynolds, 2009] Reynolds, R. W., 2009. What's new in Version 2. [Available at http//www.ncdc.noaa.gov/oa/climate/research/sst/papers/whats_new_v2.pdf.]

[Ríos et al., 1992] Ríos, A. F., Pérez, F. F., Fraga, F., 1992. Water masses in the upper and middle North Atlantic Ocean east of the Azores. Deep Sea Research Part A. Oceanographic Research Papers 39(3), 645-658.

[Rodríguez-Puebla et al., 1998] Rodríguez-Puebla, C., Encinas, A.H., Nieto, S., Garmendia, J. 1998. Spatial and temporal patterns of annual precipitation variability over the Iberian Peninsula. International Journal of Climatology 18, 299–316.

[Roemmich and Gilson, 2009] Roemmich, D., Gilson, J., 2009. The 2004–2008 mean and annual cycle of temperature, salinity, and steric height in the global ocean from the Argo Program. Progress in Oceanography 82(2), 81-100.

[Roemmich et al., 2012] Roemmich, D., Gould, W. J., Gilson, J., 2012. 135 years of global ocean warming between the Challenger expedition and the Argo Programme. Nature Climate Change 2(6), 425-428.

[Sáenz et al., 2001] Sáenz, J., Zubillaga, J., Rodríguez Puebla, C., 2001. Interannual winter temperature variability in the north of the Iberian Peninsula. Climate Research 16:169–179.

[Sagarminaga and Arrizabalaga, 2010] Sagarminaga, Y., Arrizabalaga, H., 2010. Spatio-temporal distribution of albacore (Thunnus alalunga) catches in the northeastern Atlantic: Relationship with the thermal environment. Fisheries Oceanography 19 (2), 121–134, doi:10.1111/j.1365-2419.2010.00532.x.

[Saha et al., 2010] Saha, S., Moorthi, S., Pan, H. L., Wu, X., Wang, J., Nadiga, S., ... & Reynolds, R. W. 2010. The NCEP climate forecast system reanalysis. Bulletin of the American Meteorological Society, 91(8), 1015-1057, doi:10.1175/2010BAMS3001.1.

[Saldias et al., 2012] Saldías, G.S., Sobarzo, M., Largier, J., Moffat, C., Letelier, R. 2012. Seasonal variability of turbid river plumes off central Chile based on high-resolution MODIS imagery. Remote Sensing of Environment, 123, 220-233, doi:10.1016/j.rse.2012.03.010.

[Sánchez and Olaso, 2004] Sánchez, F. Olaso, I., 2004. Effects of fisheries on the Cantabrian Sea shelf ecosystem. Ecological Modelling 172(2), 151-174.

[Santos et al., 2005] Santos, A.M.P., Kazmin, A.S., Peliz, A., 2005. Decadal changes in the Canary upwelling system as revealed by satellite observations: their impact on productivity. Journal of Marine Research 63, 359–379.

[Santos et al., 2011] Santos, F., Gómez-Gesteira, M., deCastro, M., Alvarez, I., 2011. Upwelling along the western coast of the Iberian Peninsula: Dependence of trends on fitting strategy. Climate Research 48, 213–218, doi:10.3354/cr00972.

[Santos et al., 2012a] Santos, F., Gomez-Gesteira, M., deCastro, M., Alvarez, I., 2012a. Variability of coastal and ocean water temperature in the upper 700 m along the Western Iberian Peninsula from 1975 to 2006. PLoS One 7(12), 1–7, doi:10.1371/journalpone.0050666.

[Santos et al., 2012b] Santos, F., Gómez-Gesteira, M., deCastro, M., Alvarez, I., 2012b. Differences in coastal and oceanic SST trends due to the strengthening of coastal upwelling along the Benguela current system. Continental Shelf Research 34, 79–86, doi:10.1016/j.csr.2011.12.004.

[Santos et al., 2012c] Santos, F., deCastro, M., Gómez-Gesteira, M., Alvarez, I., 2012c. Differences in coastal and oceanic SST warming rates along the

Canary upwelling ecosystem from 1982 to 2010. Continental Shelf Research 47, 1–6, doi::10.1016/j.csr.2012.07.023.

[Saunders and Lea, 2008] Saunders, M.A., Lea A.S. 2008. Large contribution of sea surface warming to recent increase in Atlantic hurricane activity. Nature 451, 557–560.

[Saunders, 1982] Saunders, P. M., 1982. Circulation in the eastern North Atlantic. Journal of Marine Research 40, 641-657.

[Selig et al., 2010] Selig, E. R., Casey, K. S., Bruno, J. F., 2010. New insights into global patterns of ocean temperature anomalies: implications for coral reef health and management. Global Ecology and Biogeography 19(3), 397-411, doi:j.1466-8238.2009.00522.x.

[Somavilla et al., 2009] Somavilla, R., González-Pola, C., Rodriguez, C., Josey, C.A., Sánchez, R.F., Lavín, A., 2009. Large changes in the hydrographic structure of the Bay of Biscay after the extreme mixing of winter 2005. Journal of Geophysical Research: Oceans 114, C01001, doi:10.1029/2008JC004974.

[Somavilla et al., 2011] Somavilla, R., González-Pola, C., Ruiz-Villarreal, M., Lavín, A., 2011. Mixed layer depth (MLD) variability in the southern Bay of Biscay. Deepening of winter MLDs concurrent with generalized upper water warming trends?. Ocean Dynamics 61:1215:1235.

[Soto-Navarro et al., 2012] Soto-Navarro, J., Criado-Aldeanueva, F., Sánchez-Garrido, J.C., García-Lafuente, J., 2012. Recent thermohaline trends of the Atlantic waters inflowing to the Mediterranean Sea. Geophysical Research Letters 39, doi:10.1029/2011GL049907.

[Sura, 2011] Sura, P., 2011. A general perspective of extreme events in weather and climate. Atmospheric Research 101(1), 1-21.

[Sverdrup, 1953] Sverdrup, H., 1953. On conditions for the vernal blooming of phytoplankton. Journal du Conseil International pour l'Exploration de la Mer, 18: 287–295.

[Taboada and Anadon, 2012] Taboada, F., Anadon, R., 2012. Patterns of change in sea surface temperature in the North Atlantic during the last three decades: Beyond mean trends. Climatic Change, doi:10.1007/s10584-012-0485-6.

[Thieltges, 2006] Thieltges, D. W., 2006. Parasite induced summer mortality in the cockle *Cerastoderma edule* by the trematode *Gymnophallus choledochus*. Hydrobiologia *559*(1), 455-461.

[Thompson and Wallace, 1998] Thompson, D. W., Wallace, J. M. (1998). The Arctic Oscillation signature in the wintertime geopotential height and temperature fields. Geophysical Research Letters, 25(9), 1297-1300.

[Thompson and Wallace, 2000] Thompson, D. W., Wallace, J. M. 2000. Annular modes in the extratropical circulation. Part I: month-to-month variability. Journal of Climate, 13(5), 1000-1016.

[Timmermann et al., 1998] Timmermann, A., Latif, M., Voss, R., Grötzner, A. 1998. Northern hemispheric interdecadal variability: a coupled air-sea mode. Journal of Climate, 11(8), 1906-1931.

[Trigo et al., 2009] Trigo, R. M., Ramos, A. M., Nogueira, P. J., Santos, F. D., Garcia-Herrera, R., Gouveia, C., Santo, F. E., 2009. Evaluating the impact of extreme temperature based indices in the 2003 heatwave excessive mortality in Portugal. Environmental Science & Policy 12(7), 844-854.

[UNESCO, 1983] UNESCO, 1983. Algorithms for computation of fundamental properties of seawater. UNESCO Technical Paper in Marine Science, 44 (53 pp.).

[Usabiaga et al., 2004] Usabiaga, J. I., Sáenz, J., Valencia, V., Borja, Á., 2004. Climate and meteorology: variability and its influence on the Ocean, In: Oceanography and Marine Environment of the Basque Country. Elsevier Oceanography Series, 70, 75-95.

[Valencia et al., 2003] Valencia, V., Borja, A., Fontán, A., Pérez, F.F., Ríos, A.F., 2003. Temperature and salinity fluctuations in the Basque Coast (SE Bay of Biscay) from 1986 to 2000 related to the climatic factors. ICES Marine Science Symposia 219, 340–342.

[Valencia et al., 2004] Valencia, V., Franco, J., Borja, Á., Fontán, A., 2004. Hydrography of the southeastern Bay of Biscay. In: Borja, A., Collins, M. (Eds.), Oceanography and Marine Environment of the Basque Country Elsevier Oceanography Series vol. 70. Elsevier, Amsterdam, pp. 159–194.

[van Aken, 2000] van Aken, H.M. 2000. The hydrography of the mid-latitude northeast Atlantic Ocean. II: The intermediate water masses. Deep Sea Research Part I: Oceanographic Research Papers 47, 789–824.

[Vizy and Cook, 2010] Vizy, E.K., Cook, K.H., 2010. Influence of the Amazon/Orinoco plume on the summertime Atlantic climate. Journal of Geophysical Research 115, D21112, doi:10.1029/2010JD014049.

[Voerman et al., 2013] Voerman, S.E., Llera, E., Rico, J.M., 2013. Climate driven changes in subtidal kelp forest communities in NW Spain. Marine Environmental Research 90, 119–127, doi:10.1016/j.marenvres.2013.06.006.

[Wang et al., 2010] Wang, C., Dong, S., Munoz, E., 2010. Seawater density variations in the North Atlantic and the Atlantic meridional overturning circulation. Climate Dynamics 34(7-8), 953-968.

[Wethey et al., 2011] Wethey, D.S., Woodin, S.A., Hilbish, T.J., Jones, S.J., Lima, F.P., Brannock, P.M., 2011. Response of intertidal populations to climate: Effects of extreme events versus long term change. Journal of Experimental Marine Biology and Ecology 400, 132–144.

[Wong et al., 2013] Wong, A., Keeley, R., Carval, T., the Argo Data Management Team 2013. Argo Quality Control Manual, Version 2.8. http://www.argodatamgt.org/content/download/15699/102401/file/argo-quality-control-manual-version2.8.pdf.

List of publications

Articles

[Gómez-Gesteira et al., 2013] Gómez-Gesteira, M., deCastro, M., Santos, F., Álvarez, I., **Costoya, X**., 2013. Changes in ENACW observed in the Bay of Biscay over the period 1975-2010. Continental Shelf Research 65, 73-80, doi: 10.1016/j.csr.2013.06.014.

[Costoya et al., 2014a] **Costoya, X**., deCastro, M., Gómez-Gesteira, M., 2014. Thermohaline trends in the Bay of Biscay from Argo floats over the decade 2004-2013. Journal of Marine Systems 139, 159-165, doi: 10.1016/j.jmarsys.2014.06.001.

[Costoya et al., 2014b] **Costoya, M**., deCastro, M., Gómez-Gesteira, M., Santos, F., 2014. Mixed layer depth trends in the Bay of Biscay over the period 1975-2010. PLoS ONE 9(6):e99321, doi: 10.1371/journal.pone.0099321.

[Costoya et al., 2015] **Costoya, X**., deCastro, M., Gómez-Gesteira, M., Santos, F., 2015. Changes in sea surface temperature seasonality in the Bay of Biscay over the last decades (1982-2014). Journal of Marine Systems 150, 91-1001, doi: 10.1016/j.jmarsys.2015.06.002.

[deCastro et al., 2014] deCastro, M., Gómez-Gesteira, M., **Costoya, X**., Santos, F., 2014. Upwelling influence on the unmber of extreme hot SST days along the Canary upwelling ecosystem. Journal of Geophysical Research:Oceans 119, 3029-3040, doi:10.1002/2013JC009745.

[Costoya et al., in press] **Costoya, X**., Fernández-Nóvoa, D., deCastro, M., Santos, F., Lazure, P., Gómez-Gesteira, M., in press. Modulation of sea surface temperature warming in the Bay of Biscay by Loire and Gironde Rivers. Journal of Geophysical Research:Oceans.